科技部補助專題研究計畫成果報告
期末報告

碳分子篩型水氣轉移膜反應器於IGCC系統捕獲CO2及提升H2產率之開發與老化再生機制評估(第3年)

計 畫 類 別 ： 個別型計畫
計 畫 編 號 ： MOST 103-2221-E-040-001-MY3
執 行 期 間 ： 105年08月01日至106年12月31日
執 行 單 位 ： 中山醫學大學職業安全衛生學系暨碩士班

計 畫 主 持 人： 曾惠馨

計畫參與人員： 碩士班研究生-兼任助理：李靜怡
博士班研究生-兼任助理：莊國良

報 告 附 件 ： 出席國際學術會議心得報告

中 華 民 國 107 年 03 月 31 日

中 文 摘 要 ： 本計畫中將整合薄膜氣體分離技術與水氣轉移反應，構成碳分子篩型水氣轉移膜反應器；應用薄膜連續地移除H2或CO2克服反應的熱力學限制而提高CO的轉換率及H2的產率。由於多孔無機碳分子篩選薄膜可被操作於高溫、高壓及組成較複雜的進氣環境中，當其構成膜反應器時，往往以管柱型模組內填充觸媒以提供足夠的停留時間；因此，在本計畫第一年將進行管柱型碳分子篩選薄膜的開發及多成份氣體測試系統、第二年則是建構碳分子篩型水氣轉移膜反應器系統與老化機制評估、第三年則是發展疏水性碳分子篩型膜反應器與再生方法評估；期使能在高溫環境下(200-300 oC)提高CO轉換率及H2產率，並將二氧化碳與氫氣分離，達到潔淨能源之目的。
本研究利用真空輔助浸塗法來製備出管柱式高分子薄膜，使用聚醚醯亞胺（Polyetherimide, PEI）作為高分子前趨物，使用N-甲基吡咯酮（N-methyl-2-pyrrolidone, NMP）與三氯甲烷做為溶劑，塗佈於多孔管柱式氧化鋁基材上。第一年研究結果顯示，真空輔助系統確實能提升碳膜對於氣體的選擇率，最佳的製程參數為真空輔助浸塗時，以氯仿做為溶劑配製10 wt.% PEI、基材浸漬與浸沒與抽出速度為1 mm/s、塗佈5次，此時PH2 為519 Barrer、H2/N2 為9.25。
接著利用共沉澱法製備出Cu/Zn/SBA－16水氣轉移觸媒，將其應用於固定床催化反應中，結果顯示CO轉化率、H2生成率隨反應溫度提高、空間速度降低皆有增加之趨勢。最佳之催化效果出現於操作在反應溫度為300 ℃、空間速度2,500 h-1及水氣含量S/C (Steam /CO ratio) = 1時，CO轉化率為82.76%。最後以相同操作參數將Cu/Zn/SBA－16觸媒應用於薄膜反應器內，結果顯示CO轉化率相較於固定床反應器提升了4.19%，透過使用催化型薄膜反應器不僅能有效提升CO轉化率和H2生成率，同時能夠縮短反應達平衡的時間。
在第三年研究中，水氣轉移觸媒Cu/Zn/SBA-16仍係以共沉澱法製備。當膜反應器之操作條件為反應溫度300 oC，空間速度2,500 h-1，水汽比為1.5時，膜反應器的CO轉化率可達到99%以上，H2的回收率可達76%，且H2回收率則是隨著水汽比越高而有提升之趨勢，在S/C=2時，膜反應器之氫氣回收率亦可達100%，然其CO轉化率卻降至89%。由於水汽含量高時容易吸附於碳膜活性位基，導致碳膜老化。因此，在研究中利用疏水材進行碳膜改質，並發現其在S/C=2時仍可得到高CO轉化率；相較於固定床，膜反應器在CO轉化率及H¬2回收率都有更佳的表現。

中 文 關 鍵 詞 ： 膜反應器、碳分子篩、水氣轉移、二氧化碳分離、氫能、清潔能源

英 文 摘 要 ： In this research, a H2/CO2- selective carbon molecular sieve membrane was incorporated into the WGS reactor as a membrane reactor (MR) to improve efficiency through continually remove either H2 or CO2 to overcome the thermodynamic constraints of the reaction, resulting in a higher CO conversion. Generally, WGS-MR design is similar to a tube heat exchanger, which can provide longer retention time. In the first year, the tube-type carbon molecular sieve membrane will fabricate and evaluate with multi-gas permeation test; in the second year, the tube-type WGS-MR will fabricate, and the aging mechanism will

study. Finally, in the third year, a hydrophobic tube-type WGS-MR will synthesis to improve the lifetime, and the generation mechanism will also study.
In the first year, the thin tubular CMS membranes were obtained by one step of vacuum-assisted dip-coating and pyrolysis procedure. The polyethyleneimine (PEI) and two kind of solvent which NMP and chloroform was used to prepare casting solution to coat on the porous alumina tube via dip-coating method. The effects of vacuum-assisted dip-coating parameters, such as immersion speed, vertical withdrawal speed and coating times on the membrane structure and gas separation performance. The results indicated that the vacuum assisted system can increase the gas selectivity. The best gas permeability and selectivity is PH2 519 Barrer and H2/N2 9.25, respectively, by opportune parameters that chloroform as solvent to prepare 10 wt % PEI casting solution, immersion velocity and withdrawal velocity is 1 mm/s, coating five times with vacuum-assisted system.
Furthermore, we synthesized Cu/Zn/SBA－16 catalyst with co-precipitation. The results indicated that the CO conversion and H2 yield of reaction become higher with the raising operating temperature and decreasing GHSV in the traditional fixed-bed reactor. The optimal reaction temperature, GHSV and steam contain of Cu/Zn/SBA－16 catalyst were 300 ℃、2,500 h-1and S/C (Steam /CO ratio) = 1with CO conversion 82.76%. Finally, Cu/Zn/SBA－16 catalyst were used in catalytic membrane reactor with the same condition above, result in increasing the CO conversion about 4.19%. With the MR we not only successfully prepared with high CO conversion and fine H2/CO2 selectivity, but also cutting the time of reaction equilibrium.
In the third year, the Cu/Zn/SBA-16 catalyst synthesized by co-precipitation were used in WGSR. With the 300 C reaction temperature, 2,500 h-1 GHSV (Hourly space velocity) S/C=1.5, the CO conversion efficiency of membrane reactor could reach to 99% and the recovery of H???2 was about 76%. However, as the S/C increasing to 2, the H2 recovery was increased to 99 % with the CO conversation decreased to 89% due to the water vapor adsorbed on the active site. The hydrophobic Si/C membrane was further synthesized and showed good performance with S/C equal to 2. Compared to fixed-bed reactor, the performance of membrane reactor showed higher CO conversion and H?2 recovery simultaneously.

英文關鍵詞：Membrane reactor, carbon molecular sieve, water-gas shift, CO2 capture, hydrogen energy, clean energy

附件一

科技部補助專題研究計畫成果報告

（□期中進度報告/☑期末報告）

碳分子篩型水氣轉移膜反應器於IGCC 系統捕獲CO_2及提升H_2產率之開發與老化再生機制評估

計畫類別：☑個別型計畫　□整合型計畫

計畫編號：MOST　103－2221－E－040－001－MY3

執行期間：103 年 08 月 01 日至 106 年 12 月 31 日

執行機構及系所：中山醫學大學 職業安全衛生學系

計畫主持人：曾惠馨

共同主持人：無

計畫參與人員：博士班研究生 莊國良

碩士班研究生 鄭博育、涂逸寧、李靜怡

專題生 毛婉驊、劉靖圓、林鈺婷、林奕辰、儲億凡

本計畫除繳交成果報告外，另含下列出國報告，共 _3_ 份：

☑執行國際合作與移地研究心得報告

☑出席國際學術會議心得報告

☑出國參訪及考察心得報告

中　華　民　國　107 年 03 月 14 日

摘要

本計畫中將整合薄膜氣體分離技術與水氣轉移反應，構成碳分子篩型水氣轉移膜反應器；應用薄膜連續地移除 H_2 或 CO_2 克服反應的熱力學限制而提高 CO 的轉換率及 H_2 的產率。由於多孔無機碳分子篩選薄膜可被操作於高溫、高壓及組成較複雜的進氣環境中，當其構成膜反應器時，往往以管柱型模組內填充觸媒以提供足夠的停留時間；因此，在本計畫第一年將進行管柱型碳分子篩選薄膜的開發及多成份氣體測試系統、第二年則是建構碳分子篩型水氣轉移膜反應器系統與老化機制評估、第三年則是發展疏水性碳分子篩型膜反應器與再生方法評估；期使能在高溫環境下(200-300 ºC)提高 CO 轉換率及 H_2 產率，並將二氧化碳與氫氣分離，達到潔淨能源之目的。

本研究利用真空輔助浸塗法來製備出管柱式高分子薄膜，使用聚醚醯亞胺（Polyetherimide, PEI）作為高分子前趨物，使用 N-甲基吡咯酮（N-methyl-2-pyrrolidone, NMP）與三氯甲烷做為溶劑，塗佈於多孔管柱式氧化鋁基材上。第一年研究結果顯示，真空輔助系統確實能提升碳膜對於氣體的選擇率，最佳的製程參數為真空輔助浸塗時，以氯仿做為溶劑配製 10 wt.% PEI、基材浸漬與浸沒與抽出速度為 1 mm/s、塗佈 5 次，此時 P_{H2} 為 519 Barrer、H_2/N_2 為 9.25。

接著利用共沉澱法製備出 Cu/Zn/SBA–16 水氣轉移觸媒，將其應用於固定床催化反應中，結果顯示 CO 轉化率、H_2 生成率隨反應溫度提高、空間速度降低皆有增加之趨勢。最佳之催化效果出現於操作在反應溫度為 300 ℃、空間速度 2,500 h^{-1} 及水氣含量 S/C (Steam /CO ratio) = 1 時，CO 轉化率為 82.76%。最後以相同操作參數將 Cu/Zn/SBA–16 觸媒應用於薄膜反應器內，結果顯示 CO 轉化率相較於固定床反應器提升了 4.19%，透過使用催化型薄膜反應器不僅能有效提升 CO 轉化率和 H_2 生成率，同時能夠縮短反應達平衡的時間。

在第三年研究中，水氣轉移觸媒 Cu/Zn/SBA-16 仍係以共沉澱法製備。當膜反應器之操作條件為反應溫度 300 ºC，空間速度 2,500 h^{-1}，水汽比為 1.5 時，膜反應器的 CO 轉化率可達到 99%以上，H_2 的回收率可達 76%，而 H_2 回收率則是隨著水汽比越高而有提升之趨勢，在 S/C=2 時，膜反應器之氫氣回收率亦可達 100%，然其 CO 轉化率卻降至 89%。由於水汽含量高時容易吸附於碳膜活性位基，導致碳膜老化。因此，在研究中利用疏水材進行碳膜改質，並發現其在 S/C=2 時仍可得到高 CO 轉化率；相較於固定床，膜反應器在 CO 轉化率及 H_2 回收率都有更佳的表現。

關鍵詞：膜反應器、碳分子篩、水氣轉移、二氧化碳分離、氫能、清潔能源

ABSTRACT

In this research, a H_2/CO_2- selective carbon molecular sieve membrane was incorporated into the WGS reactor as a membrane reactor (MR) to improve efficiency through continually remove either H_2 or CO_2 to overcome the thermodynamic constraints of the reaction, resulting in a higher CO conversion. Generally, WGS-MR design is similar to a tube heat exchanger, which can provide longer retention time. In the first year, the tube-type carbon molecular sieve membrane will fabricate and evaluate with multi-gas permeation test; in the second year, the tube-type WGS-MR will fabricate, and the aging mechanism will study. Finally, in the third year, a hydrophobic tube-type WGS-MR will synthesis to improve the lifetime, and the generation mechanism will also study.

In the first year, the thin tubular CMS membranes were obtained by one step of vacuum-assisted dip-coating and pyrolysis procedure. The polyethyleneimine (PEI) and two kind of solvent which NMP and chloroform was used to prepare casting solution to coat on the porous alumina tube via dip-coating method. The effects of vacuum-assisted dip-coating parameters, such as immersion speed, vertical withdrawal speed and coating times on the membrane structure and gas separation performance. The results indicated that the vacuum assisted system can increase the gas selectivity. The best gas permeability and selectivity is P_{H2} 519 Barrer and H_2/N_2 9.25, respectively, by opportune parameters that chloroform as solvent to prepare 10 wt % PEI casting solution, immersion velocity and withdrawal velocity is 1 mm/s, coating five times with vacuum-assisted system.

Furthermore, we synthesized Cu/Zn/SBA–16 catalyst with co-precipitation. The results indicated that the CO conversion and H_2 yield of reaction become higher with the raising operating temperature and decreasing GHSV in the traditional fixed-bed reactor. The optimal reaction temperature, GHSV and steam contain of Cu/Zn/SBA–16 catalyst were 300 ℃、2,500 $h^{-1}$and S/C (Steam /CO ratio) = 1with CO conversion 82.76%. Finally, Cu/Zn/SBA–16 catalyst were used in catalytic membrane reactor with the same condition above, result in increasing the CO conversion about 4.19%. With the MR we not only successfully prepared with high CO conversion and fine H_2/CO_2 selectivity, but also cutting the time of reaction equilibrium.

In the third year, the Cu/Zn/SBA-16 catalyst synthesized by co-precipitation were used in WGSR. With the 300 °C reaction temperature, 2,500 h^{-1} GHSV (Hourly space velocity) S/C=1.5, the CO conversion efficiency of membrane reactor could reach to 99% and the recovery of H_2 was about 76%. However, as the S/C increasing to 2, the H_2 recovery was increased to 99 % with the CO conversation decreased to 89% due to the water vapor adsorbed on the active site. The hydrophobic Si/C membrane was further synthesized and showed good performance with S/C equal to 2. Compared to fixed-bed reactor, the performance of membrane reactor showed higher CO conversion and H_2 recovery simultaneously.

Keywords: Membrane reactor, carbon molecular sieve, water-gas shift, CO_2 capture, hydrogen energy, clean energy

目錄

表目錄

圖目錄

第一章 研究背景與目的

1.1 計畫背景--潔淨發電程序

依據國際能源局的統計資料顯示，發電廠是碳排放最大的點源，將最有可能受到氣候變化法的影響，需要在未來投資決策和營運策略中考慮碳管理[1]。因此，20世紀80年代起，美國、日本和歐盟等政府相繼佈署"潔淨煤發展計畫"，並將CO_2捕集與封存（carbon dioxide capture and storage，CCS）技術視為是碳管理的重要手段之一。時至西元2007年，美國能源部在該計劃中對天然氣複循環發電技術（NGCC）、超臨界煤粉燃燒（Supercritical PC）、亞臨界煤粉燃燒（PC Sub）、整合煤氣化複循環發電系統（IGCC）等進行了技術評估，由於煤炭初估有200 年以上之蘊藏量，其價格相較於石油與天然氣已漸趨穩定，也逐漸拉大IGCC與NGCC之經濟差異，而使IGCC系統（含CCS系統）的投資與發電成本為最低。目前，美國、英國、荷蘭、西班牙、德國、日本、印度等國紛紛建起了IGCC商用化示範電站[2]。

IGCC是指將煤炭、生物質、石油焦、重渣油等多種含碳燃料進行氣化，將得到的合成氣淨化後與高效的聯合迴圈相結合的先進動力系統。這種系統不僅可以符合2005-2010年日益嚴格的脫硫脫硝除塵要求，而且可以符合2010-2020年排上日程的微顆粒（PM_{10}、$PM_{2.5}$）和金屬元素（如汞）的排放要求，同時也克服了天然氣供應不足和價格昂貴的問題，正代表21世紀潔淨煤發電技術的發展方向[2]。

在該程序中，運用薄膜氣體分離技術進行二氧化碳捕獲與氫氣分離，已被視為是減少溫室氣體排放的潛力技術之一[3,4]。如圖1-1所示該程序又稱為燃燒前碳捕獲技術（pre-combustion capture），化石燃料如煤將於高溫環境下氣化形成合成氣，此時主要組成為H_2：25-45 mol%、CO：40-50 mol%及CO_2：10-35 mol%，之後再經由水氣轉移反應器（water-gas shift，WGS reactor），將CO與H_2O反應生成高壓的CO_2及H_2；此產物經分離後即可將CO_2予以貯存，而H_2則可被使用於發電程序[5]。因此，該程序可產生無碳燃料且可於高壓環境下進行碳捕獲。

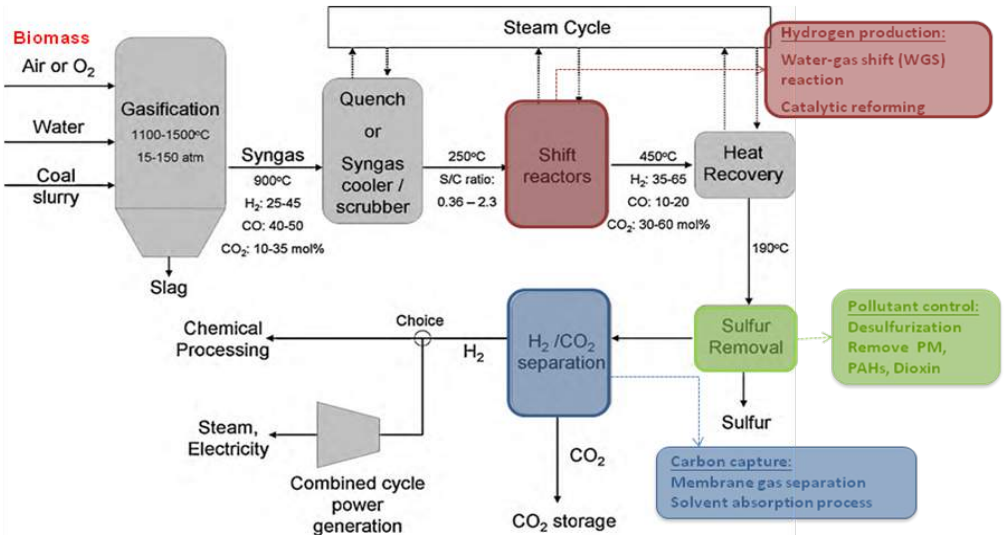

圖 1-1 預燃燒碳捕捉整合水氣轉移於煤氣化複循環發電程序

目前已知有金屬膜及多孔無機膜等被應用於燃燒前碳補獲程序，雖各有其優/缺點；然而運用薄膜氣體分離技術整合水氣轉移反應，構成水氣轉移膜反應器（membrane reactor，MR），因另具有突破水氣轉移反應之熱力學限制而可提高氫產率之優勢，故已相繼被法國、澳洲及美國等國家的

能源發展相關部門列入改善現有共生廠(ready cogeneration plant) 碳排放與氫分離的可行技術之一[6]或整合煤氣化複循環發電系統(integrated gasification combined cycle，IGCC)的淨煤技術。

1.2 水氣轉移膜反應器概念

在固定式水氣轉移反應器中，CO轉換平衡是溫度與H_2O/CO劑量比的函數（方程式(1)）[7]。由於該反應為放熱反應，因此在低溫環境下或提高H_2O含量，皆可提高CO轉換率及H_2產率；故就經濟觀點而言，學者建議當化學計量比為0.9~1.5時可使既有氣體的熱值獲得較佳的效益[8]；然而，要使複循環達最大效益，則合成氣的溫度不能低於200 ºC。因此，固定式水氣轉移反應器受限於複循環往往較難獲得高CO轉換率及H_2產率。

$$CO + H_2O \leftrightarrow CO_2 + H_2 \quad \Delta H_{298}=-41.1\ kJ/mol \tag{1}$$

此外，低H_2O/CO比可能會產生非預期的副反應，而生成碳或甲烷[8]。取決於催化反應、系統條件及動力行為，可能發生下列反應（方程式(1)、(2)），若該反應較為顯著，則可能產生碳沉積於WGS-MR而導致觸媒失活、減低氣體通量及設備阻塞。

$$2CO \leftrightarrow C + CO_2 \tag{2}$$

$$2CO + 2H_2 \leftrightarrow CO_2 + CH_4 \tag{3}$$

應用薄膜連續地移除H_2或CO_2是有利於WGS反應的，因為它可克服反應的熱力學限制而提高CO的轉換率；因此，可將H_2-或CO_2-選擇性薄膜整合至WGS反應器，而成為水氣轉移膜反應器[9]，其概念如圖1-2所示。適合此類反應目的之膜反應器稱之為"移除型膜反應器（extractor）"，如右圖1-3所示。一般而言，WGS-MR的設計與殼狀或管狀的熱交換器相似，薄膜多為中空纖維型，觸媒則填充於薄膜內；以一般可逆反應為例：A+B ↔ C+D，可將C或D自反應系統中移除，使整個反應的熱力學平衡有利於往產物的方向進行以提高產率（如圖1-3(a)所示），或是限制進入膜反應器之反應物，以避免二次反應的發生（如圖1-3(b)所示）此時的薄膜為控制傳輸的材料。在該反應器中，藉由提高薄膜的選擇率、催化劑的活性、穩定度以及改變接觸時間、反應物濃度、反應溫度，或是提高催化劑與膜面積的比例等操作參數，皆可增加產率[10]；因此，催化劑本身的活性以及膜本身的性能，將是反應的限制因子。

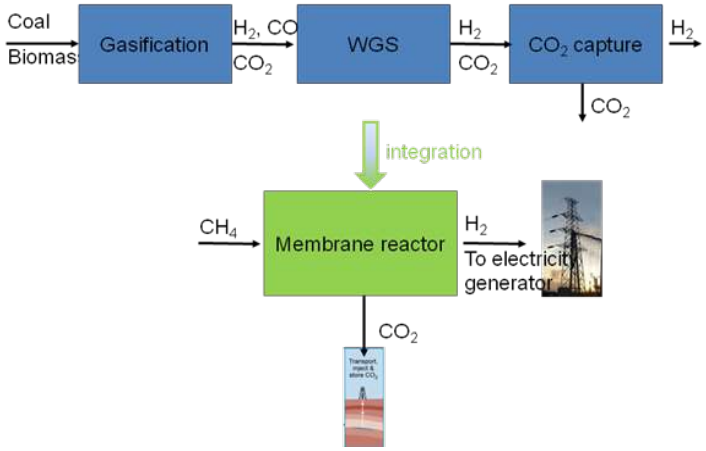

圖 1-2 水氣轉移膜反應器的設計概念

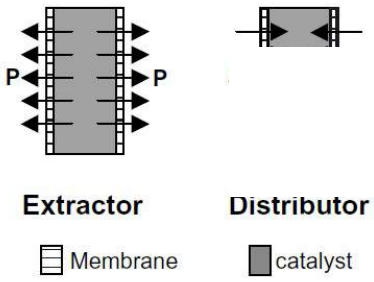

圖 1-3 移除型膜反應器示意圖[17]
(P：product，A：reactant)

1.3 具發展潛力的膜反應器材料

目前已知有金屬膜及多孔無機膜等被應用於燃燒前碳補獲程序。於氫氣選擇性薄膜(H_2-selective membranes) 種類中，金屬鈀膜(或鎳、銅、鐵等合金型薄膜)可產生純度高於99.99%的氫氣[11]，當鈀膜溫度為300～500 °C下，氫分子可在鈀膜的高壓側解離成氫原子，溶於鈀並擴散到

低壓側，然後結合成氫氣。然而，金屬鈀膜存在許多問題而減少其應用於大規模H_2分離的潛力，例如：(1) 低溫時(<300 ºC)氫氣易使鈀金屬脆化[11]、(2)進氣中的污染物會抑制氫氣解離與再結合的反應[12]，(3)對硫化物、CO、NH_3及氯化物等較敏感物質，會使鈀金屬因膨脹而破壞其結構[13]，此外，(4)鈀膜使用期限短，約數個月即需予以更換，因此高額的操作及維護費亦是促使鈀膜無法被大規模使用的潛在問題[14]。

相反地，多孔無機膜如沸石膜及碳分子篩選薄膜(carbon molecular sieve membrane，CMSM)等，則可被操作於高溫、高壓及組成較複雜的進氣環境中[15]。

多孔無機膜係利用氣體分子動力尺寸的差異來達到分選的目的，如利用分子篩選機制將小分子的氫氣(2.8Å)自大分子CO_2 (3.3Å)、O_2 (3.46Å)、N_2 (3.64Å)或CH_4 (3.8Å)中分離；表面處理亦可以增加孔壁對氫氣的吸附能力，透過提升氫氣在孔壁的表面遷移速率而改善氫氣的選擇率，此即表面擴散；或藉由孔洞表面的吸附擴散，自較小分子中分離出特定的大分子等，因此，多孔無機膜有多種傳輸機制。一般而言，多孔無機薄膜的氣體通量比高分子膜高數百倍以上，但缺點是價格高，且薄膜的面積/模組體積比僅為高分子薄膜的1/100至1/1000。

然而，分子篩選型多孔無機薄膜可藉由製程條件調整薄膜內孔洞尺寸，而使分子篩選薄膜具有將氫氣或二氧化碳自任何氣體中分離的能力，且具有高通量。其中，碳分子篩選薄膜係在高溫、惰性的環境下經由裂解有機高分子前驅物製備而得，可經由調整高分子前驅物種類、前處理、熱裂解條件及後處理等程序[16]，改變膜結構中微孔及超微孔的分佈比例，而使其兼具分子篩選與表面擴散的作用機制。

1.4 碳分子篩膜反應器及其老化行為

由於碳分子篩選機制係一種活化擴散程序，因此，以碳分子篩選薄膜所建構的反應器，其優點在於可被操作於低溫或高溫等環境下(250-450 °C)，係一種在高溫環境下亦可達高滲透率與高選擇率，且對環境忍受度高的膜反應器，因此相當具有發展潛力[17-19]。而隨著水氣轉移反應觸媒的發展迅速，許多研究已提出可展現高催化活性的觸媒，如Cu-Zn觸媒[20,21]。因此，若能整合低溫水氣轉移觸媒與碳分子篩選薄膜於一反應單元內，構成碳分子篩型水氣轉移膜反應器，應可應用於IGCC系統中，於高於200 °C的環境下，突破反應之熱力學限制而達到提高氫產率之目的。

然而，如同矽膜，碳膜亦可能因高濃度的水氣而失活。碳膜雖然是一種疏水性材料，但表面含氧官能基及高孔隙率的性質，易使得水氣吸附於孔洞內，並填滿碳膜的微孔洞而減少有效孔洞的含量。含氧官能基通常作為吸附水份子的起始位置，被吸附的水分子將會與其他水分子以氫鍵方式鍵結而導致水團簇的形成，進而減少氣體分子穿透的有效孔洞，導致薄膜分離效能的損失，此即為碳材的老化現象。

對於碳膜的老化現象，可以藉由(1)表面改質的方法，使薄膜表面趨於穩定，以防止氧基團對極性水分子產生親和力[22]，或是(2)添加疏水性的材料，以減少多孔結構中對水吸附的親和性，減緩薄膜老化速率[23]；此外，透過再生程序，如熱再生，化學再生及電熱再生等，皆可恢復碳膜本身的活性能，增加碳膜的使用週期。

1.5 研究目的

因此，在本計畫中將應用碳分子篩膜反應器(carbon membrane reactor，CMR)於IGCC程序進行碳捕獲與氫氣分離，整合水氣轉移反應器與氣體分離薄膜於單一系統中，使其能在高於250 ºC的環境下達到高CO轉換率、高H_2產率，並將二氧化碳與氫氣分離，達到潔淨能源之目的。此外，在本計畫中亦將評估碳膜反應器的老化機制、改善碳膜的疏水性質、並提出改善策略。茲將三年研究目標及執行方法簡述如下：

A. 第一年

(1) 研究目標：管柱型碳分子篩選薄膜的開發。本計畫第一年著重於管柱型碳膜及多成份分離系統的開發。管柱型基材多以浸沾式塗佈法(dip-coating)鍍膜，但容易有塗佈厚度不均等問題；且由於製備碳膜的前驅物為有機材料(如 PEI、PI、PFA 等)與氧化鋁無機基材間的相容性或結合性較差，容易於碳化後產生缺陷，而降低碳膜的選擇率。

(2) 研究方法：本研究將回顧浸沾式塗佈法之塗佈機制，探討相關塗佈參數及其經碳化後與基材間的黏附情形；並同時組裝多成份系統，進行混合氣的滲透分選效能測試。

B. 第二年

(1) 研究目標：碳分子篩型水氣轉移膜反應器的開發與老化機制評估

(2) 研究方法：水氣轉移觸媒將以中孔沸石 SBA-15 為擔體附載 Cu-Zn 活性相。研究將(1)摻雜異質原子如 Al、Zr 於 SBA-15 擔體，評估觸媒的酸鹼度、疏水性、熱穩定性對轉換率及選擇率之影響；(2)探討進氣含水氣、硫或氮氧化物、不同反應溫度對觸媒燒結、毒化及碳膜老化現象之影響。

C. 第三年

(1) 研究目標：發展疏水性碳分子篩型膜反應器與再生方法評估

(2) 研究方法：製備疏水性 C/Si 複合膜改善老化現象。於鑄膜液中摻雜疏水性高分子前驅物或疏水性無機材，如 methyltriethoxysilane (MTES) 提高碳膜的疏水性，以避免水氣沉積於薄膜孔洞內部，減少分離效能。並將評估熱再生或化學再生的操作條件。

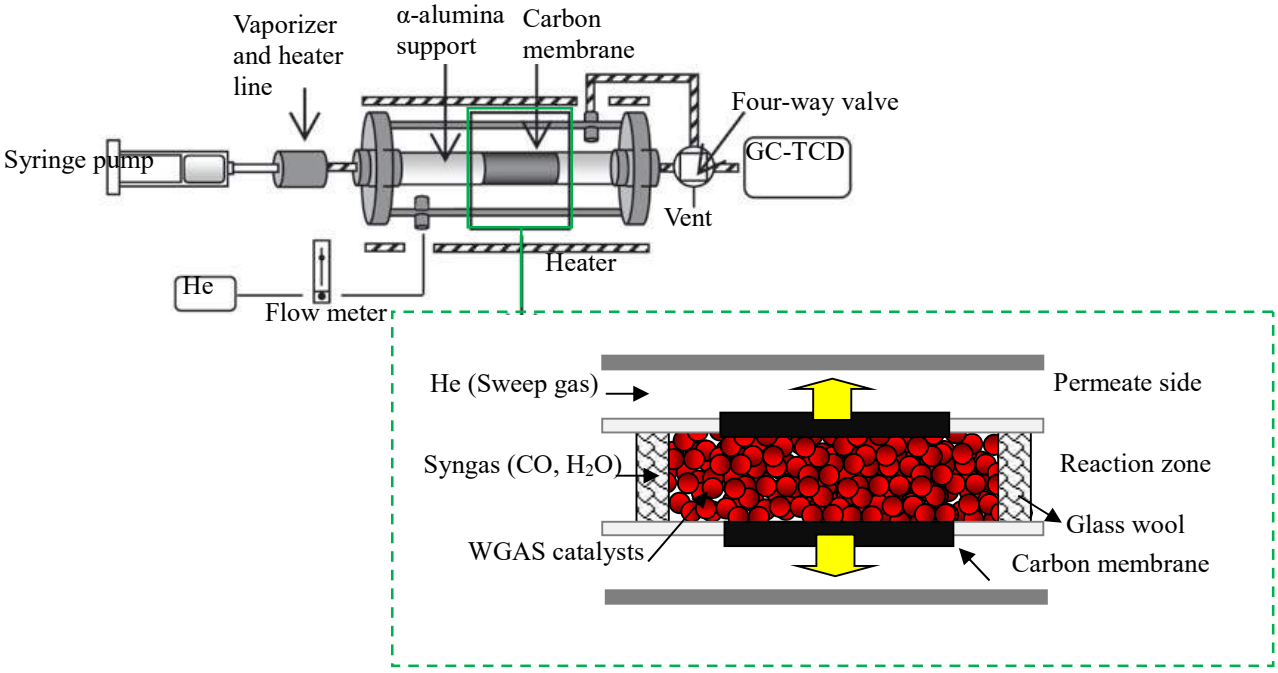

圖 1-4 碳分子篩膜反應器裝置示意圖

第二章 文獻回顧

為提升碳分子篩選薄膜的機械強度及減少膜厚，碳膜除碳中空纖維外，多以基材支撐式為主要模組型式。一般而言，碳膜的製備步驟依序為：(1) 高分子前驅物的選擇、(2) 高分子薄膜之製備、(3) 薄膜預處理、(4) 熱裂解/碳化、(5) 薄膜後處理及 (6) 模組建構。其中，高分子薄膜之製備亦為影響碳分子篩選薄膜結構的重要條件。製備高分子薄膜時根據所使用的方法而有適合的最佳操作條件，並於塗佈過程中需注意基材上的高分子溶液是否均勻分佈、塗佈量及黏度是否恰當，且高分子溶液不會破壞基材結構造成材料變質等；若所製備的高分子薄膜品質不良，則經由碳化過程，碳膜將出現裂縫或缺陷而無法表現出好的氣體分選效能。

2.1 浸塗法的作用機制

浸塗法（dip-coating）是最常被用於將高分子溶液塗佈在管柱式基材上的方法，為一種極簡易且使用已久的塗佈技術，具有不浪費溶劑、設備容易建立和操作簡單等優點[24]。該方法係將基材從牛頓流體（Newtonian fluid）或非牛頓流體（non-Newtonian fluid）中垂直浸入並拉出，使塗佈液塗佈於基材表面。當鑄膜液為非牛頓流體時，浸塗過程將涉及溶劑蒸發所引起的濃度、黏度梯度和表面張力的改變；然而，在膜沉積期間，黏度變化、液體的蒸發冷卻及化學反應等影響並不易評估，是個複雜的動態過程[25]。僅管如此，縱使難以規範單一參數對薄膜結構的影響，但浸塗法過程公認受兩大機制作用，分別為：(1) 毛細現象機制 (Capillarity regime)、(2) 黏性阻力機制 (Draining regime)。機制示意圖如圖 2-1 所示，茲說明如下：

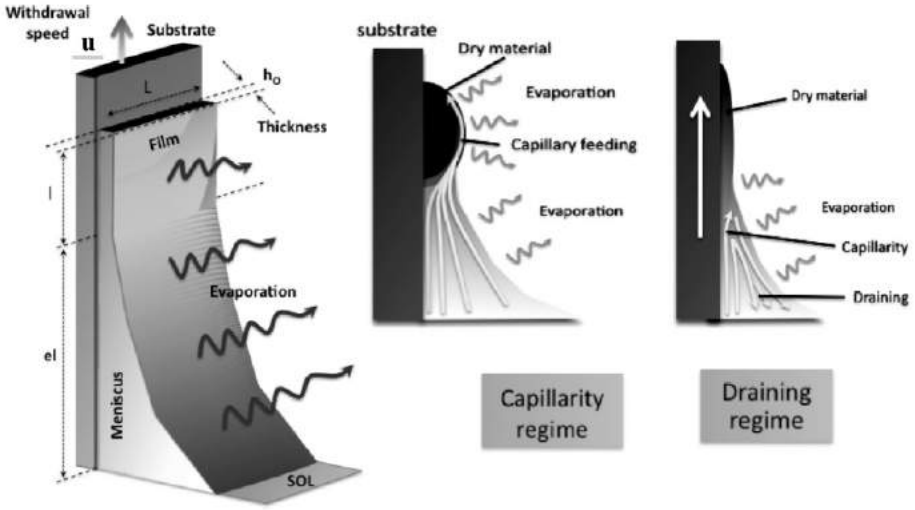

圖 2-1 浸塗法的作用機制示意圖[25]

(1) 毛細現象機制

在低基材浸沒與抽出速度時，毛細現象為影響成膜的主要機制（同時作用於浸沒與抽出階段），其原因為當基材由大氣緩慢浸入塗佈液內，經靜置與緩慢的拉伸（一般指速度< 0.1 mm/s 時）[24, 25] 過程中，基材對於溶液的毛細現象和因大氣溫度使得塗佈液產生的蒸發行為，兩者相互密切影響，進而影響成膜行為。因此在低基材浸沒與抽出速度時，毛細管現象與塗佈液蒸發行為皆為重要影響因素；故於此作用機制下，主要影響成膜因子包括：基材浸沒與抽出速度、黏性阻力（受毛細管現象和塗佈液體蒸發行為改變）、大氣溫度。

(2) 黏性阻力機制

在高基材抽出速度時（僅作用於抽出階段），黏性阻力及重力作用力為影響成膜的主要機制，其原因為當基材由塗佈液內快速的拉伸（一般指速度> 1 mm/s 時）[24, 25]，可忽略受時間影響的

毛細管現象與液體蒸發行為[24, 25]，此時成膜機制只與基材抽出速度和液體黏滯度產生的作用力與重力間的合力有密切關係。

此外，在操作時尚有數個重要參數：（1）塗佈液的混合程度[26]、（2）塗佈液的黏滯度[24-26]、（3）基材在塗佈液的停留時間[26]、（4）基材的浸漬速度[24-27]、（5）基材的抽出速度[24-27]、（6）環境溫度[24,25]等。

因此，對於浸塗法，學者普遍認為：（1）高表面張力的液體難以均勻塗佈在基材上、（2）極低濃度或極高黏稠溶液，膜厚難以控制、（3）沉積在多孔材料時，會滲入並修飾材料特性、（4）膜厚並非隨著基材的抽出速度增加而總是增加、（5）適當的製成條件，任何塗佈液皆可形成薄膜[24]。

2.2 基材結構的影響

除了製備方法外，另一項影響支撐型薄膜結構的關鍵為基材性質，基材表面的粗糙度會影響薄膜層的分子鏈排列情形[28,29]，孔洞大小也會使得塗佈時塗佈液的滲入程度不同[30]。好的支撐材需具備表面無缺陷、低的粗糙度、高孔隙率和小孔徑、好的機械強度、氣體擴散特性、熱穩定性，而屬於多孔陶瓷的氧化鋁因出色的穩定性和市場需求被廣為使用做為薄膜的支撐材[31]。

因此，本研究利用真空輔助系統來調整塗佈液與基材間的滲入情形，進一步修飾基材表面粗糙度以及提升薄膜層與層間的穩定性。

近年來，為了優化薄膜氣體分選上之效能，各方研究學者無不盡力研發各種薄膜的改質技術來達到此目的。在薄膜之改質技術方面，主要可分為對稱型薄膜其針對薄膜本身之分離選擇層進行奈米無機材的添加[32,33]，以及非對稱型薄膜針對薄膜之支撐層基材性質作為改質重點加文獻。其中在基材的改質方面主要著重於內部孔徑與表面粗糙度，過去文獻曾提及基材之表面粗糙度會影響薄膜分選層分子之排列，同時孔洞的大小亦會影響製程中鑄膜液的滲入情形[34-36]，對薄膜之後續氣體分選能力造成很大的影響，因此基材的性質對於薄膜之製備亦是成敗關鍵。

Tseng 等學者[37]提出以 sol–gel 法進行二氧化鈦(TiO_2)中間層改質平板型氧化鋁基材，最終以 400 ℃燒結溫度進行鍛燒；透過中間層修飾基材藉此降低原始基材之表面粗糙度與提升機械強度，製備出 TiO_2/Al_2O_3 複合基材；並於改質基材上塗覆高分子材料，經高溫碳化後得到 $Carbon/TiO_2/Al_2O_3$ 碳分子篩選薄膜，其研究結果顯示在於氣體分離效率方面，基材的改質會改變高分子與基材間之機械互鎖與化學鍵結情形，進而影響碳膜之氣體滲透選擇率。Qi 等學者[38]則提到將 TiO_2 粉末摻雜於 Al_2O_3 粉末製備出巨孔之 Al_2O_3/TiO_2 混合基材，透過不同配置比體之混合以及燒結溫度，探討這些參數對於基材之影響；該混合材料在燒結過程中主要受緻密化反應與固化反應等作用力所影響，結果顯示當燒結溫度提高至超過 1300 ℃以上時，Al 轉移至 TiO_2 與其發生反映生成 Al_2TiO_5 之鈦酸鋁，此 Al_2TiO_5 結晶可提高基材之機械強度與耐腐蝕性，且其在基材中生成之數量將會左右基材整體之開放孔隙率。

2.3 影響水氣轉移反應活性之主要因素

以觸媒進行水氣轉移反應之活性試驗，除了觸媒本身之特性會影響反應之外，整體試驗之操作因子亦會使反應之轉化率、氫氣產量等結果產生不同表現。在觸媒之催化反應下，反應整體之轉化主要受制於動力學，根據阿瑞尼士定律（Arrhenius law）溫度對反應速率的影響，以下針對個操作參數進行說明：

1. 反應溫度

在一定的溫度範圍內，操作溫度越高，反應速率越高；主要原因為當溫度升高時反應物分子內之動能隨之增加，高過反應所需低限能之反應物分子亦隨之增加[39]，見圖 2-2；由阿瑞尼士

方程式可得知反應速率與活化能之關係，反應速率經常隨著溫度升高而成指數函數增長[40]。

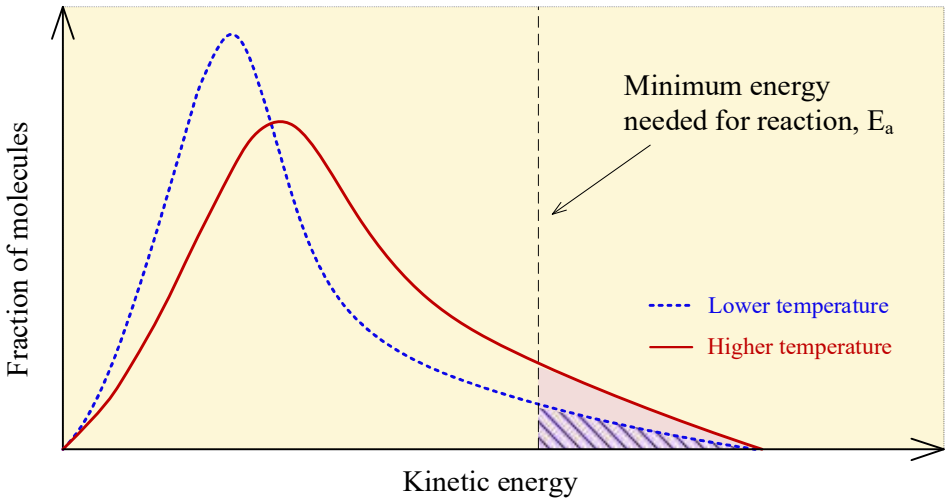

圖 2-2 反應物分子對溫度之動能分布曲線[39]

一般工程應用觸媒催化水氣轉移反應之操作溫度範圍約落於 150–500 ℃之間，視不同種類之觸媒而有其適合之反應溫度，當反應溫度超過其適合之範圍時，便可能使觸媒出現燒結或是揮發等現象，導致其失活而造成反應轉化率下降[41]。

2. 空間速度

空間速度係指在單位時間內，反應物分子通過觸媒床體積之體積流量，其關係式如下列所示：

$$\text{空間速度}(hr^{-1}) = \frac{\text{通過觸媒床之氣體流量}(Nm^3/hr)}{\text{觸媒床體積}(m^3)} \quad (4)$$

空間速度愈大代表合成氣於觸床之停留時間愈短，反應物分子與觸媒因接觸時間短，致使催化反應發生之機率降低，故其轉化率較低；反之，空間速度愈小，反應物分子與觸媒因接觸時間延長，反應的轉化率因而提升。一般而言，以觸媒催化水氣轉移反應，通常控制在較低之空間速度（約 $< 20000\ h^{-1}$）之下有較佳的轉化率[42]；然而為了有效提升 CO 轉化率，往往會將空間速度降至 400–2500 h^{-1} 之範圍[43,44]。此外，根據不同觸媒種類、反應器形式以及合成氣特性，亦需針對其適當之空間速度進行調整。

3. 水蒸汽添加量

水蒸汽作為反應物，其含量的多寡自然會影響反應之進行；在進行水氣轉移反應過程中，經常會加入超過化學反應平衡劑量（Steam/ CO ratio，S/C > 1）之水蒸汽，用以提升 CO 之轉化率[45]。根據碰撞學說解釋反應物濃度效應：當提高反應物之濃度時，整體反應物分子與觸媒顆粒表面之間的碰撞頻率亦隨之增加，進而提高反應之轉化率。Mendes 等人[46]針對多篇文獻進行整理，得出當 S/C 自 1/1 提高至 5/1 時，CO 之轉化率從原先 65% 增加至 98% [47-56]。Galuszka 等人[45]以催化型薄膜反應器進行水氣轉移反應，結果顯示提高 S/C 不僅能夠提升膜反應器整體 CO 之轉化率，同時提升反應的平衡轉化率，至使轉化率提高至 98%。

2.4 基材與選擇層的界面接合效應

碳分子篩選薄膜一般是以非對稱型態製備而成，因此，當高分子鑄膜液塗覆於多孔無機基材表面時常會面臨兩界面間因受到不同熱膨脹係數而導致兩者間產生接合之相容性問題。

Tseng 等人[57]曾提及欲製備出一具有良好分選能力之次微孔碳分子篩選薄膜，其選擇層的選用是相當重要的，其中考慮條件包含基材之表面粗糙度、孔隙率及孔洞分布情形等。當基材表面粗糙度過大，兩相之間容易有界面間隙產生，且由於兩材料性質之差異，經高溫熱裂解過程，兩相之熱膨脹係數不同會有應力集中之現象，當應力分佈不均則可能產生相分離使結構崩解而導致薄膜結構產生缺陷；此外，當塗覆其上之高分子鏈因摺疊而呈現不規則排列，分子鏈經過碳化後的層間距會拉大，進而導致薄膜孔隙增大而不利於氣體選擇。

因此，為了改善碳分子篩選薄膜面臨上述情況，Okubo 等人[58]利用 sol-gel 法製備單水鋁石(boehmite)溶膠凝膠溶液於中空的管柱式基材內層鍍一層 γ-Al_2O_3 薄膜作修飾；而 Smid 等人[59]則是直接以浸塗法在管柱式基材的外層塗布一層 γ-Al_2O_3 薄膜，但是內文中沒有提供太多細節。另有學者 Oyama [60]等人認為將大顆粒氧化鋁沉積於多孔基材可填補較大的孔洞，然而也由於顆粒較大，顆粒與顆粒間亦會產生間隙，故導致有些表面的孔洞不易填補；至於若直接以小顆粒氧化鋁沉積於基材上，雖可以填補所有孔洞，然而，則容易產生破裂情形，詳見圖 2-3。因此，欲得到較平整的表面，可先將大粒徑之氧化鋁顆粒沉積於基材；再以小粒徑之氧化鋁顆粒沉積於其上，預期可得到較平整的表面形貌，如圖 2-3(c)所示，並藉由調整水解時間與加入酸之強度，製備出不同顆粒大小的 boehmite sol，再藉由浸塗方式將溶膠凝膠溶液塗佈於管柱式基材上。

Tseng 等人[57]則曾提出利用 sol-gel 法製備 TiO_2 溶液並塗佈於平板式基材表面，藉此作為有機與無機相間的中間層，以增加兩相間的黏附情形，並於 400°C 下進行燒結。探討兩相間的黏附機制包含機械互鎖、化學鍵結及吸附作用的情形及利用中間層修飾基材表面粗糙度對於後續碳膜製備之影響。研究結果顯示，TiO_2 中間層可有效填補氧化鋁基材之巨孔洞，並修飾基材表面粗糙度以避免高分子溶液直接滲入基材內部；另外，藉由 TiO_2 的塗覆可增加基材與高分子鍵之間形成氫鍵鍵結，進而改變兩相之間的黏附情形。

既然 TiO_2 中間層之表面粗糙度與孔洞內部修飾效果顯著，進一步探討水解縮合製程條件是必要的。水解縮合過程之製備參數對於所合成之 TiO_2 顆粒尺寸的影響之大。據過去的研究[61]得知在酸性環境下(<pH=2)時，隨著 H^+濃度增加水解之速度；反之，在 pH 值>pH 2 時，隨著 OH^-濃度增加，聚合速度越快，而 pH=2 左右是等電點(isoelectric point)，屬於穩定區域，此時凝膠時間變長。當水解反應速率比縮合反應速率快，生成之顆粒偏小且為線性網狀結構；反之，當縮合反應速率比水解反應快，容易生成粒徑大之顆粒；此外，隨著 sol-gel 溫度越高，合成之顆粒越大；反之則越小[62]。

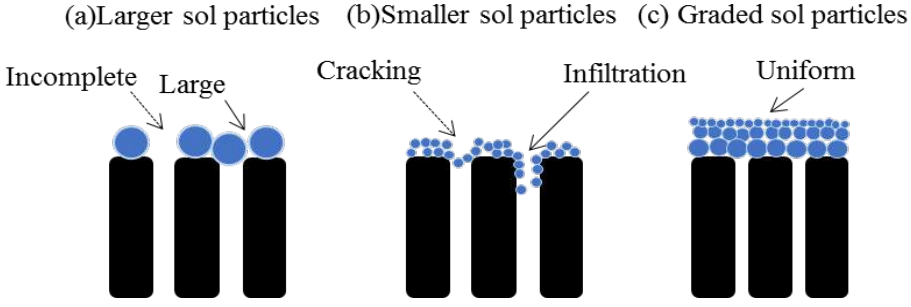

圖 2-3 不同尺寸之顆粒沉積於薄膜孔洞之情形(a)在孔洞上沈積大顆粒，(b)在孔洞上沉積小顆粒、(c)在孔洞上先沉積大顆粒再沉積小顆粒

2.5 碳膜反應器的老化現象

雖然碳分子篩薄膜在氣體分離表現上具有高滲透及高選擇率，但在實際使用時仍存在一些缺陷。碳膜之碳結構上的奈米微晶表面是由石墨烯層所構成，其中部份奈米微晶的邊界會形成 C-H 鍵或 C-O 含氧官能基。雖然碳材屬於疏水的性質，但這些含氧表面官能基會對極性水分子有較高的親和力，導致容易吸附水分子，並以氫鍵結合於碳材表面，水分子吸附於含氧官能基後通常作為會取代吸附的位置並作為起始位置，開始與其他水分子以氫鍵方式鍵結而形成水團簇，進而阻塞碳膜的微孔洞，致使氣體滲透率下降，導致薄膜喪失分離效能，造成碳膜的老化現象[63,64]。

為了改善碳膜上述使用上之瓶頸，因此近年來有許多學者相繼研究如何延緩碳膜老化的速度或經由再生方式，將碳膜重複使用。對於碳膜的老化現象，目前已開發幾種改質方法－第一種方式是在碳膜表面改質，如塗佈高疏水性的材料來作為碳膜保護層，避免薄膜表面與水氣發生吸附作用；第二種則是添加疏水性的材料，以減少多孔結構中對水吸附的親和性，延緩薄膜老化速率；亦或是透過再生如熱再生或化學再生等方式使碳膜可以再重複使用。

Arkles 學者[69]曾提及藉由在一界面層之表面鍵結終端官能基可有效促使此表面成為親水或疏水的表面。常見於改質界面使其轉變為低表面能之疏水薄層之官能基如單一烷基鏈、非極性之甲基團(CH_3)及三氟甲基(CF_3)等。此外，對於提高表面活性之官能基包含常見的硫醇基(SH)、矽烷基(trichlorosilane 或 $SiCl_3$)及羧基團；其中，矽烷基物質又因嫁接不同官能基而有疏水與親水性之區分，疏水性矽烷物質帶有之官能基如甲基、具有單鏈或支鏈之烷基、氟化烷基、芳基(Arly)或雙達(Dipodal)等。

此外，為了使膜面達到疏水效果，許多學者紛紛提出疏水性材料之塗覆，例如，Lee 等人[65]以氟系矽氧烷基材料(FAS)作為多孔氧化鋁中空纖維膜接觸器之表面疏水性改質，並將薄膜暴露至 CO2/N2 混合 20 wt.%之 MEA 溶液中，藉此分析其對於 CO_2 之吸附通量；含氟官能基之所以可以成為超疏水材料是由於氟原子之電負度大，因此當氟原子與物質接觸時彼此之間容易產生較強的排斥力，因此分子間作用力弱，導致此表面呈現疏水性[70]；而矽氧烷(silane)系列則是因為主鏈具柔軟而有彈性，使分子間之作用力比主鏈為碳之化合物弱，因此可使得表面呈現疏水性。Selivanova 等人[68]則是利用 Trichlorododecylsilane 及 3-mercaptopropyl)-trimethoxysilane 材料進行兩界面之疏水改質，並以 AFM 進行表面能之分析。亦有學者利用 TFPTES 進行薄膜表面改質之研究。為防止疏水材料在操作至較高溫反應下即揮發，選擇沸點較高之材料亦是必要之考量。在眾多疏水材料中，由於十二烷基三氟矽烷(Trichlorododecylsilane)之沸點高達 297 ºC，因此較適用於本研究所使用。Kansara 等人[71]提出使用簡單的一步合成方式即可進行超疏水材料之回收。研究中使用 PP 織物作為膜材料，並透過混合二氧化矽粉末及十二烷基三氯矽烷(比例為 1:1)將超疏水材料利用簡單的浸塗法塗覆於膜表面 10 分鐘，遂將 PP 取出並放置 60 ºC 烘箱中乾燥 30 分鐘。

表 2-1 常見之疏水材料相關應用

Application	Hydrophobic material	Hydrophobic functional group	Ref.
alumina(Al_2O_3) hollow fiber membrane contactor	Fluoroalkylsilane(FAS)	-	[65]
Carbon composite membrane (hollow fiber)	Fluoropolymer (a) perfluoro-2,2-dimethyl-1,3-dioxole (b) tetrafluoroethylene	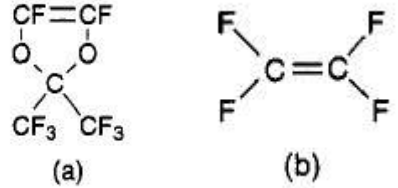	[66]
CMSM	Methyl-modified－PPO	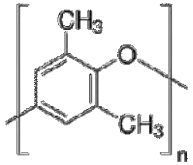	[67]
two different types interface- liquid crystal films and silane monolayers	(a)Trichlorododecylsilane (b)Mercaptopropyltrimethoxysilane	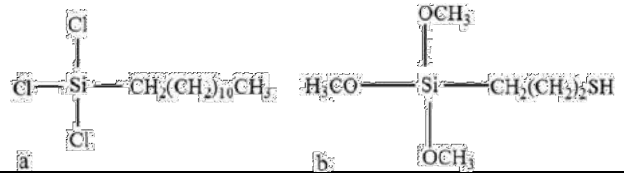	[68]

第三章 計畫第一年執行方法與成果

3.1. 執行方法

3.1.1. 材料

本研究所使用之 α-氧化鋁管係由永晉電陶瓷股份有限公司所提供（O.D. 1.2 cm, I.D. 0.8 cm, L 5 cm），依純度及鍛燒溫度不同，共有四種不同結構。分別以 SX-Y 表示，其中 X 代表氧化鋁純度，Y 代表燒結溫度。高分子前趨物為聚醚醯亞胺（Polyethylenimine, PEI）（Sigma-Aldrich Chemical Co. USA）。溶劑為 N-甲基吡咯酮（N-methyl-2-pyrrolidone, NMP）（Mallinckrodt Chemical Co.USA）、三氯甲烷（Trichloromethane, TMP）（純度>50 %，Mallinckrodt Chemical Co. USA）。

3.1.2. 管柱式碳分子篩選薄膜的製備

取適量高分子前驅物 PEI 分別溶解於 NMP 和 TMP，並於 80 °C（NMP 為溶劑）和 50 °C（TMP 為溶劑）環境下以 60 rpm 攪拌 24 小時，以製備 8、10、12 wt.%的高分子塗佈液。待完全溶解後靜置 24 小時去除氣泡。塗佈液則以塗佈機（ DX-5 型，智果整合有限公司）將管柱式氧化鋁基材依設定條件進行塗佈，其程序依序為浸沒、停滯、抽出等三個步驟。當基材完全浸沒於塗佈液後，於停滯時期（10 秒鐘）輔以真空減壓系統使塗佈液滲入基材孔隙內，接著抽出即完成一次塗佈。完成後放置室溫乾燥 24 小時，接著置於真空管狀爐中以 5 °C/min 加熱至 240 °C 持溫 6 小時進行薄膜預處理，之後便升溫至升溫至 600 °C 持溫 2 小時進行碳化程序，即可製備出管柱式碳分子篩選薄膜。浸塗法操作條件：基材之浸漬速度與抽出速度 1、6 mm/s、塗佈次數 5、6、7 次。薄膜樣品命名為 MW-X-Y(Z)，其中 W 代表高分子溶液濃度、X 代表基材之浸漬與抽出速度、Y 代表塗佈次數、Z 代表使用溶劑（N 代表 NMP、T 代表三氯甲烷）。

3.1.3. 氣體滲透實驗

本研究藉由氣體滲透測試做為薄膜分離效能之依據，主要依單一氣體進行滲透實驗，給予一進氣壓由薄膜上游端通入 2 kg/cm^2 氣壓，藉由氣體通過薄膜進行滲透過程中之壓力變化經公式計算數氣體滲透率，而兩氣體滲透率之比值即為薄膜對此兩種氣體之選擇率。氣體滲透自組裝置如圖 3-1 所示。

$$P_g = \left[\frac{dp}{dt}\right]\frac{\ell \cdot T_0 \cdot V}{A \cdot \Delta p \cdot T \cdot p_0}$$

其中：dp/dt 為達穩定狀態時，壓力隨時間變化曲線之斜率（cmHg/sec），V 為薄膜下游之體積（cm3），ΔP 為薄膜上、下游端起始之壓力差（cmHg）、A 為薄膜有效面積（cm^2）、L 為薄膜厚度（cm）、P_0 與 T_0 分別為標狀態下之壓力及溫度（76 cmHg、273 K）、T 為量測時之溫度（K）。

理想氣體氣體分離系數 $\alpha = {}^{P_A}/_{P_B}$。

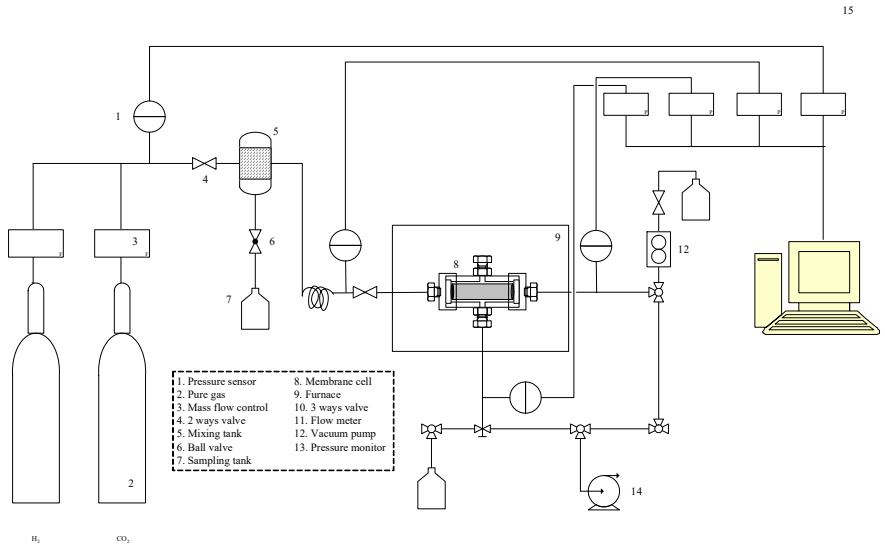

圖 3-1 氣體滲透設備圖(自組設備)

3.1.4. 特性分析

本研究將以原子力顯微鏡（Atomic Force Microscope, AFM，Veeco DI-3100，中興大學貴重儀器中心）分析氧化鋁基材表面粗糙度；比表面積分析儀（Brunauer-Emmett-Teller, BET，Model ASAP2010，Microorifice 公司）量測表面積大小、孔徑分佈情形；場發射掃描式電子顯微鏡（Field-Emission Scanning Electron Microscope, FE-SEM，JEOL JSM-6700F，OXFORD INCA ENERGY 400，中興大學貴重儀器中心）觀察基材表面特徵與量測薄膜厚度。樣品進行分析前接進行 100 ℃乾燥 24 小時。

3.2. 計畫執行成果

3.2.1. 管柱式氧化鋁基材之選擇

本研究所使用的管柱式氧化鋁基材，係以氧化鋁粉為原料、氧化鋅為助熔劑，經改變兩者間的比例、添加適量添加劑後、擠出成型，再經改變燒結溫度來控制成品之孔洞大小及孔隙度。表 3-1 所示，為氧化鋁管基材的孔洞結構及表面粗糙度。

表 3-1 氧化鋁基材之比表面積、平均孔徑、孔洞體積及表面粗糙度

Sample code	S_{BET} (m^2/g)	D_{proe} (Å)	V_{total} (cm^3/g)	(cm^3/g)			Ra (nm)
				V_{micro}	V_{meso}	V_{maro}	
S50-1330	22.80	16.91	0.0096	0.0026	0.0065	0.0005	436±37
S70-1400	11.78	49.78	0.0146	0.0025	0.0112	0.0010	431±32
S82-1200	12.34	70.30	0.0217	0.0038	0.0162	0.0016	427±90
S98-1400	4.72	76.29	0.0089	0.0023	0.0007	0.0058	299±85
Disk substrate[14]	4.3	74.10	0.0080	0.0011	0.0062	0.0005	42.8

根據本研究室過去之研究經驗指出[14, 15]，當氧化鋁基材具有低比表面積（4.3 m^2/g）孔隙率（0.008 cm3/g）、小的平均孔徑（74.10 Å）及低粗糙度（42.8 nm）時，可使碳膜層完整披覆於基材表面，並獲致較佳的孔洞結構及分選效率。因此，本研究首先探討管柱式氧化鋁基材的孔洞結構、表面粗糙度與碳膜結構及氣體分選效率三者間的關係。

依據泥漿流變行為之研究指出，當氧化鋁對助熔劑的體積比增加（即純度增加）時，成品的孔隙度及平均孔徑均會增加；若是燒結溫度增加，亦或是燒結時間增加，則平均孔徑會增加，但此時

孔隙度會變小。這是因為當燒結溫度提高時，氧化鋁粉形態會開始由顆粒轉換成十四面體，使得顆粒粗化及重新堆疊，顆粒與顆粒間因重新排列而相互擠壓，顆粒接合界面面積增加而壓縮孔洞，使得孔隙度、孔徑和孔體積因而下降[72]；然而，若氧化鋁基材達緻密化時則會對氣體傳輸產生阻力，進而減少氣體的滲透通量，便不適合做為薄膜基材。

因此，為使基材孔洞結構均勻，且具有低孔隙率及小孔徑，但又不能達緻密化，本研究初步選擇四種支撐材進行評估。表 3-1 所示為該四種基材之孔洞結構分析，結果指出，經改變氧化鋁含量及燒結溫度後（SX-Y，其中 X 為氧化鋁純度 Y 為燒結溫度），隨著氧化鋁純度提升至 98 wt.%、燒結溫度提升至 1400 ℃，基材結構略呈現孔徑隨之增加、孔體積隨之減少的趨勢；另以 AFM 觀察表面粗糙度發現，在相同鍛燒溫度 1400 ℃下，高助熔劑含量具高的氧化鋁基材粗糙度 S70-1400 與 S90-1400 其 Ra 值分別為 431、299 nm，而在相近的溫度下，也呈現出相同趨勢(S50-1330、S70-1400 及 S98-1400)，Ra 值隨著助熔劑的量增加而由 299 nm 依序增加至 431、436 nm，整體而言氧化鋁粗糙度 Ra 值隨著助熔劑添加量的增加而增加。此結果與 FESEM 顯微圖相當吻合，當助熔劑含量高且燒結溫度高時（S50-1330 及 S70-1400），將會增加液相、擴大燒成範圍，故如圖 3-2(a)及 3-2(b)所示，基材微結構呈現塊狀，孔徑及孔隙率低，但粗糙度高；相反地，當助熔劑含量低且燒結溫度低時（S82-1200），則因液相相對減少，減少燒成範圍，基材微結構呈現顆粒狀，故孔徑、孔體積較大，尤其是巨孔及中孔體積；進一步地於助熔劑含量低時（S98-1400），提高燒結溫度可觀察到基材型能仍維持顆粒狀，但孔隙體積因高溫燒結而減少，尤其是中孔體積。

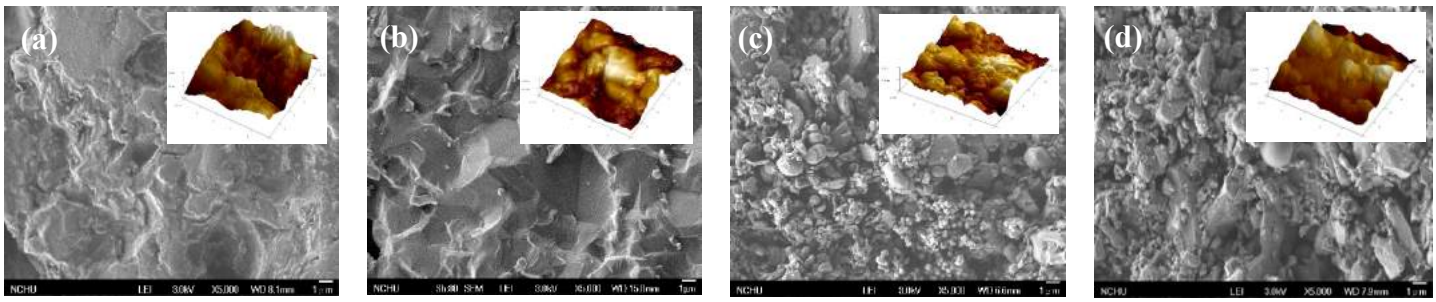

圖 3-2 氧化鋁陶瓷基材的表面 FE-SEM 顯微圖及粗糙度分析：(a) S50-T1300、(b) S70-T1400、(c) S82-T1200、(d) S98-T1400。

將上述四種基材以相同條件製備：溶劑與濃度 10 wt.% NMP、浸漬速度 1 mm/s、抽出速度 1 mm/s、塗佈 5 次、600 ℃持溫 2 小時，所獲得之管柱式碳分子篩選薄膜的氣體滲透率及選擇率如圖 3-3 所示。由圖 3-3(a)可知，在相同製備條件下，以 S50-1330 及 S70-1400 為基材之碳膜，其氣體滲透率與選擇率皆低，此可能因這二種基材微觀結構呈塊狀，平均孔徑較小，而使其所披覆之碳膜幾乎呈緻密結構；以 S82-1200 及 S98-1400 為基材時，通量明顯增加，PH_2 通量可達 498.9 GPU，但 H_2、CO_2、O_2、N_2 及 CH_4 等氣體滲透通量大小並不隨氣體動力直徑增加而減少，反倒與氣體分子量之均方根倒數呈正相關；此結果顯示，當以 S98-1400 為碳膜基材時，可獲得較為理想的通量，然氣體擴散機制因孔徑較大，故仍遵循 Kundsen 擴散機制，故本研究初步選擇以 S98-1400 陶瓷為碳膜基材，進行後續研究。

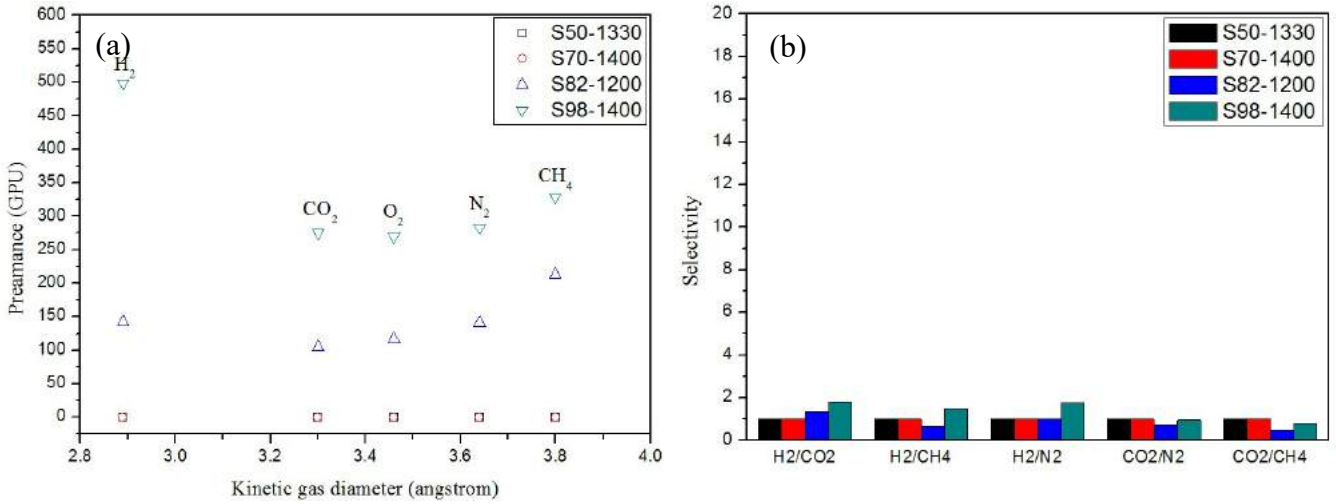

圖 3-3 基材前處理條件對管柱式碳分子篩選薄膜氣體分離表現之影響：(a)氣體滲透率、(b)氣體選擇率

3.2.2. 浸沒與抽出速度之影響

浸塗法的製備程序係將基材浸入塗佈液後再予以拉出。於浸沒入塗佈液階段，基材與塗佈液接觸面會發生毛細現象而產生作用力，使塗佈液滲入基材。於拉出階段，塗佈液的黏滯力會受到重力的影響，抽出速度越高代表能縮短將附著於基材上的塗佈液受重力的影響時間，故膜厚較厚。離開液體後為乾燥階段，此時塗佈液的揮發速度為影響膜結構關鍵，通常薄膜底端因重力影響，導致塗層較厚、結構亦較為緻密[26]，且薄膜表面會因溶劑流動而較不平整。有鑑於此，本研究初步先討論浸沒與抽出速度對碳膜膜厚的影響，如圖 3-4 所示，相同的浸沒與抽出速度為：0.1、1、6 mm/s，層數為 5、6 層。

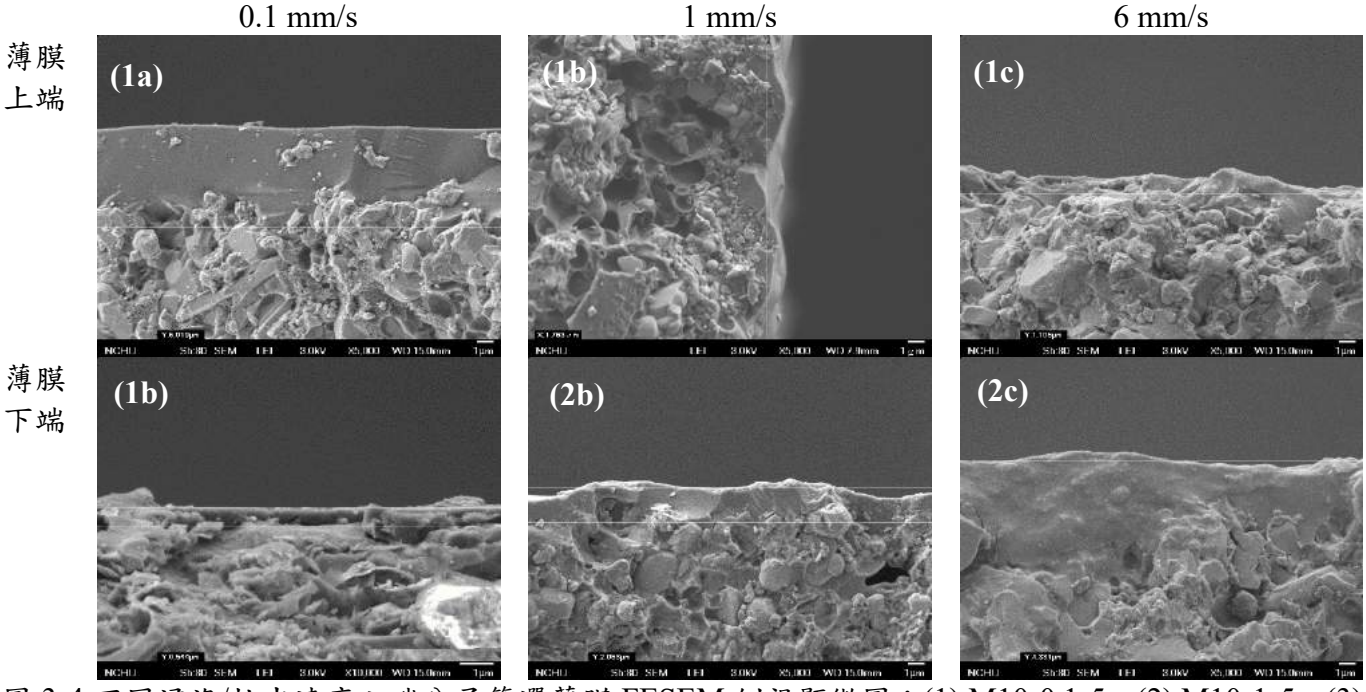

圖 3-4 不同浸沒/抽出速度之碳分子篩選薄膜 FESEM 側視顯微圖：(1) M10-0.1-5、(2) M10-1-5、(3) M10-6-5 及(a)薄膜上端與(b) 薄膜下端

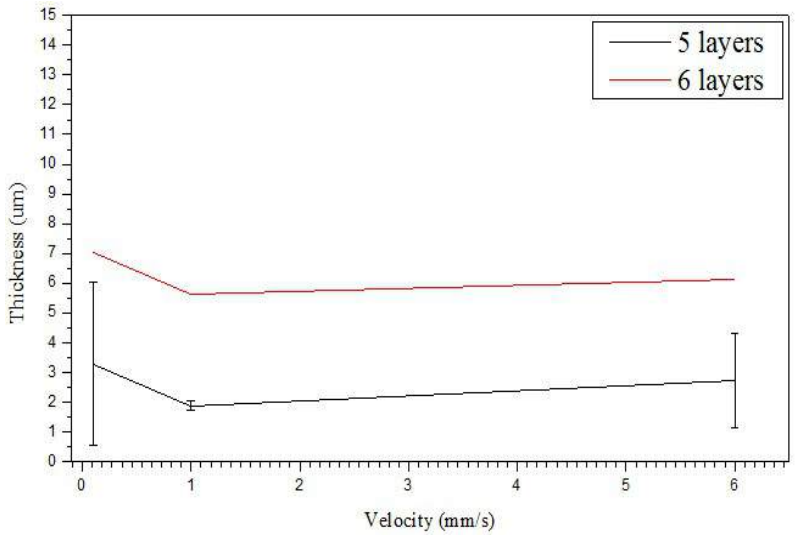

圖 3-5 相同浸沒與抽出速度與層數對碳膜膜厚的影響

首先，從圖 3-4 為在塗佈 5 次搭配不同浸沒與抽出速度之碳膜膜厚顯微圖，可以發現在低浸沒與抽出速度（0.1 mm/s），薄膜厚度呈現上厚下薄之趨勢，這是因為在低的速度下，成膜機制受到毛細作用力所支配，越低的速度則基材與塗佈液間接觸的時間越長，造成基材下端因毛細作用力使得孔洞被塗佈液充滿的程度大於基材上端，另一方面，基材下端因重力影響使得厚度較厚，整體膜厚介於 0.544～6.019 μm；而在高的速度下，成膜機制受到黏性阻力和重力的影響，而基材抽出速度與黏性阻力成反比，因此當速度越高時，重力與黏性阻力的合力較小，使得膜厚隨著速度越快而增加，此時影響薄膜厚度均一性的因素為重力，薄膜下端膜厚 4.331 μm 高於薄膜上端 1.106 μm。可以觀察到當速度介於中間過渡區時（即 1 mm/s），薄膜上端與下端厚度較為平均分別為 1.763 μm 與 2.063 μm，因過渡區域能使得毛細作用機制與黏性阻力機制兩者成膜機制相互抗衡，毛細作用力、黏滯度作用力與重力相互牽制，出現最低膜厚值且薄膜上端與下端厚度差異不大。將其膜厚值繪製於圖 3-5，可以發現，當塗佈層數由 5 增加至 6 時，三種速度所生成的膜厚都有增加之趨勢，且最低膜厚值與標準偏差值最小皆出現在速度為 1 mm/s；觀察在速度為 0.1 mm/s 所生成的薄膜厚度受毛細作用力影響，速度越慢影響程度更加明顯，膜厚標準偏差值變動幅度最大；在速度為 6 mm/s 所生成的薄膜厚度受到塗佈液本身黏滯度產生的黏性阻力影響，速度越高越可忽略黏滯阻力與毛細作用力影響程度，可以發現膜厚標準偏差值變化量較低。這意味著速度為 1 mm/s 下所製備出的薄膜其膜厚均質性較高，而毛細作用力影響薄膜厚度程度較重力來得顯著，為減緩毛細作用力的影響，故輔以真空系統，於浸滯階段將孔隙填滿使膜厚均勻，欲達到更平整的薄膜結構。

3.2.3. 溶劑組成與真空輔助系統之影響

如前所述，為減緩毛細作用力所造成的膜厚不均，本研究分別選用了 NMP（b.p. 202°C）及 TMP（b.p. 61.2 °C）等兩種溶劑來配製 PEI 鑄膜液，探討（1）溶劑沸點高低對於溶劑揮發度，及（2）高分子與溶劑間的交互作用對毛細作用力的影響。

圖 3-6(a)與(b)分別基材經使用 NMP 與 TMP 做為溶劑配成的 10 wt.% PEI 塗佈液，在浸漬速度與抽出速度皆為 1 mm/s，塗佈 5 次製備而成的管柱式高分子薄膜之外觀圖。由圖 3-6(a)與(b)可明顯發現，使用 NMP 做為溶劑所製成的薄膜表面較不平整，且在底端的部分因溶劑沸點較高使得揮發速率較慢，導致底端薄膜厚度較厚；相較之下，以 TMP 做為溶劑所製成的薄膜表面較為平整且具有光澤感，底端厚度也沒有增加太多，此可能因溶劑低沸點特性，使得溶劑快速揮發並完成相轉換，減緩了溶液的流動性。而使用真空輔助系統後，如圖 3-6(c)與(d)，可以發現到 NMP 做為溶劑所製程的薄膜表面較無因溶液流動性所造成的不平整，且底部膜厚較未使用真空輔助系統前來得薄，此可能是因為在基材浸泡過程中使用真空輔助系統，使得基材孔隙備足夠充滿塗佈液體，使得基材在抽出過程中減緩了毛細作用力所造成的塗部液滲入程度；而 TMP 做為溶劑所製成的薄膜，

使用真空系統後薄膜表面無明顯差異。

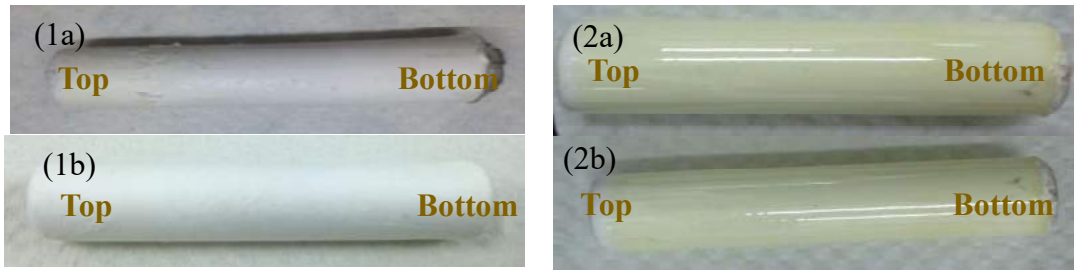

圖 3-6 使用不同溶劑之管柱式高分子薄膜外觀圖：(1) M10-1-5(N)、(2) M10-1-5-(T)、(a)未使用真空輔助系統與(b)使用真空輔助系統

碳分子篩選薄膜是由高溫裂解高分子薄膜而得，高分子鏈與其支鏈物質會受到破壞，只剩下碳鏈，因此碳膜厚度皆會低於原高分子膜。然而，氣體的滲透分選能力與膜厚間又有顯著關係。

圖 3-7(1a)、(2a)分別為以 NMP、TMP 做為溶劑的碳膜膜厚，皆為未使用真空輔助系統的碳膜，膜厚值約為 2 μm；圖 3-7(1b)、(2b)分別為以 NMP、TMP 做為溶劑的碳膜膜厚，為使用真空輔助系統的碳膜，選擇層較為平整，厚度較厚約分別為 2、4μm。在真空輔助系統的協助下，利用抽真空所產生的作用力加強塗佈液滲入基材的行為，欲使讓足夠的滲入量來修飾基材表面粗糙度，藉此提升選擇層的平整度，能避免塗佈於基材上的塗佈液在成膜過程中，因毛細作用力持續產生的滲入行為，使選擇層不均且厚度減少；另一方面，由圖 3-7 可了解到毛細作用力影響薄膜膜厚來得顯著，真空產生的作用力減緩了毛細作用力，因此在基材浸沒與抽出速度為 1 mm/s 時屬於中間過度區，更能使得毛細作用力與重力相互抵消，形成最薄且膜厚均一度高的薄膜。

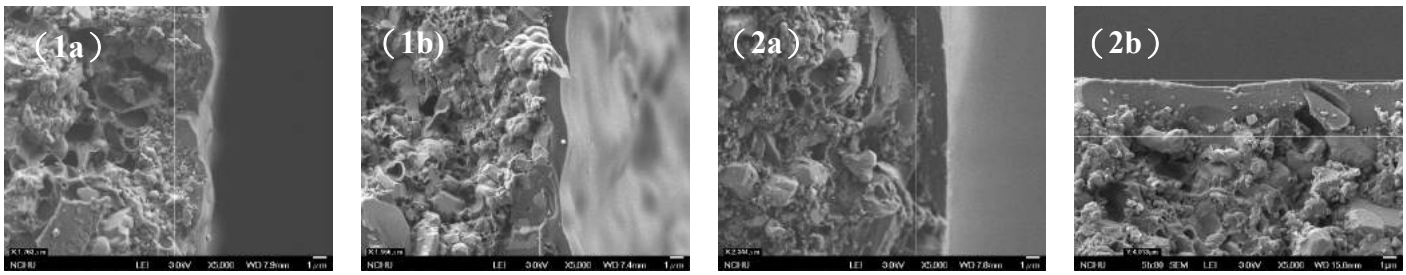

圖 3-7 不同溶劑組成之碳分子篩選薄膜的 FESEM 側視顯微圖：(1) M10-1-5(N)、(2) M10-1-5(T)、(a)未使用真空輔助系統、(b)使用真空輔助系統。

此節討論溶劑組成與有無真空輔助系統所製成的薄膜結構與氣體滲透分選能力的影響，從圖 3-6 可以看出 NMP 做為溶劑所製成的高分子薄膜表面不平整，這導致在碳化過程薄膜易產生缺陷；而以 TMP 做為溶劑所製成的高分子薄膜表面較為平整；而從圖 3-6 可以明顯發現，真空輔助系統可以提升選擇層的平整度。圖 3-8 為有無真空輔助下之 M10-1-5(N)、M10-1-5(T) 碳膜氣體滲透率與選擇率，比較無使用真空輔助系統的 M10-1-5(N)與 M10-1-5(T)，可以發現前者具有高滲透低選擇特性，這可能為碳膜表面產生缺陷所導致，後者具有低滲透高選擇特性，因為使用 TMP 做出的碳膜表面，因溶液本身高揮發特性，減少了液體流動所造成表面缺陷。而搭配真空輔助系統，M10-1-5(N)氣體滲透量明顯減少，PH_2 由 879.6 降低至 149.8 Barrer，雖已從 Kundsen 擴散機制逐漸變成隨著氣動直徑越大氣體滲透量越小之分子篩選機制，但屬於氣動直徑最大的 CH_4 仍無法降低滲透量而導致氣體選擇率無法提升；相較之下，M10-1-5(T)表現出高的氣體滲透率與高選擇率，PH_2 519 Barrer、H_2/N_2 9.25，但 PCH_4 仍略高於 PN_2。

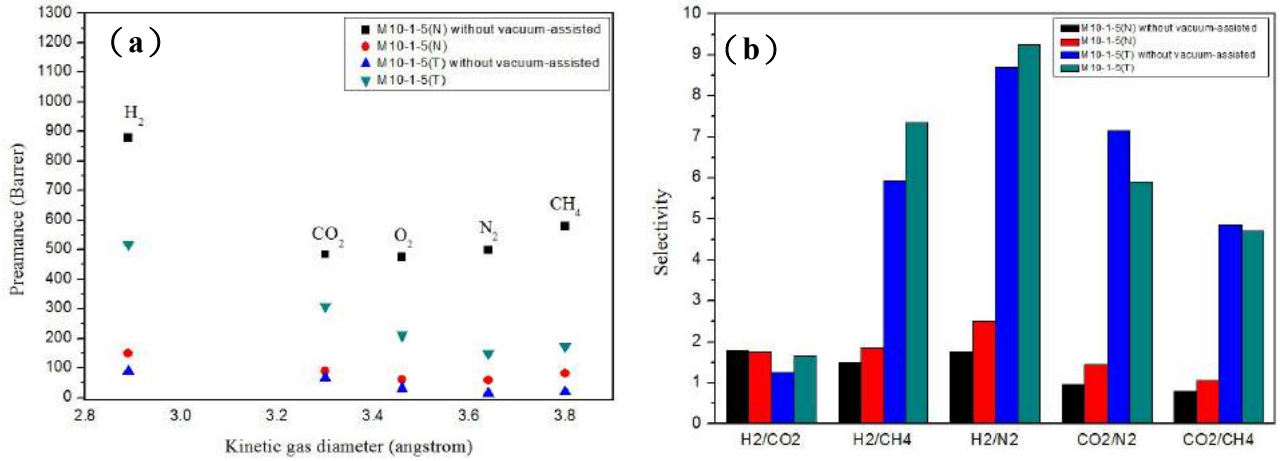

圖 3-8 不同溶劑組成與真空輔助系統之碳分子篩選薄膜的氣體分離表現：(a) 氣體滲透率、(b) 氣體選擇率。

3.2.4. 塗佈層數的影響

由上一小節，已知使用 TMP 做為溶劑且搭配真空輔助系統，有助於提升碳膜之氣體滲透分選特性。因此，此節討論使用 TMP 做為溶劑，在兩種的浸漬與抽出速度為 1、6 mm/s，改變塗佈次數分別為 5、6、7 次，以了解薄膜厚度對於薄膜結構與應用在氣體滲透分選上的影響。首先是浸漬與抽出速度為 1 mm/s 之下，改變塗佈次數之結果，從圖 3-9(a) 可以發現當塗佈 5 次時，碳膜表面有部分呈現無光澤的暗灰色，可能原因為基材之粗糙度不均使得薄膜滲入情形不均一，故在塗佈 5 次仍無法獲得結構完整之選擇層；當塗佈次數增加至 6 層，如圖 3-9(b)，碳層表面呈現具光澤感的黑色；當提升基材之浸漬與抽出塗佈液速度時，藉由速度的改變來影響成膜機制，通常厚度會隨著速度增快而變厚。從圖 3-9(d) 可以發現當速度由 1 增加至 6 mm/s 在相同的塗佈次數 5 次時，速度為 6 mm/s 所製備出的碳膜已展現出具光澤感的碳層表面，這代表較高速度下所塗佈的塗佈層達到修飾基材表面效果，使選擇層結構完整。而不論基材之浸漬與抽出速度的高低，當到達塗佈 7 層時，碳層出現裂痕剝落，這是因為橫向拉力大於層與層間的吸附力，使得裂痕產生[24]，其中速度為 6 mm/s 所製備出的碳膜剝落程度更為嚴重。

圖 3-9 不同浸沒抽出速度、塗佈次數之管柱式碳分子篩選薄膜外觀圖：(a) M10-1-5(T)、(b) M10-1-6(T)、(c) M10-1-7(T)、(d) M10-6-5(T)、(e) M10-6-6(T)與(f) M10-6-7(T)

圖 3-10 為 TMP 做為溶劑分別在基材浸沒與抽出速度為 1、6 mm/s 和塗佈次數 5、6 次之碳膜側視圖。兩種速度下塗佈次數由 5 增加至 6 次時，膜厚度均跟著增加從圖 3-10(a)與(b)可以觀察到膜厚由 4 增加至 14 μm；圖 3-10(c)與(d)膜厚則由 26.2 增加至 36.2 μm。而在相同的層數下，提高基材的浸沒與抽出速度，可以發現膜厚也隨之上升。因基材抽出速度的提升，使得成膜機制轉移到黏性阻力機制，此機制特性為膜厚隨著基材抽出速度增加而增加，而原本基材浸沒速度會影響到基材與塗佈液的接觸時間，進而影響到毛細作用力的作用時間，改變基材滲入情形，但本研究利用真空輔助系統使得不論高或低的基材浸沒速度並不在顯助的影響到薄膜結構，因為基材孔洞皆已被

塗佈液充滿。

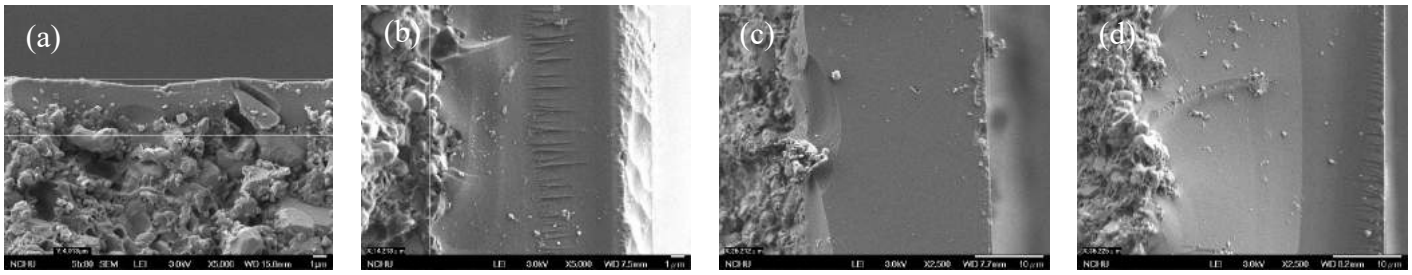

圖 3-10 不同浸沒抽出速度、塗佈次數之管柱式碳分子篩選薄膜的 FESEM 側視顯微圖：(a) M10-1-5(T)、(b) M10-1-6(T)、(c) M10-6-5(T)、(d) M10-6-6(T)

圖 3-11 為不同塗佈層數與速度 1、6 mm/s 的碳膜氣體滲透分選率，當塗佈 7 層時發現薄膜結構已不完整，因而無法進行氣體滲透試驗。在基材浸沒與抽出速度 6 mm/s，所製成的碳膜厚度較高，氣體滲透單位乘以膜厚得 Barrer 氣體滲透量，使其具高氣體滲透量。不同的速度與塗佈層數，對於大氣動直徑的氣體滲透率下降情形仍不明顯，這原因為製成的碳膜孔徑大小約介於 6 Å，增強了 CH_4 氣體分子吸附行為因而滲透率上升[72]。這樣的結果導致氣動直徑較小的氣體（如 H_2、CO_2），在膜厚增加的情形下滲透率有明顯下降；反觀氣動直徑較大的氣體（如 N_2、CH_4）因薄膜孔徑介於 6 Å，即使薄膜厚度增加也無法有效降低其氣體滲透率，使得 H_2/CH_4、H_2/N_2、CO_2/CH_4 之選擇率無法有效提升。

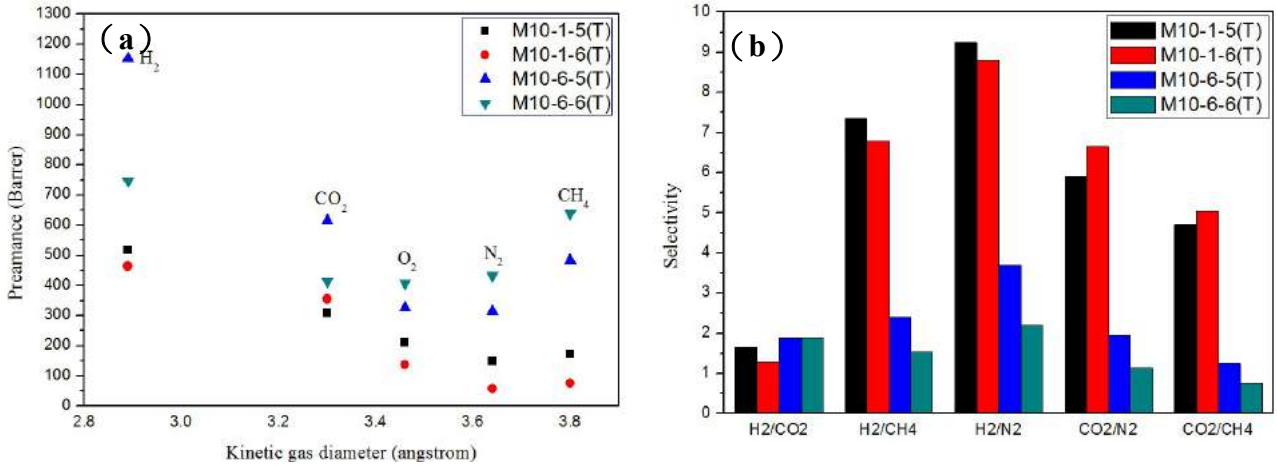

圖 3-11 不同塗佈層數之管柱式碳分子篩選薄膜的氣體分離表現：(a)氣體滲透率、(b)氣體選擇率

3.2.5. 溶液濃度之影響

此節透過調整溶液的濃度來提升塗佈次數為 6 次的碳膜氣體分選能力。探討濃度分別為 8、10、12 wt.% PEI 塗佈液，相同浸漬與抽出速度為 1 mm/s。圖 3-12 為不同塗佈液濃度所製備出的碳膜表面形貌，當在低濃度 8 wt.%的塗佈液時，因為黏滯度相對較低，易滲入基材結構內，因而無法在基材表面形成碳膜；當濃度提升至 12 wt.%時，薄膜表面的碳層，有小部分的的方發生剝落，使得結構受損。因此過低或過高的濃度皆無法有效製備出無缺陷的碳分子篩選薄膜。

圖 3-12 不同鑄膜液濃度之管柱式碳分子篩選薄膜 FESEM 圖：(a) M8-1-6(T)、(b) M10-1-6(T)、(c) M12-1-6(T)

3.3. 小結

本計畫的第一年研究主題係在管柱式碳分子篩選薄膜的開發，評估製參數如：溶液組成與濃度、真空輔助系統之影響、塗佈層數、基材浸沒與抽出速度。實驗共設計兩種溶劑、三種濃度、有無真空輔助系統、三種塗層、兩種基材移度速度，對碳膜表面結構觀察與進行氣體滲透試驗，來找出最佳的操作條件。

研究結果發現，使用高揮發性的氯仿做為溶劑，能製備出表面無缺陷的碳分子篩選薄膜，而在浸塗過程中使用真空輔助系統，增強了碳層與基材間的滲入行為，使得基材能夠被有效修飾，大幅提升氣體間的選擇率。本研究發現使用真空輔助系統，以氯仿作為溶劑之 10 wt.% PEI，基材浸漬與浸沒與抽出速度為 1 mm/s、塗佈 5 次，具有最佳的氣體滲透與分選能力，PH_2 519、PCO_2 308.4、PO_2 210.1、PN_2 149.7、PCH_4 172.9 Barrer、H_2/CH_4 為 7.35、H_2/N_2 為 9.25。

第四章 計畫第二年執行方法與成果

4.1. 計畫執行方法

4.1.1. 管柱式碳分子篩選薄膜製備方法

本研究所使用之薄膜擔體為 α-氧化鋁，係由永晉電陶瓷股份有限公司所提供之多孔氧化鋁管(O.D. 1.2 cm, I.D. 0.8 cm, L 5 cm)；以非對稱薄膜的型式將商業用之管柱式多孔氧化鋁基材作為碳分子薄膜之支撐層，製備出管柱式碳分子篩選薄膜。管柱式氧化鋁基材係委託廠商製備，於實驗前皆須先以 50vol%/ 50vol%之(乙醇/ DI Water)經超音波震盪清洗 2 小時，重複 1 至 2 次並置於 80 ℃烘箱中隔夜乾燥。本研究所製備之管柱式碳分子篩選薄膜，根據基材是否經過 TiO_2 修飾層改質可分為兩類；首先將針對製薄參數進行調整，接著進一步透過基材的改質進行碳分子篩選薄膜分選效能之優化。

基材經改質之 TiO_2 修飾層製備係採用溶膠凝膠法，於 30 ℃恆溫水浴之環境下，將 14.65 ml 之 TTIP 緩慢地加入 100 ml 之無水乙醇中混合攪拌 30 分鐘，使其均勻地溶解於溶液中；接著加入 0.3 ml 之硝酸及 1 ml 之去離子水，此時之溶液 pH 值約為 4，遂經恆溫攪拌 2 小時後即製備出 TiO_2 凝膠前驅溶液。最後再以含浸塗佈法（含浸沒、浸滯、抽出三步驟）將 TiO_2 凝膠塗覆於管柱式氧化鋁基材，固定浸沒、抽出速度為 1 mm/s，浸滯抽真空時間為 20 秒（抽真空壓力值固定約為 0.8 atm)，塗佈次數為 3、4 或 5 次；經隔夜乾燥後置於高溫爐分別以 400 ℃、1300 ℃、1350 ℃或 1400 ℃進行鍛燒。

表 4-1 TiO_2 修飾層之命名方式

Code		Sintered temperature (℃)			
		400	1300	1350	1400
TiO_2 Coating Layers	3	Ti3 – 400	Ti3 – 1300	Ti3 – 1350	Ti3 – 1400
	4	Ti4 – 400	Ti4 – 1300	Ti4 – 1350	Ti4 – 1400
	5	Ti5 – 400	Ti5 – 1300	Ti5 – 1350	Ti5 – 1400

碳分子篩選薄膜層之作法，首先製備 12、15、20 wt.%高分子前驅溶液：取適量高分子前趨物聚醚醯亞胺(Polyethylenimine, PEI)溶解於 NMP 之溶劑，於 80 ℃環境下以 60 r.p.m.攪拌 24 小時，待完全溶解後靜置 24 小時去除氣泡。利用塗佈機(Dip-coater)將管柱式氧化鋁基材依設定條件進行塗佈，透過含浸塗佈法（含浸沒、浸滯、抽出三步驟）將高分子前趨溶液塗覆於管柱式氧化鋁基材（含未修飾以及經 TiO_2 修飾過），固定浸沒、抽出速度為 1 mm/s；當基材完全浸泡在塗佈液時，開啟真空輔助系統浸滯抽真空時間為 10、20、100 或 200 秒（抽真空壓力值固定約為 0.8 atm），塗佈次數為 2 次（高濃度）或 5 次（低濃度）；經 24 小時隔夜乾燥後，置於真空高溫爐以 240 ℃持溫進行薄膜之欲處理步驟，遂升溫至 600 ℃持溫 2 小時進行碳化裂解之程序，期間之升溫速率為 5 ℃/min。薄膜樣品命名為 **m-w-s-L**，其中 m 代表經基材經改質之 TiO_2 修飾層（未經修飾則不標示），w 代表高分子溶液濃度，s 代表浸滯在塗佈液內抽真空時間，L 代表塗覆的層數。

4.1.2. Cu/ZnO/SBA – 16 水氣轉移觸媒之製備

觸媒之製備包含兩個部分，首先為觸媒之 SBA – 16 擔體之製備，遂將其與活性相金屬結合製備出 Cu/ZnO/SBA – 16 觸媒。以水熱合成法自製 SBA-16 觸媒擔體，在 2M HCl 酸性溶劑下添加膜板 F127 於室溫下攪拌使其溶解，續逐滴添加矽源 TEOS 於常溫下攪拌均勻；經攪拌 3 小時後，以高溫水熱法於 100 ℃反應 24 小時使其結構穩定；最後將所得之沉澱物進行淋洗、過濾及乾燥，並於高溫 500 ℃下鍛燒 6 小時以利移除模板，即可得到體心立方型態之多孔 SBA-16 粉末。接著將

所合成出之 SBA – 16 擔體以改良之共沉澱法結合沉積-沉澱法合成 Cu/ZnO/SBA-16 觸媒，其 Cu：Zn：Si 的莫爾比為 3：3：1。將水合硝酸銅與水合硝酸鋅以固定比例於 65 ℃下以 300 r.p.m.攪拌溶解於適量的去離子水，同時將碳酸鈉以固定比例加入去離水中於 65 ℃下以 300 r.p.m.攪拌溶解，製備成金屬前驅溶液與沉澱試劑；秤取適量的 SBA-16 擔體加入去離子水中，於 65 ℃下以 300 r.p.m.攪拌使其均勻散佈於水溶液中，接著將上述的金屬前驅溶液與沉澱試劑以滴定的共同沉澱方式加入 SBA-16 水溶液中，將金屬活性相批覆於 SBA-16 擔體上，整個滴定過程中 pH 值維持在 6.5 – 7 之間，溫度控制在 65 ℃並以 300 r.p.m.持續攪拌；達滴定終點意即金屬前驅溶液滴定完畢，於於 65 ℃下以 300 r.p.m.攪拌熟化一小時，續經淋洗數次於 110 ℃隔夜乾燥，並於 350 ℃鍛燒 3 小時。

4.1.3. 氣體滲透實驗

本研究於第一階段藉由氣體滲透測試做為碳分子篩選薄膜分離效能之依據，主要依單一氣體進行滲透實驗，方法為在薄膜的上游端予以一進氣壓力，藉氣體通過薄膜所造成之下游端單位時間內壓力變化值，透過公式計算求得氣體之滲透率；而兩種氣體分別通過薄膜之滲透率的比值即為薄膜針對此二種氣體之選擇率。

$$P_g = \left[\frac{dp}{dt}\right]\frac{\ell \cdot T_0 \cdot V}{A \cdot \Delta p \cdot T \cdot p_0}$$

其中P_g表示氣體選擇率（barrer）；$\frac{dp}{dt}$為達穩定狀態時，壓力隨時間變化曲線之斜率(cm-Hg/ sec)；V為薄膜下游端之體積(cm^3)；Δp為薄膜上、下游端起始之壓力差(cmHg)；A為薄膜之有效滲透面積(cm^2)；L為薄膜之厚度(cm)； P_0與T_0分別代表標狀態下之壓力及溫度（76 cm-Hg、273 K）；T為量測時之溫度(K)。

理想氣體氣體分離系數 $\alpha = P_A/P_B$

4.1.4. 催化反應實驗

第二階段與第三階段分別為混合氣體之觸媒固定床催化反應測試和薄膜反應器之催化反應與氣體分離測試；其中薄膜反應器之觸媒與薄膜結合的方式，為將觸媒披覆於石英棉上，捲成條狀後再將其填充於擔載碳分子篩選薄膜之多孔氧化鋁管內。此二階段之實驗操使用同一套設備，唯不同在於固定床反應器所使用用於填充觸媒之氧化鋁基材為緻密無孔洞之觸媒床體，形成一封閉管路氣體不會自管內洩漏。將反應氣體在固定壓力下通入薄膜反應器之反應床進行催化反應，藉薄膜反應器上游端、下游端（含滲透端及濃縮端）之氣體濃度差值，經公式計算求得氣體滲透率，此處分析氣體濃度的方式為在固定時間間格採氣針打入 GC 進行氣體分析；而兩種氣體滲透率之比值即為薄膜針對此二種氣體之選擇率。此設備包括 CO/H_2/CO_2/N_2 四種氣體之質量流量計，以模擬氣化合成氣氣體之組成；氣體先經過混和瓶並於此處續壓，且系統設置前須先在混合瓶中注入定量之液態水，此處同時為水蒸氣之產生位置，如此能確保氣體與水蒸氣之均勻混合；薄膜反應器之反應槽體外設有加熱器，以便於不同溫度下進行反應；系統內設有掃流氣，以利反應生成之小分子氣體（H_2）在通過薄膜後能夠被立即地帶離反應槽進入滲透端管線；濃縮端設有背壓閥以及質量流量控制器，使催化反應後所生成之氣體以連續流方式且在維持穩定壓力的狀態下持續滲透薄膜；滲透端與濃縮端後方皆設有冷凝裝置，以利後續氣體之採氣針進 GC 儀器進行分析。整個反應過程之數據皆以 GC 分析取得，數據可透過一系列的公式計算求得：觸媒催化反應之 CO 轉化率、H_2 回收率，薄膜分離氣體之氣體滲透率及選擇率。

$$X_{CO} = \frac{[\ CO_{feed\ in}\ ] - [\ CO_{feed\ out}\ ] - [\ CO_{sweep\ out}\ ]}{[\ CO_{feed\ in}\ ]} \quad (5)$$

其中：X_{CO}代表 CO 轉化率；$[CO_{feed\ in}]$為 CO 上游端進氣之濃度；$[CO_{feed\ out}]$為 CO 濃縮端出口之濃度；$[CO_{sweep\ out}]$為 CO 滲透端出口之濃度。

$$Pro_{H_2} = \frac{\left[H_{2\ sweep\ out}\right] \times \left[H_{2feed\ out}\right] \quad \left[H_{2feed\ in}\right]}{\left[H_{2feed\ in}\right]} \tag{6}$$

其中：Pro_{H_2}代表 H_2 生成率；$\left[H_{2feed\ in}\right]$為 CO 上游端進氣之濃度；$\left[H_{2feed\ out}\right]$為 CO 濃縮端出口之濃度；$\left[H_{2\ sweep\ out}\right]$ H_2 滲透端出口之濃度。

$$P_g = \frac{n_i \cdot T_0 \cdot L}{A \cdot T \cdot P_0} \tag{7}$$

其中P_g表示氣體選擇率（barrer）；n_i為氣體通過膜後之通量（mol/s）；A為薄膜之有效滲透面積(cm^2)；L為薄膜之厚度(cm)； P_0與T_0分別代表標狀態下之壓力及溫度（76 cm-Hg、273 K）；T為量測時之溫度(K)。

$$\alpha_{A/B} = \frac{P_A}{P_B} \tag{8}$$

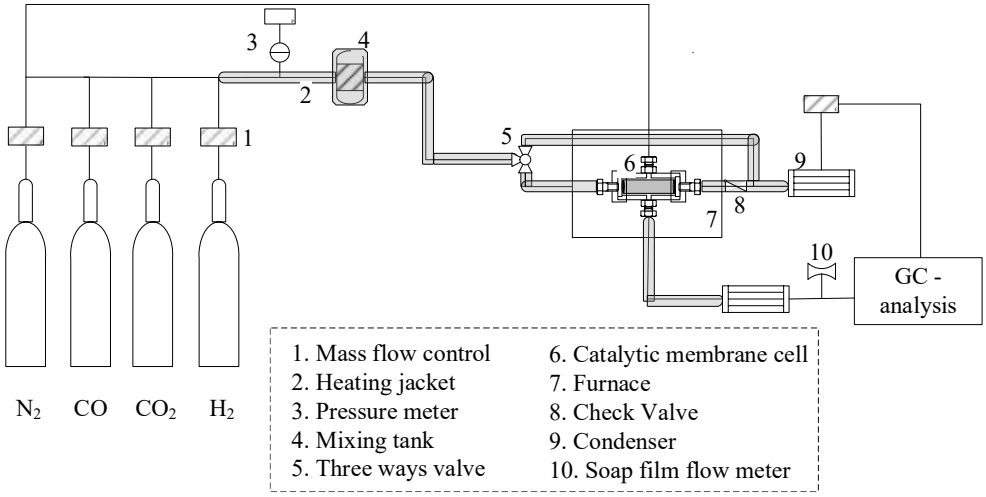

圖 4-1 混合氣體於薄膜反應器之催化分離測試設備示意圖（自組設備）

4.1.5. 特性分析

本研究將以原子力顯微鏡(Atomic Force Microscope，AFM)分析氧化鋁基材表面粗糙度；比表面積分析儀(Brunauer-Emmett-Teller，BET)量測薄膜基材與觸媒表面積大小、孔徑分佈情形；場發射掃描式電子顯微鏡(Field-Emission Scanning Electron Microscope，FE-SEM)觀察薄膜之基材表面特徵並量測薄膜厚度以及觸媒之表面微觀形貌；高解析 X 光粉末繞射分析儀（High Resolution X－Ray Diffractometer , HR-XRD 觸媒晶相和其結晶程度。

4.2. 計畫執行成果

根據第三章之研究方法，本實驗將透過以下三個方向來進行實驗與結果的討論：（1）薄膜之基本特性：碳分子篩選薄膜之基本特性分析，如 AFM 與 FE － SEM 並分別探討 H_2、CO_2、O_2、N_2 和 CO 此五種氣體之單一氣體滲透測試。（2）觸媒之基本特性：Cu/ZnO/SBA-16 觸媒之基本特性，如 FE － SEM、XRD 與 BET 分析等，藉此瞭解其表面形態、化學鍵結與孔洞結構；模擬

氣化合成氣 CO、H_2、CO_2、N_2 之混合氣配比，以此混合氣配比進行水氣轉移反應探討操作參數對 CO 轉化率之影響，並進一步探討此觸媒與傳統上經常使用之 $Cu/ZnO/Al_2O_3$ 觸媒其催化效能上的差異。（3）將上述薄膜與觸媒結合，將之構成催化型碳分子篩選薄膜反應器；用以進行合成氣之催化與分離試驗，並與固定床之催化反應進行數據分析比較。

4.2.1. 薄膜特性分析

本研究以 Sol – gel 程序製備 TiO_2 作為修飾層將柱狀氧化鋁管進行改質，並以不同之鍛燒溫度來控制樣本的表面粗糙度、孔洞大小與孔隙度。

圖 4 – 2 為以不同參數製備 TiO_2 修飾層之基材表面微結構 FE – SEM 分析圖，圖 4 – 2 (a) 為原始氧化鋁基材表面，其呈現大小顆粒不均一之堆疊形式，經 TiO_2 修飾層改質後，其表面形貌出現明顯的變化。如圖 4 – 2 (b) ~ (d)所示，塗覆 Sol – gel 溶液之基材經過 400 ℃的鍛燒溫度後，在基材表面形成明顯的 TiO_2 修飾層且出現許多大小不一的裂痕；而隨著塗覆層數的提高，因應力增加之影響而使 TiO_2 修飾層破裂的情形加劇。然而由於 TiO_2 修飾層與氧化鋁基材表面兩相之間的並無良好的化學鍵結，故無法提供足夠的機械強度供碳膜生長。圖 4 – 2 (e) ~ (m)分別將鍛燒溫度提升至 1300、1350、1400 ℃，使 TiO_2 修飾層與氧化鋁基材表面產生 Al_2TiO_5 結晶相，此結晶相的生成能提供足夠的機械強度以利碳膜的生長[73,74]。隨著鍛燒溫度的提升，TiO_2/Al_2O_3 的燒結情形亦加劇，可發現其表面隨鍛燒溫度之提升有逐漸緻密化的情形；然而在增加層數方面則無明顯的變化趨勢[75]。

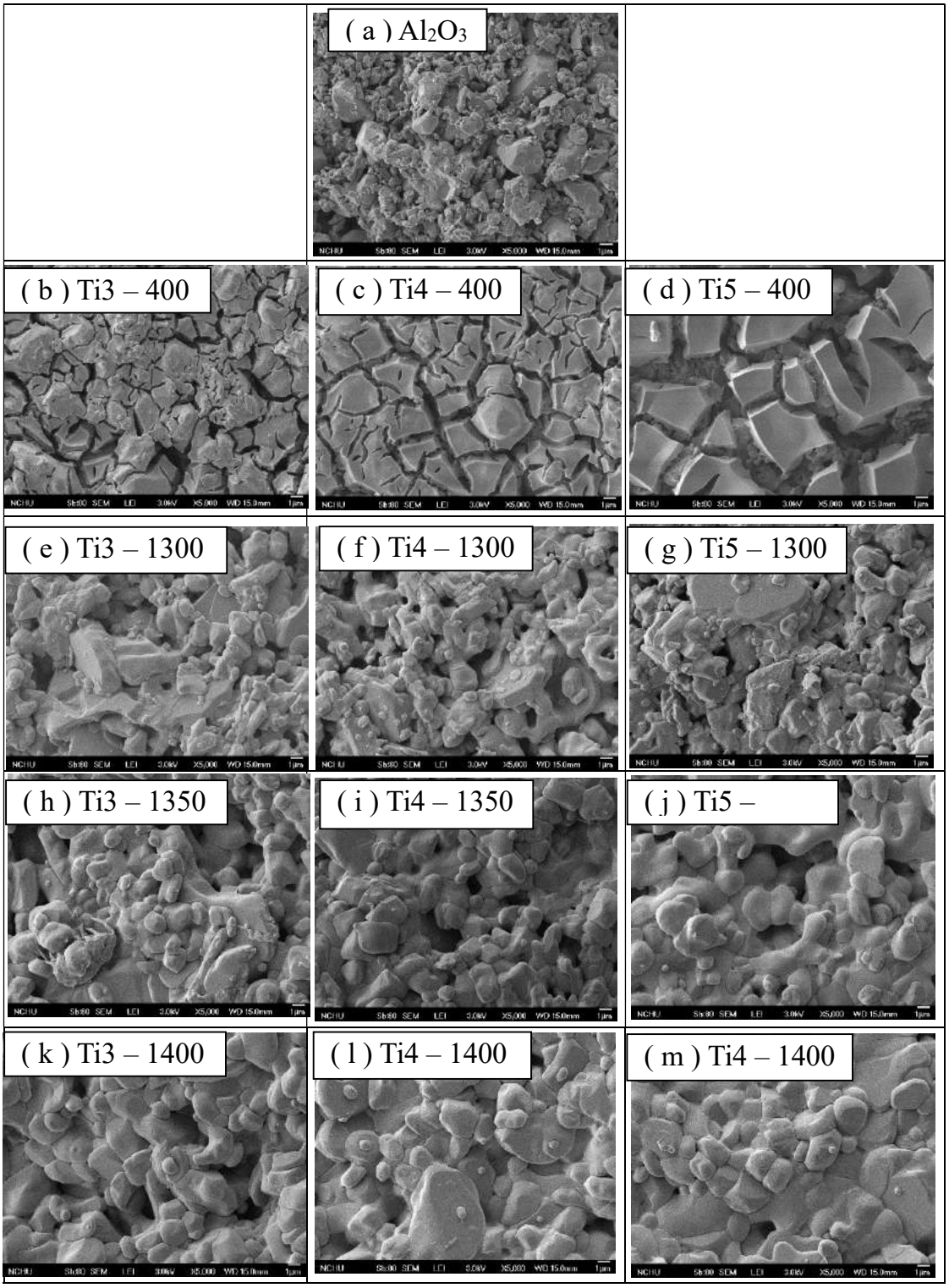

圖 4-2 以不同參數製備 TiO_2 修飾層之基材表面微結構 FE – SEM 分析圖

表 4-2 為以不同參數製備 TiO_2 修飾層之基材比表面積、孔洞半徑與孔體積分析結果，氧化鋁基材經過 TiO_2 修飾層改質後，其比表面積上升而孔徑則有下降的情形。推測由於塗覆 Sol – gel 溶液時，抽真空輔助浸塗過程中 TiO_2 粒子進入氧化鋁基材內部填補孔洞，使得提高比表面積、降低孔徑；而鍛燒溫度的升高使 TiO_2 與 Al_2O_3 反應加劇，提高 Al_2TiO_5 結晶程度，導致孔洞略為增加[73]。從各孔徑的孔體積分布圖亦可觀察到巨孔的結構從原先的 7.67%下降至 6.91%～4.18%，結果顯示由於多數的 TiO_2 在內部進行堆積，因此可以修飾基材內部孔洞過大的缺陷。

表 4-2 氧化鋁基之比表面積、孔洞半徑及孔洞體積分析結果

Sample code	S_{BET} (m^2/g)	D_{pore} (Å)	V_{total} (cm^3/g)	BJH adsorption cumulative Pore Volume of pores between 3.5 Å and 1000 micros Radius (cm^3/g)		
				Vmicro	Vmeso	Vmacro
Raw	32.7	46.3	0.0379	0.0055 (*14.55%*	0.0294 *77.78%*	0.0029 *7.67%*
Ti3 – 1300	54.5	23.6	0.0321	0.0050 *15.57%*	0.0252 *78.51%*	0.0019 *5.92%*
Ti4 – 1300	62.5	19.2	0.0301	0.0041 *13.62%*	0.0245 *81.40%*	0.0015 *4.98%*
Ti5 – 1300	57.1	21.2	0.0303	0.0042 *13.86%*	0.0243 *80.20%*	0.0018 *5.94%*
Ti3 – 1350	46.3	28.5	0.0330	0.0042 *12.74%*	0.0270 *81.89%*	0.0018 *5.37%*
Ti4 – 1350	57.1	33.9	0.0484	0.0067 *13.84%*	0.0391 *80.79%*	0.0026 *5.37%*
Ti5 – 1350	59.8	30.5	0.0455	0.0071 *15.60%*	0.0365 *80.22%*	0.0019 *4.18%*
Ti3 – 1400	38.5	34.6	0.0333	0.0057 *17.12%*	0.0253 *75.98%*	0.0023 *6.91%*
Ti4 – 1400	43.4	37.3	0.0405	0.0065 *16.08%*	0.0320 *79.15%*	0.0019 *4.77%*
Ti5 – 1400	39.3	34.4	0.0338	0.0062 *18.34%*	0.0259 *76.63%*	0.0017 *5.03%*

圖 4-3 為利用原子力顯微鏡（AFM）分析以不同參數製備 TiO_2 修飾層之基材表面粗糙係數(Ra)；由分析結果可觀察到，原始氧化鋁基材表面粗糙係數為 501 nm (圖 4-3 (a))，而經過 TiO_2 修飾層改質後，在低溫 400℃鍛燒之下基材表面粗糙係數明顯地下降；然而當鍛燒溫度提升至 1300、1350、1400 ℃時，由於 TiO_2 修飾層與氧化鋁基材反應產生 Al_2TiO_5 結晶相，而致使表面粗糙度未能獲得改善。基材表面的形貌會影響後續塗佈薄膜後兩者的接合情形，尤其表面的孔隙與粗糙度更是直接影響機械互鎖的關鍵因素之一；在基材粗糙過高的情形下，容易使披覆其上之高分子鏈折疊而呈現不規則狀態，分子鏈之間產生之折疊愈為明顯，致使裂解碳化後所得之層間巨變大，造成氣體選擇率下降；因此良好之薄膜基材，須擁有適當之表面粗糙度才能使薄膜黏附而不致於使高分子鏈折疊造成缺陷[74]。

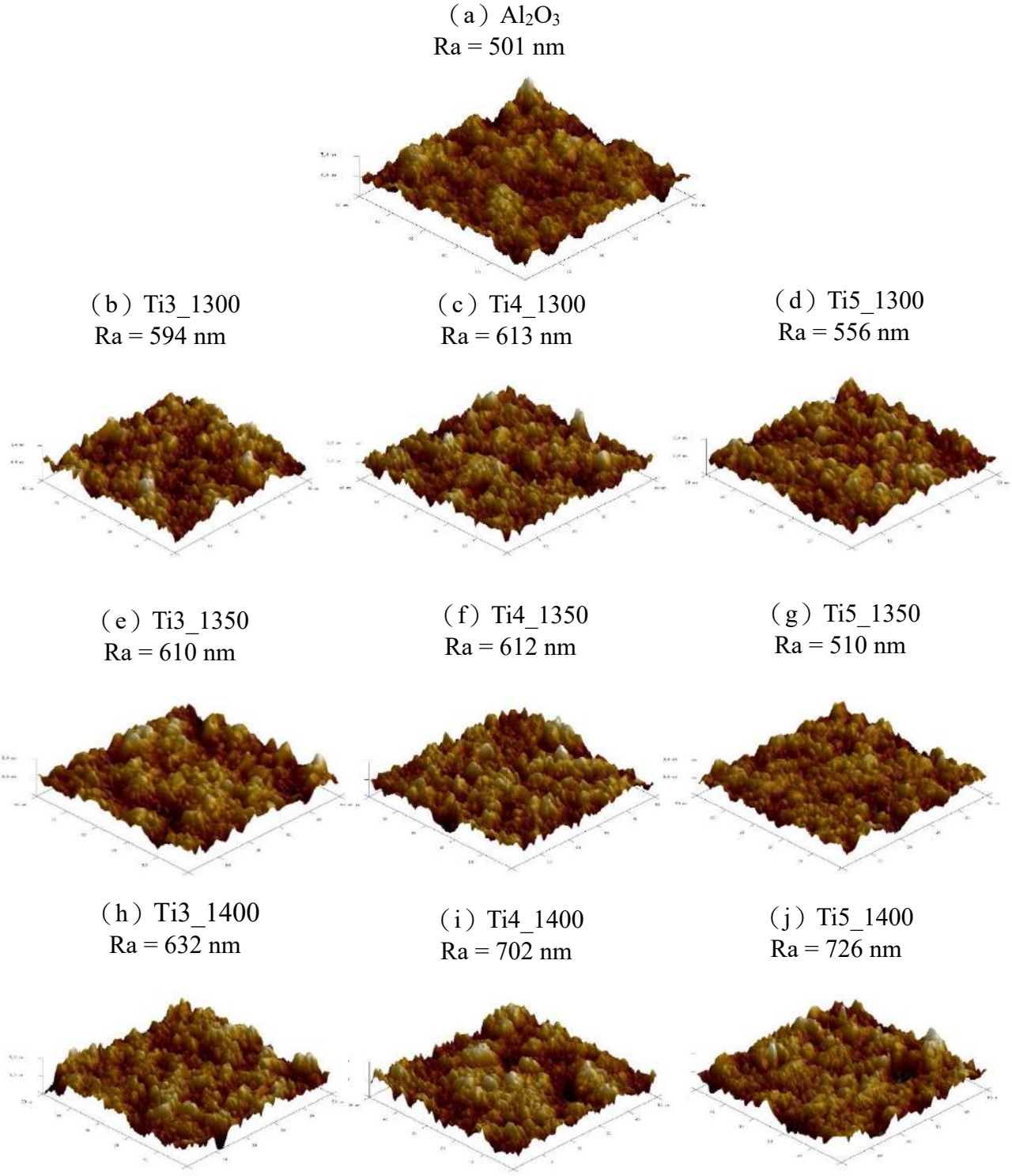

圖 4-3 以不同參數製備 TiO_2 修飾層之基材表面粗糙度 AFM 分析 （a）Al_2O_3、（b）Ti3-400、（c）Ti4-400、（d）Ti5-400、（e）Ti3-1300、（f）Ti4-1300、（g）Ti5-1300、（h）Ti3-1350、（i）Ti4-1350、（j）Ti5-1350、（k）Ti3-1400、（l）Ti4-1400、（m）Ti5-1400

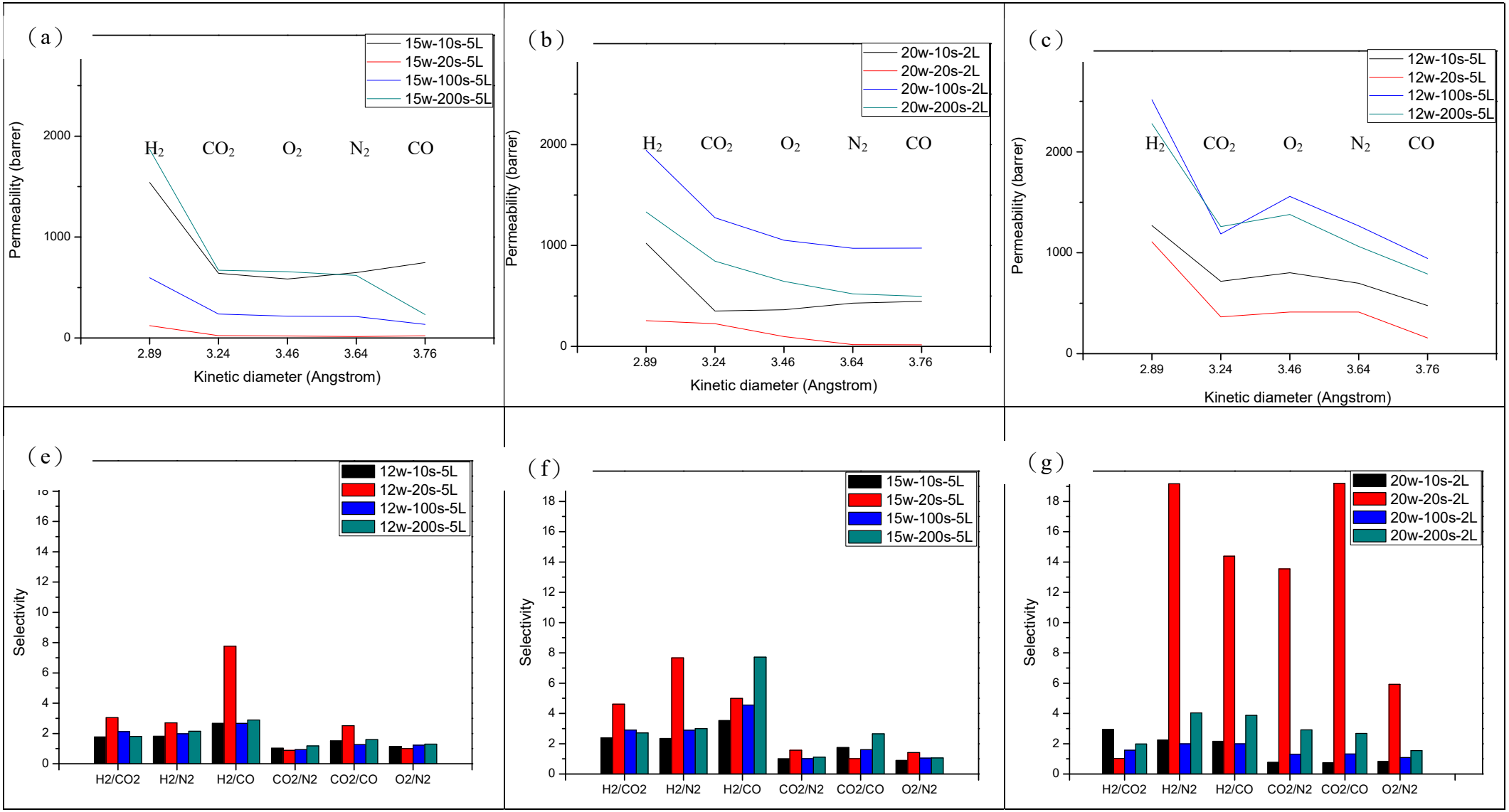

圖 4-4 不同鑄膜液濃度與真空輔助抽真空時間之碳分子篩選薄膜 (a)、(b)、(c)氣體滲透率，(d)、(e)、(f)氣體選擇率

圖 4-4 為碳膜之氣體滲透選擇數據，在未改質基材之碳分子篩選薄膜方面，薄膜之製備參數為：使用 12、15、20 wt.% PEI/ NMP 鑄膜液，真空輔助系統浸滯抽真空時間為 10、20、100 與 200 秒，以 240 ℃持溫進行薄膜之欲處理步驟，遂升溫至 600 ℃持溫 2 小時進行碳化。其中 12、15 wt.%塗覆的層數為 5 層，而 20 wt.%為 2 層；20 wt.%塗覆至三層以上(含)時，由於高分子層的橫向拉力大於層與層間的吸附力，製使所得之碳膜表面變會產生嚴重的裂痕剝落狀態[75]。在比較不同鑄膜液濃度方面，從圖 4－4 可觀察到本研究所製備出來之碳分子篩選薄膜普遍具有高的滲透率，其濃度對應滲透率的關係分別為 12 wt.%＞20 wt.%≧15 wt.%。濃度的提升代表單位塗佈業體積內所含的分子數量較多；以同樣具有最低通量之抽真空浸滯 20 秒之參數為例，在相同塗佈層數下，濃度自 12 wt.%增加至 15 wt.%，各氣體的滲透率有下降的趨勢，H_2、CO_2、 O_2、N_2、CO 依序從 1109.1、364.5、413.4、413.0、155.5 下降至 122.1、23.2、19.6、13.7、21.3 Barrer，而選擇率 H_2/CO_2 由 3.04 提升至 4.61，H_2/N_2 由 2.70 提升至 7.67。而當濃度提升至 20 wt.%，僅塗覆兩層高分子層，在氣動直徑較小的氣體方面滲透率無明顯變化，但在大氣動直徑的氣體滲透率方面則有些微的提升；在選擇率方面 20w-20s-2L 抽真空浸滯 20 秒之參數在分離大氣動直徑的分子上有顯著的提升，分別為 H_2/N_2 19.2、H_2/CO 14.4，CO_2/N_2 13.5，CO_2/N_2 19.2，O_2/N_2 5.9，然而在小氣動直徑的氣體之 H_2/CO_2 卻沒有獲得提升。

進一步透過 TiO_2 進行基材內部孔洞之修飾，選擇以上述具有最佳大氣動直徑氣體選擇率之 20w-20s-2L 參數作為製備改質基材之碳膜的條件。由圖 4-5 可觀察到經 TiO_2 改質基材之碳膜在滲透通量方面有明顯的提升，推測原始基材缺陷孔隙大可能造成高分子滲入嚴重，造成低的滲透通量.。藉 TiO_2 的填補缺陷縮小巨孔的比例，降低高分子滲入的情形，進而使滲透率提高。而在小氣動直徑氣體的分離上亦有所提升，H_2/CO_2 自 1.0 增至 3.6。

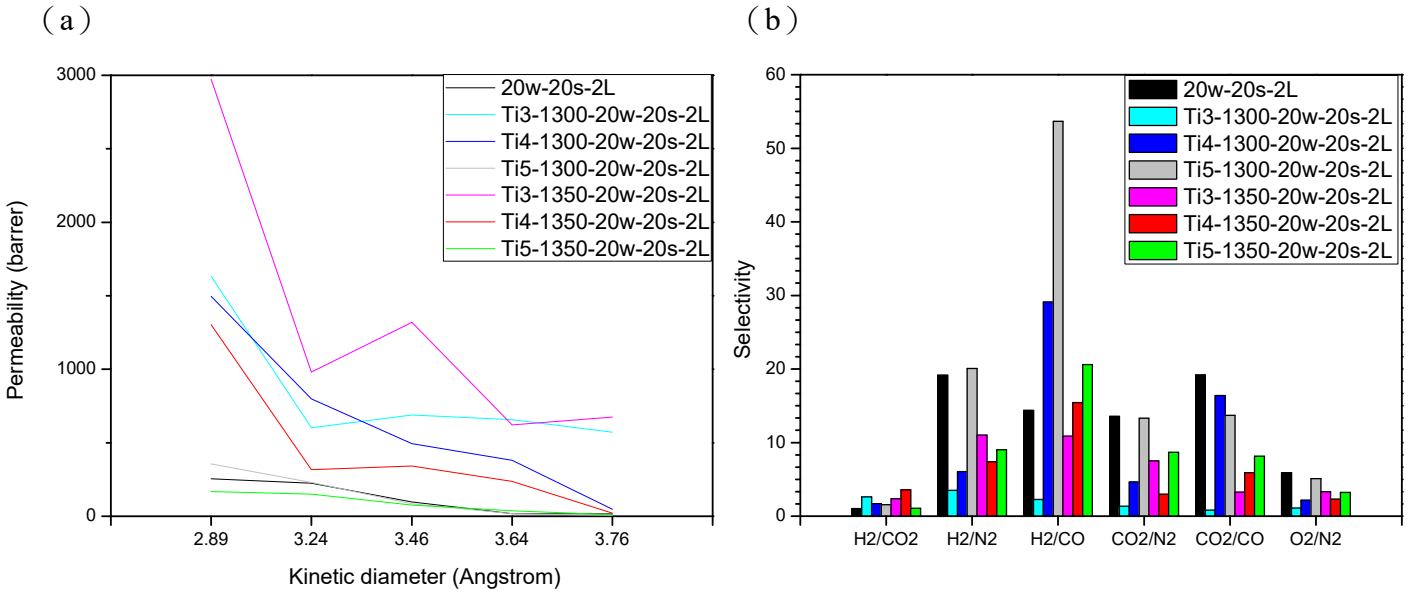

圖 4-5 不同鑄膜液濃度與真空輔助抽真空時間之碳分子篩選薄膜 (a)氣體滲透率、(b)氣體選擇率

4.2.2. 觸媒特性分析

以水熱法合成 SBA－16 擔體，並以沉澱沉積法合成 Cu/ZnO/SBA–16 觸媒應用於模擬 IGCC 發電系統中以氣化合成氣進行水氣轉移反應；其合成氣配比為 CO：40%、H_2：30%、CO_2：10%以及 N_2：20%，固定反應溫度為 300 ℃，空間速度為 10,000 h^{-1}、5,000 h^{-1} 或 2,500 h^{-1}，探討空間速度以及模反應器之使用對觸媒催化反應之影響。

圖 4-6 觸媒之表面微觀結構 FE－SEM 圖，從圖 4－6 (a) 可觀察到在放大倍率為 100,000 倍之 SBA–16 擔體表面微觀結構，在披覆活性相 Cu、Zn 金屬後明顯的改變，Cu/ZnO/SBA–16 觸媒表面呈現由許多球狀顆粒堆疊而成的片狀結構。評估催化反應之操作因子，以下針對 Cu/ZnO/SBA–16

觸媒在不同空間速度之下對整體催化反應之影響進行比較。

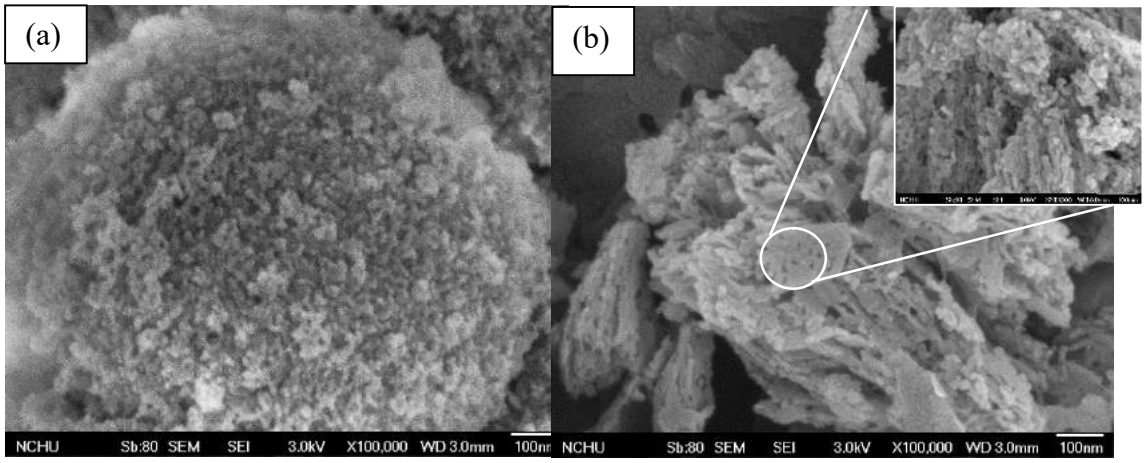

圖 4-6 觸媒之 FE – SEM 圖 (a) SBA–16 擔體 (b) Cu/ZnO/SBA–16 觸媒

圖 4-7 (a) 顯示在 10,000 h^{-1} 的空間速度下，反應經過 4 小時 CO 之轉化率僅達 50.43%；而將空間速度降低至 5,000 h^{-1} 之後，CO 轉化率於反應的第一點即獲得提升，反應經 2 小時後達到平衡且轉化率接近 90%；進一步將空間速度降低至 2,500 h^{-1}，結果顯示反應經 1.5 小時後達到平衡，轉化率相較於間速度為 5,000 h^{-1} 時高出 1 ~ 2%。空間速度越小，單位時間內反應物與觸媒的接觸面積越多，增加反應發生之機率，進而加速反應達平衡並提升整體之轉化率[76]。

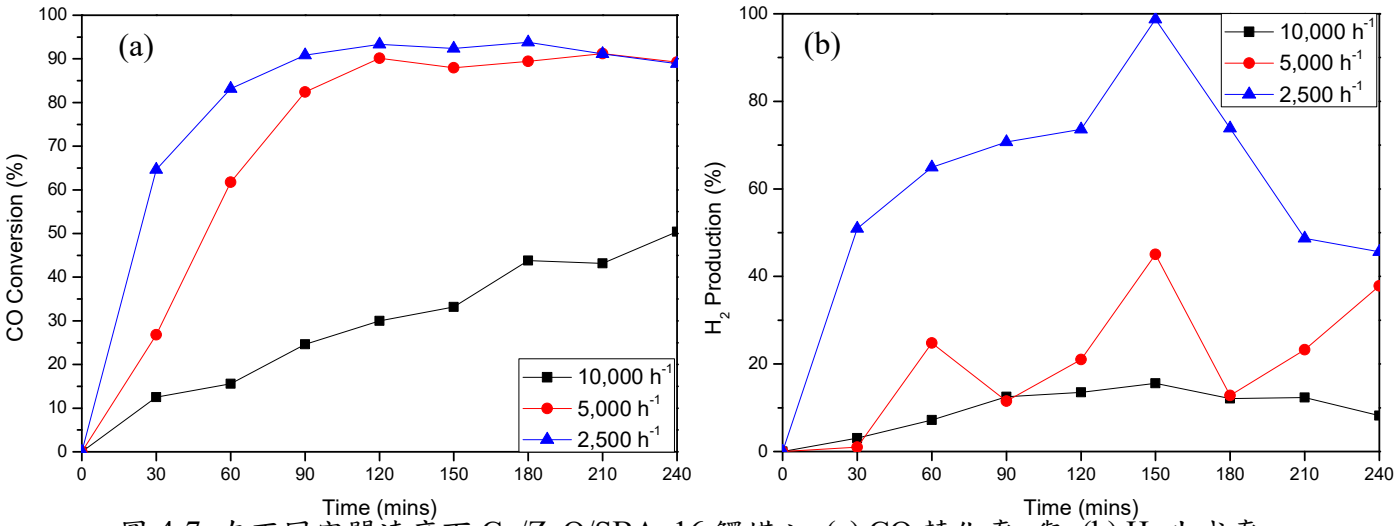

圖 4-7 在不同空間速度下 Cu/ZnO/SBA–16 觸媒之 (a) CO 轉化率 與 (b) H_2 生成率

4.2.3. 催化型薄膜反應器

初步針對固定床反應器與催化型膜反應器之效能進行比較，反應的操作參數為：固定反應溫度 300 ℃，空間速度為 5,000 h^{-1} 反應 5 小時。圖 4–8 (a) 顯示在未使用膜反應器的情形下轉化率約可達 90%，而在使用膜反應器後雖 CO 轉化率明顯的下降，但 H_2 之生成卻有顯著的提升。推測是由於本研究所製備之碳分子篩選薄膜滲透率過高而針對 CO 的截流能力不是太好的情況下，使得未反應之 CO 自膜反應器內滲透，導致整體的 CO 轉換率呈現降低的趨勢。

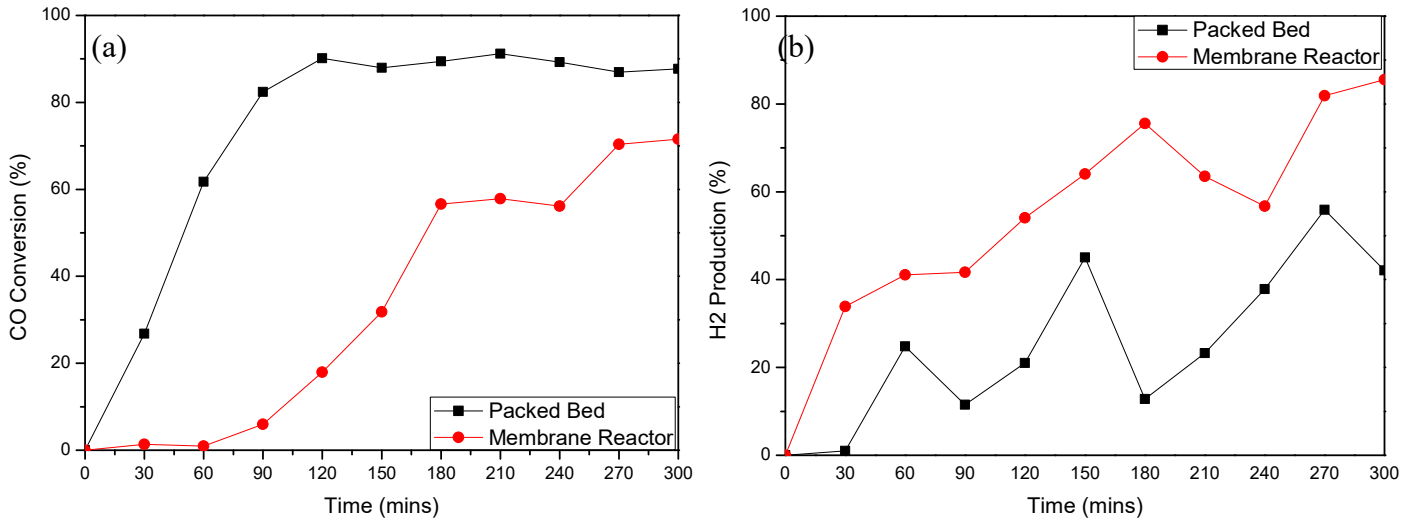

圖 4-8 比較固定床反應器與催化型膜反應器之 (a) CO 轉化率 與 (b) H_2 生成率

4.3 小結

本研究第二年研究主題係在碳分子篩型水氣轉移膜反應器的開發與老化機制評估，針對第一年所開發出來之管柱式碳分子篩選薄膜進行改良，評估鑄膜液濃度、基材浸於鑄膜液內抽真空浸滯時間以及透過 TiO_2 修飾層改質基材，對管柱式碳分子篩選薄膜於氣體分選效能之影響；並製備出以 SBA－16 作為擔體之 Cu/ZnO/SBA–16 低溫水氣轉移觸媒，評估其反應最適當之空間速度；並將上述兩者結合成為碳分子篩型水氣轉移膜反應器，比較與傳統之觸媒固定床反應器在催化反應上效能之差異。

研究結果顯示，使用高濃度的鑄膜液，以特性的抽真空浸滯時間塗覆低層數之高分子層，大幅提升氣體分子間之選擇率。透過 TiO_2 改質基材，使基材內部之巨孔結構得以受到有效之修飾，能夠有效改善鑄膜液滲入的情形增加薄膜之滲透率。水氣轉移催化反應方面，降低空間速度能夠有效的加速反應達平衡，並提高 CO 轉化率與氫氣生成率。使用碳分子篩型水氣轉移膜反應器進行催化反應，能夠致使氫氣的生成率大幅提升。

第五章 計畫第三年執行方法與成果

5.1. 計畫執行方法

5.1.1. 基材前處理

本研究所選用之多孔管柱式氧化鋁基材之內部缺陷較多且表面粗糙度大，為了有效改善此現象並提升高分子對無機基材之黏附情形，本研究選擇以塗佈 TiO_2 溶膠凝膠溶液的方式改質基材。本實驗室在過去的研究中[77,78]曾提出藉由 TiO_2 塗佈使基材表面增加化學吸附力並改善其表面粗糙度；另外，在 Ti 溶膠凝膠溶液塗佈後進行基材鍛燒可有效使鈦和鋁顆粒間產生燒結作用藉此提升基材之機械強度[79]。一般而言，TiO_2 在常溫下是無晶型結構，經鍛燒溫度至 200ºC 以上時，易呈現銳鈦礦晶型，若再高溫加熱至 600ºC 左右，銳鈦礦晶型將會轉變為熱力學穩定之金紅石晶型[80]。因此，可預期透過 800ºC 高溫鍛燒後的 TiO_2/Al_2O_3 管柱之機械強度有提升的趨勢，亦利於後續拋光步驟的進行。

本研究用基材之前處理步驟依序為：(1)清洗、(2)塗佈 Ti 中間層及(3)機械拋光等，以減少基材表面粗糙度，進而減少碳膜的塗佈厚度。

(1) 清洗

實驗前先將氧化鋁管以 50 / 50 vol.% 之乙醇/去離子水浸泡，並於恆溫 80 °C 的超音波震盪機中清洗 1 小時，並重複 1 至 2 次，隨後將其置於 110 °C 烘箱中乾燥至隔夜。

(2) 塗佈 Ti 中間層

Ti 中間層係以溶凝膠法製備 Ti 前驅液進行塗佈。首先於恆溫水浴槽中，將 14.65 ml TTIP 緩慢地加入無水乙醇中以配製不同濃度之 Ti 前驅液，充分攪拌約 30 分鐘後，使其均勻地溶解於溶液中；隨後加入 0.3 ml 之硝酸，經恆溫攪拌後即製備出 Ti 前驅溶液。最後再以浸沒塗佈的方式，將 Ti 前驅溶液塗覆於管柱式氧化鋁基材表面。浸沒塗佈程序依序為浸沒、浸滯、抽出三步驟；其中，浸沒、抽出速度固定為 1 mm/s；浸滯時輔以真空幫浦進行，待塗佈數次，在室溫下乾燥至隔夜後再置於高溫爐以 800 °C 進行鍛燒，升溫速率設定為 5 °C/min，並持溫 2 小時於 800 °C 鍛燒，可避免將顆粒燒結至瓷化－意即高溫燒結至鋁原子間緊密結合，致使坯體急劇收縮。到達此階段，坯體的強度及硬度雖會增大，但氣孔率迅速降低，將對氣體質量傳輸送產生阻力，不適作為擔體材料。

修飾之基材將以 **Tix_d (P)** 命名，其中 x 代表為塗佈之層數，d 為浸滯時間，而 (P)代表研磨/拋光程序，例如 Ti3_120s (P)，意即 Ti 前驅溶液塗佈 3 層，浸塗時浸滯時間為 120 秒，並緊接著進行研磨/拋光。後續用以製備薄膜之 質條件為 **Ti3_240s (P)**。

(3) 機械拋光

鍛燒後之 Ti/Al_2O_3 基材，先依序以 1000 及 2000 號砂紙個別進行 5 分鐘的研磨，隨後再以顆粒為 0.05 μm 之氧化鋁拋光液將基材表面進行拋光處理(拋光時間為 5 分鐘)。研磨時將基材固定於高速旋轉鑽孔機上，並將砂紙平鋪於基材表面，施予一固定壓力，並同時以清水洗滌基材表面。待完成拋光程序以去離子水和酒精潤洗基材表面，並放置於 60 °C 烘箱中乾燥至隔夜。

5.1.2. 碳分子篩選薄膜製備方法

高分子鑄膜液係取適量高分子前趨物 PEI 溶解於 NMP 溶劑，於 80 °C 恆溫環境下以 60 r.p.m. 攪拌 24 小時，待其完全溶解後靜置 24 小時去除氣泡。隨後以浸沒塗佈將高分子鑄膜液塗覆於管柱式 Ti/Al_2O_3 基材表面。浸塗條件為：浸沒、抽出速度固定為 1 mm/s，輔以抽真空浸滯之時間為 20 秒 (抽真空壓力值固定為 1 atm)，塗佈層數為 1、2 或 3 層；經 24 小時乾燥隔夜後，置於真空環境下，以高溫爐進行碳化。設定升溫速率為 5 °C /min 先升溫至 240 °C，並持溫 6 小時進行薄膜前處理，隨後以升溫速率 5 °C/min 分別升溫至 600、650、700 °C 並持溫 2 小時進行碳化裂解。薄膜樣品命名為 M-xL-T，x 代表塗覆層數，T 則代表碳化溫度。例如 M-1L-600，代表經 TiO_2 修飾之基材，塗覆 1 層高分子後於 600°C 下進行碳化。

5.1.3. 碳分子篩選薄膜之疏水改質

碳膜之疏水層塗佈採用一般浸鍍方式(未以抽真空輔助)。首先取適量的十二烷基三氯矽烷溶液於樣本瓶中，隨後將製備好之管柱型碳膜浸滯其中 1 分鐘，隨後將其取出放置於 60°C 烘箱中 30 分鐘使多餘的溶劑揮發。

5.1.4. Cu/Zn/SBA-16 水氣轉移觸媒的製備

SBA-16 擔體係以水熱合成法。首先在酸性條件 2M 稀鹽酸中加入 4 g 模板 F127，待其攪拌三小時完全溶解後，逐滴加入 14.2 ml 的矽源 TEOS，並持續均勻攪拌 24 小時。隨後再置入 110 °C 烘箱中 24 小時使其熟化，取出後待其冷卻，將反應產物以二次水清洗抽濾之，遂再次將其置入 110 °C 烘箱進行乾燥，最後將產物於 500 °C 條件下鍛燒 6 小時，即可得到白色粉末狀之 SBA-16。

本研究以共沉澱法合成 Cu/Zn/SBA-16 觸媒。其 Cu：Zn：Si 之莫爾比為 3：3：1[81]。首先秤量 3 g 之 SBA-16 擔體加入去離子水中，於 65 °C 下以 300 r.p.m.攪拌使其均勻分散於水溶液中。接著將 17.09 g 水合硝酸銅($Cu(NO_3)_2 \cdot 2.5H_2O$)與 21.87 之水合硝酸鋅($Zn(NO_3)_2 \cdot 6H_2O$)於 65 °C 下以 300 r.p.m.攪拌溶解於去離水，配製成 6.0 M 的金屬硝酸水溶液，以得到金屬前驅溶液；遂將 25.44 g 碳酸鈉(Na_2CO_3)溶於 150 ml 去離水中配製成 1.6 M 之碳酸納水溶液，並於 65 °C 下以 300 r.p.m.攪拌溶解，製備成沉澱試劑。接著將上述的金屬前驅液與沉澱試劑逐滴加入 SBA-16 懸浮液中使 Cu-Zn 金屬共沉澱於 SBA-16 擔體表面，期間 pH 值維持在 6.5 – 7 之間，溫度控制於 65 °C 並以 300 r.p.m. 持續攪拌。隨即於 65 °C 下以 300 r.p.m.持續攪拌一小時使其熟化，續經離心清洗數次於 110 °C 烘箱中隔夜乾燥，並於 350 °C 下鍛燒 3 小時，升溫速率為 5 °C / min。

5.1.5. 氣體滲透實驗

本研究係利用氣體滲透測試作為薄膜分離效能之評估，而滲透試驗主要以單一氣體來進行。測試方法為在薄膜的上游端予以一進氣壓力，當薄膜兩側存在壓力差時即可作為驅動力，接著於下游端記錄單位時間內壓力之變化值，續以下列公式－式(9)計算求得氣體之滲透率；而兩種氣體個別通過薄膜時之滲透率的比值即為薄膜對兩氣體之選擇率(如式(10))。本實驗之單一氣體滲透設備示意圖如圖 5-1 所示。

氣體滲透測試的流程為首先將製備完成之碳膜置於氣體滲透槽中，並以 O-ring 壓實，確保設

備密封；續以真空幫浦將管線及設備抽真空，使整個系統保持在真空狀態以避免其他氣體干擾測試結果；接著開啟氣體鋼瓶並將錶頭之進氣壓力調控於 2 kg/cm^2，待觀測上游端壓力穩定時遂開啟上游端之球閥將氣體通入系統內。在氣體滲透通過薄膜的過程中，同時以下游端之壓力計偵測壓力變化，並將讀值以電腦連線記錄單位時間內之壓力變化情形。滲透試驗完成後，經整理並繪製出下游端壓力隨時間變化曲線圖，以求得壓力值隨時間變化而上升之斜率值，並將其代入滲透率公式計算求得氣體滲透率；而薄膜之分選效能係藉由兩種氣體滲透率之比值表示之，如式(10)，因此可由上述數據評估薄膜對於氣體之滲透分選能力。

$$\mathbf{P_g} = \left(\frac{dp}{dt}\right)\frac{V \cdot T_0 \cdot L}{A \cdot \Delta p \cdot P_0 \cdot T} \tag{9}$$

其中，P_g：氣體滲透率(barrer)； dp/dt：達穩定狀態時，壓力隨時間變化曲線之斜率(cm-Hg/ sec)；V：薄膜下游端之體積(cm^3)；Δp：薄膜上、下游端之壓力差(cm-Hg)；A：薄膜之有效滲透面積(cm^2)；L：薄膜厚度(cm)；P_0 與 T_0：分別代表 STP 標準狀態下之壓力(76 cm-Hg)和溫度(273 K)；T：氣體滲透實驗之溫度(K)。

$$\alpha_{A/B} = \frac{P_A}{P_B} \tag{10}$$

其中，$\alpha_{A/B}$：A、B 兩氣體間之選擇率；P_A 與 P_B：各代表 A、B 兩氣體之滲透率(barrer)

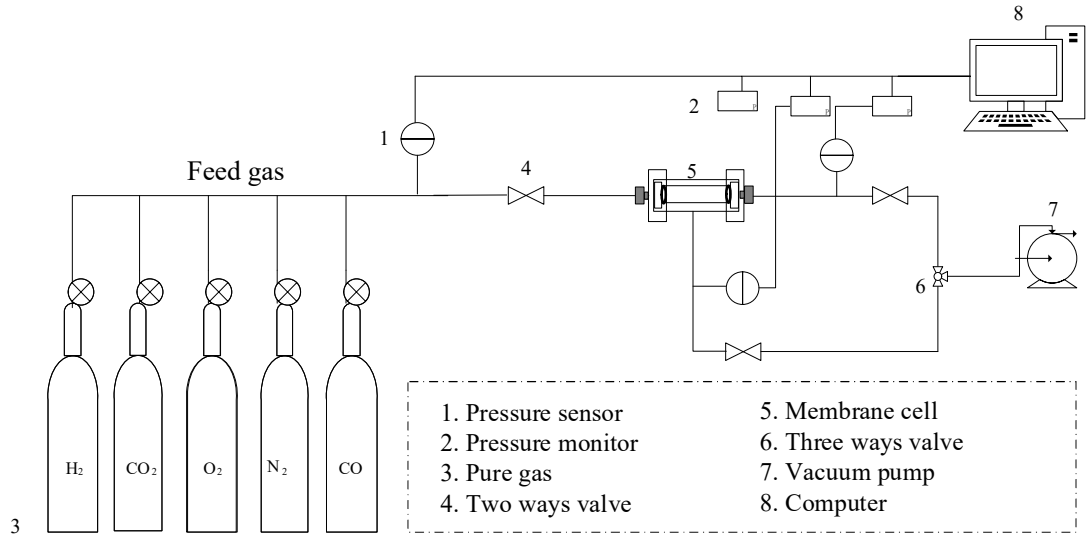

圖 5-1 單一氣體滲透設備示意圖(自組設備)

5.1.6. 催化反應實驗

本研究進行催化型膜反應裝置示意圖如圖 5-2 所示。首先將反應氣體(H_2、CO、CO_2、N_2)在固定壓力下(絕對壓力為 3 kg/cm^2)通入薄膜反應器之反應槽進行催化反應，並量測膜反應器上游端及下游端(含滲透端及濃縮端)之氣體濃度組成，經公式換算後求得氣體滲透率。此處分析氣體濃度的方式為在固定時間間隔以氣針採樣打入 GC 進行分析；而兩種氣體滲透率之比值即為薄膜對氣體之選擇率，滲透率公式如式(11)及式(12)，選擇率計算公式同式(10)。

實驗係以模擬氣化合成氣之氣體組成包括 H_2、CO、CO_2、N_2 四種氣體。首先於混合瓶中注入定量之液態水，反應前氣體會經過混和瓶並在系統內續壓，此處同時為水蒸氣產生的位置，如此能確保氣體與水蒸氣均勻混合。薄膜反應器之反應槽體外設有加熱爐，以便於不同溫度下進行反應；系統中設有掃流端提供掃流氣 N_2 之以利反應後之小分子氣體如 H_2 能夠被立即地移出滲透端；濃縮

端設有逆止閥以及質量流量控制器，使催化反應後所生成之氣體以連續流且在穩定的壓力下持續進行滲透；滲透端與濃縮端後方皆設有冷凝裝置，以利後續採氣針至 GC 儀器進行分析。整個反應過程之數據皆以 GC 分析取得，滲透數據可透過一系列的公式計算如式(11)及式(12)求得，另外，可透過式(13)及式(14)計算觸媒催化反應之 CO 轉化率(CO conversion, $\mathbf{X_{CO}}$)及 H_2 回收率(H_2 recovery, $\boldsymbol{R_{H_2}}$)。

$$\mathbf{Q_i} = \frac{\mathbf{X_i} \cdot \mathbf{Q}}{\mathbf{A}} \tag{11}$$

其中，$\mathbf{Q_i}$：通量(mL/min)；$\mathbf{X_i}$為氣體的體積濃度，由 GC 檢量線換算得知；Q ((STP) mL/s)：滲透端的總體積流率；A：薄膜之有效滲透面積(cm^2)。

$$\mathbf{P_g} = \frac{\boldsymbol{Q_i} \cdot \boldsymbol{L}}{\Delta p_i} \tag{12}$$

其中，P_g：氣體滲透率(barrer)；L：薄膜厚度(cm)；$\boldsymbol{\Delta p_i}$ (cmHg)代表特定氣體的跨膜分壓。

$$\boldsymbol{X_{CO}} = \frac{[CO_{feed\ in}] - [CO_{feed\ out}] - [CO_{sweep\ out}]}{[CO_{feed\ in}]} \tag{13}$$

其中，$\mathbf{X_{CO}}$：CO 轉化率；$[\boldsymbol{CO_{feed\ in}}]$：CO 進氣端之莫爾流率 (mol/s)；$[\boldsymbol{CO_{feed\ out}}]$：CO 濃縮出口端之莫爾流率 (mol/s)；$[\boldsymbol{CO_{sweep\ out}}]$：CO 滲透出口端之莫爾流率 (mol/s)。

$$\boldsymbol{R_{H_2}} = \frac{[H_{2_{sweep\ out}}]}{[H_{2_{sweep\ out}}] + [H_{2_{feed\ out}}]} \tag{14}$$

其中，$\boldsymbol{R_{H_2}}$：H_2 回收率；$[\boldsymbol{H_{2_{feed\ out}}}]$：$H_2$ 濃縮端出口之莫爾流率 (mol/s)；$[H_{2\ sweep\ out}]$：H_2 滲透端出口之莫爾流率 (mol/s)

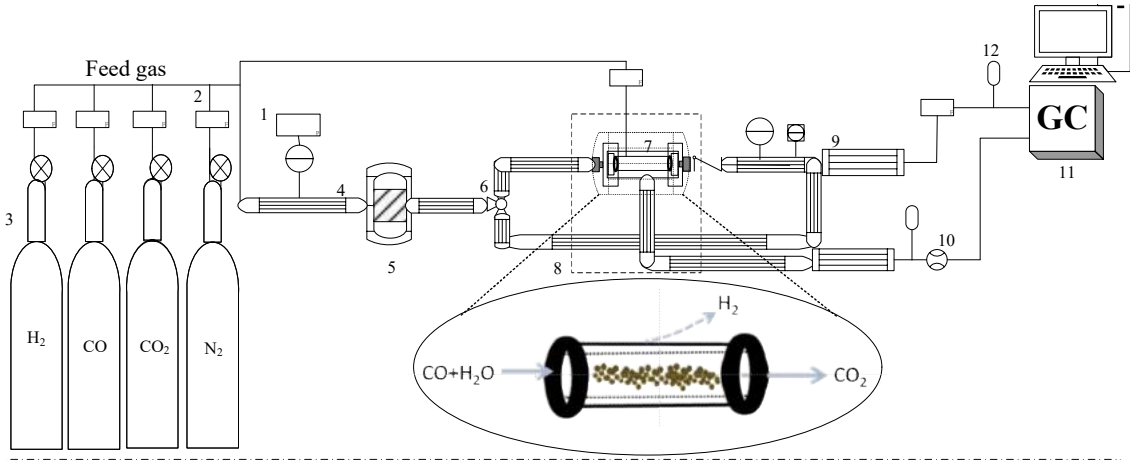

1. Pressure sensor; 2. Mass flow controller; 3. Gas cylinder; 4. Heating jacket; 5. Mixing tank; 6. Three ways valve; 7. Catalytic membrane cell; 8. Furnace; 9. Water vapor condenser; 10. Soap film flow meter; 11. GC analysis; 12. Mixing gas bottle (sampling site)

圖 5-2 薄膜反應器之水氣轉移反應與氣體分離設備整合之示意圖(自組設備)

5.1.7. 特性分析

本研究使用之場發射掃描式電子顯微鏡 (Field-Emission Scanning Electron Microscope；FE-SEM)，廠牌型號為 JEOL JSM-6700F，OXFORD INCA ENERGY 400，來自中興大學貴重儀器中心。本研究使用場發射掃描式電子顯微鏡 (Field-Emission Scanning Electron Microscope；FE-SEM)評估本研究所自製材料的外觀型態，如薄膜的結構、表面、側面形態以及膜厚之量測，或觸媒之外觀形貌等；本研究使用之原子力顯微鏡(Atomic Force Microscope；AFM)，廠牌型號為 Veeco DI-3100，來自中興大學貴重儀器中心。本研究係利用此儀器針對不同合成條件與浸塗參數之 Ti /Al_2O_3 基材表面進行掃描，主要觀察其表面形態與粗糙係數(Surface Roughness, Ra；nm)；本研究使用之高解析 X 光繞射分析儀(High Resolution X-Ray Diffractometer；HR-XRD)，廠牌型號為 BRUKER D8 SSS，來自中興大學貴重儀器中心。為了瞭解擔體與觸媒活性相的晶體結構及晶面間距，本研究藉由高解析 X 光粉末繞射分析儀進行分析，主要可透過繞射材料後出現的特徵峰提供觸媒之結晶型態與結晶度；本研究使用之比表面積分析儀(Brunauer-Emmett-Teller；BET)，廠牌型號為 Model ASAP2010，來自 Microorifice 公司。為了了解本研究所合成之擔體、觸媒及氧化鋁基材之物化性質可藉由比表面積分析儀進行分析；本研究使用之接觸角測量儀(Contact Angle Meter)，廠牌型號為 KRÜSS DSA100，來自澳登堡股份有限公司。為評估本研究所選用之疏水材對於碳膜表面之疏水改質成效，將以接觸角(contact angle)量測液/氣-界面接觸到固體表面時形成的角。

5.2. 計畫執行成果

根據上述之實驗方法，本研究將透過以下四個部分來進行實驗的結果與討論：(1) 管柱型基材之特性分析：TiO_2/Al_2O_3 基材前處理－AFM 及 FE-SEM 分析。(2) 管柱型碳分子篩選薄膜之分選效能－浸塗條件、碳化溫度及疏水性改質等測試。(3) 觸媒之基本特性：Cu/ZnO/SBA-16 觸媒之基本特性，如、XRD、SEM 及 BET 分析等。(4) 將上述薄膜與觸媒結合以構成碳分子篩選薄膜反應器，並進行水氣轉移反應催化試驗，並比較經過改質前後對膜反應器效能之影響。

5.2.1. TiO_2/Al_2O_3 基材前處理

以浸塗法將 Ti 溶液塗佈於管柱式多孔氧化鋁基材表面，其製備參數對表面粗糙度之影響如表 5-1 所示。原始氧化鋁基材表面粗糙度 Ra 為平均值為 642.8±88.52 nm，顯示原氧化鋁基材的表面粗糙度高，且各基材間粗糙度的差異度很大。經改變塗佈層數及浸塗時間後，雖然粗糙度皆較原基材粗糙度低，但所獲得的粗糙度與製備參數間並無顯著的變化趨勢。

經進一步觀察其外觀形貌如圖 5-3 可推測此現象可能由下述幾點造成：(1)各基材間原始粗糙度的差異度大，故無法反應出改質後些微的粗糙度變化（AFM 量測屬破壞性檢測，無法取得每一支基材的原始粗糙度）；(2)而此些微的粗糙度變化，可能原自於基材內部孔隙率高且孔洞較大，Ti 前驅溶液經真空輔助系統的浸鍍後，多數的 Ti 前驅溶液都直接滲入基材內部進行大孔洞的填補，而未能有效沉積於基材表面構成 TiO_2 薄層，故無法有效改善基材高表面粗糙度的問題。

表 5-1 以不同製備參數合成 TiO_2 溶液修飾基材之表面粗糙度

代號	粗糙度 (Ra, nm)
Al_2O_3	642.8±88.52
Al_2O_3 (P)	182±1
Ti3_240s (P)	109.5±7.5
Ti3_120s	467.33±79.73
Ti3_240s	618.33±74.77
Ti4_240s	526.67±99.23
Ti5_240s	545.33±20.85

(a1) Ra = 642.8±88.52 nm (b1) Ra = 618.3±74.77 nm (c1) Ra = 109.5±7.5 nm (d1) Ra = 182±1 nm

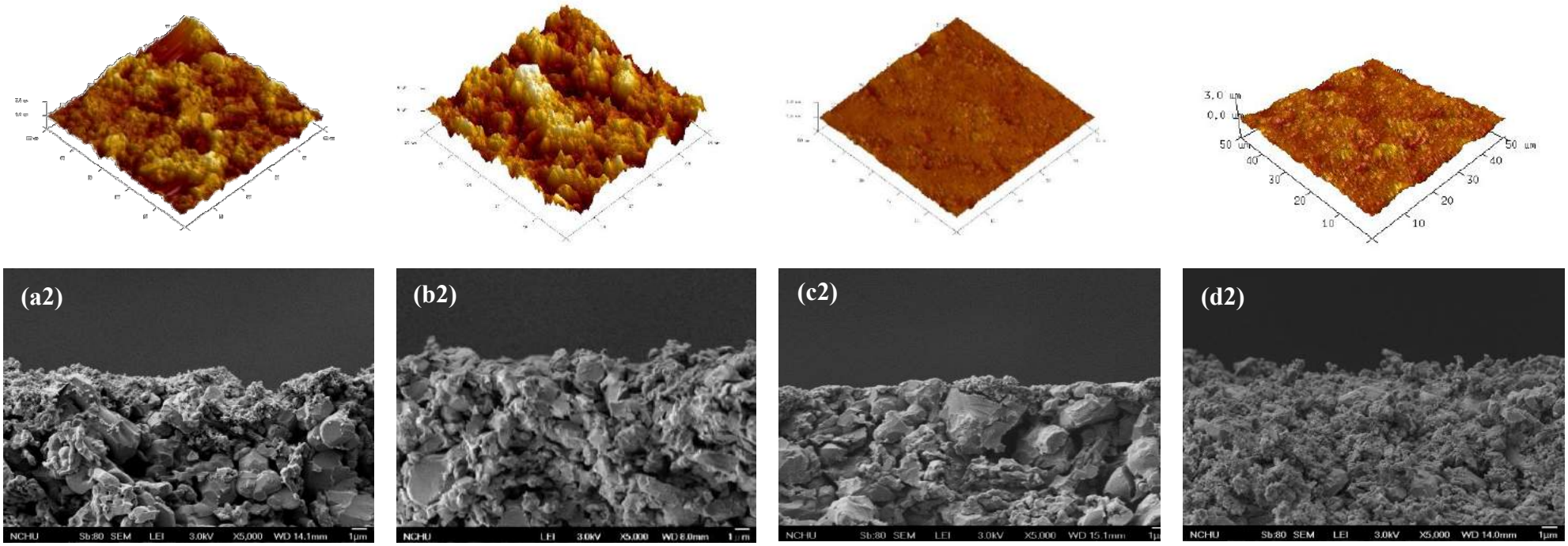

圖 5-3 (1) AFM 粗糙度分析及 (2) FE-SEM 側面照(a) raw Al_2O_3; (b) Ti3-240s, (c) Ti3-240s (P), 及 (d) raw Al_2O_3 (P)。

5.2.2. 管柱型碳分子篩選薄膜之分選效能及特性

圖 5-4 提供不同塗佈層數的碳膜之側面照及膜厚分析。根據結果顯示，在不同塗佈層數下所製備之碳膜的膜厚皆會伴隨塗佈層數越高而有增加的趨勢，如碳化溫度為 600 ºC 時，塗佈 1~3 之薄膜膜厚由 2.625μm 增加至 7.256 μm；而碳化溫度為 650 ºC 時，塗佈 1~3 之薄膜膜厚由 2.625 μm 增加至 6.266 μm；當碳化溫度為 700 ºC 時，塗佈 1~3 之薄膜膜厚更由 1.462μm 增加至 4.162μm。Grosso 學者[82]曾表示在浸塗法之中，基材是以連續式的浸滯於溶液中再以恆定的速度抽出，因此，其成膜過程將受到重力引起之黏滯阻力影響。均勻的膜厚往往取決於流體之密度、表面張力和黏滯度。

進一步比較在相同濃度與塗佈條件下由不同碳化溫度所製備之碳分子篩選薄膜之膜厚。由圖 5-4 中可以觀察到當碳化溫度提高，在相同塗佈層數下(一層和兩層)之碳膜的膜厚隨之下降，此現象推測是因為在高溫裂解時容易使高分子鏈段的層狀堆疊立體結構崩塌，因此縮短了層與層之間的間距，導致膜厚降低。在文獻中[83]曾有學者解釋道在碳化過程中，係為線性的大分子結構穩定轉化成為芳香烴梯形結構的過程[84]；因此，當熱裂解溫度升高時，大分子結構間的間距減少，膜厚通常會下降。

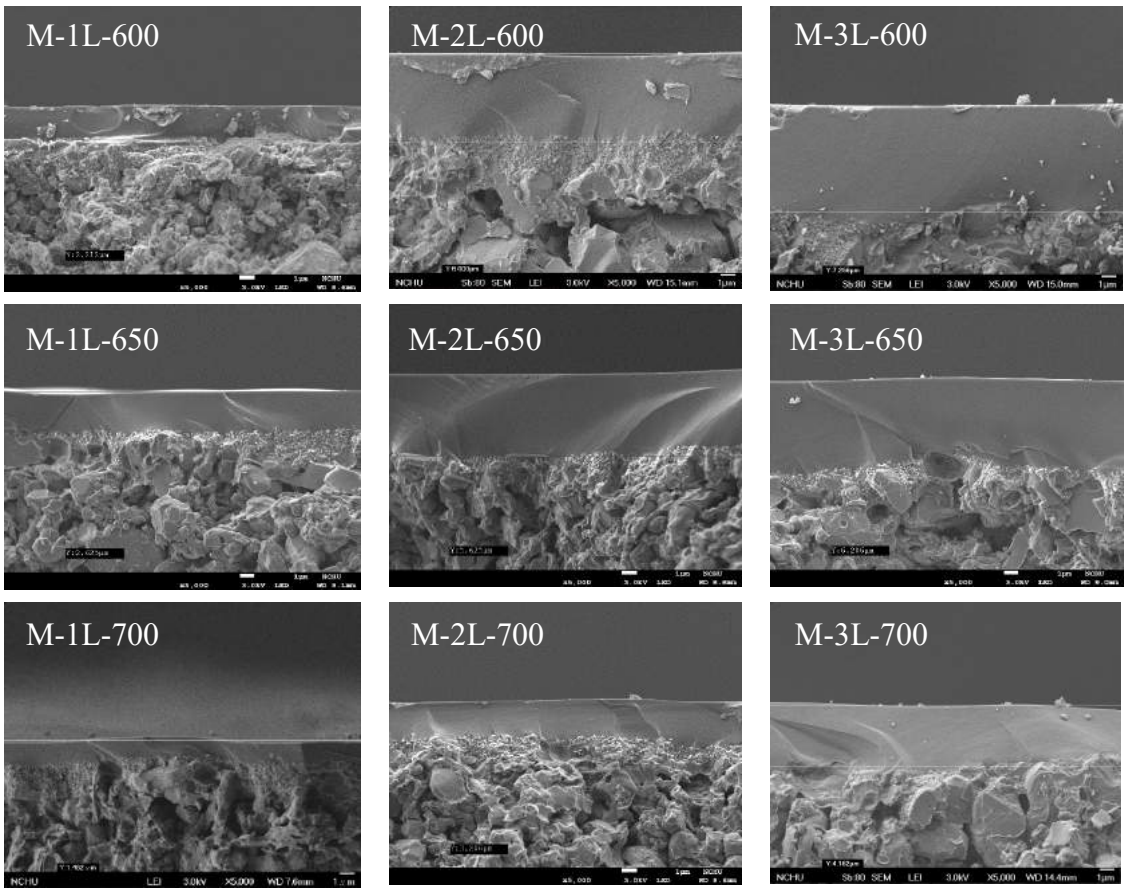

圖 5-4 以不同製備參數製備之薄膜其 FE-SEM 側面照

圖 5-5 為碳膜在不同塗佈層數及碳化溫度下對於氣體滲透分選能力的比較。由結果發現塗佈 1 層及 3 層高分子所製備而得之碳分子篩選薄膜其滲透表現較不穩定，滲透率及選擇率並無一統一趨勢。如碳化溫度為 600 ºC 下所製備出的碳膜，當塗佈層數為兩層之 M-2L-600 可獲得較佳之氣體滲透率，其次為 M-3L-600，再來是 M-1L-600，其 H_2 滲透率分別為 691.37、177.99、55.63 barrer，而 H_2/CO_2 選擇率的部分則是以塗佈 1 層之 M-1L-600 之效果最佳，其次為 M-2L-600，最後是 M-3L-600。

至於碳化溫度為 650 ºC 下所製備出的碳膜，以 M-3L-650 之 H_2 滲透率 1523.70 barrer 最高，其次分別為 M-1L-650 及 M-2L-650，各為 188.61 及 66.74 barrer；而 H_2/CO_2 選擇率則以 M-1L-650 > M-2L-650 > M-3L-650。

碳化溫度為 700 ºC 下之碳膜，H_2 滲透率趨勢為 M-3L-700 > M-2L-700 > M-1L-700，滲透率數據分別為 1100.36、55.90 及 9.63 barrer；選擇率則是以 M-2L-700 有最佳的表現，尤其是在 H_2/CO_2 及 O_2/N_2 分別有最高選擇率 5.05 及 15.14 之成果，其次則為 M-1L-700 > M-3L-700。

當塗佈層數太高使高分子層變厚，其不同層之間的受熱程度不同，拉伸應力亦不一樣，尤其若高分子在受熱時的拉伸應力大於薄膜層與基材間的吸附力，可能會導致製備好之薄膜出現裂縫，因此，塗佈層數為 2 之碳膜有較佳的氣體滲透表現。

在不同碳化溫度下所製得之碳膜以 650 ºC 時有最高之滲透率，其次是 700 ºC，最後是 600 ºC。此現象可歸究於當碳化溫度為 600 ºC 時，僅有部份熱穩定性較差之官能基及小支鏈始自高分子的主鏈段中脫附，因此留下的孔洞較少；然隨著碳化溫度升高至 650 ºC 時，由於熱裂解程度加劇會使更多官能基分解並且逐步斷鍵因而產生更多孔隙，故其滲透率較高；然而，隨著溫度再升高至 700 ºC 時，由於高分子層間收縮，改變排列的緊密度，導致滲透率稍微下降。雖然滲透率少有損失，但小氣動直徑的氣體選擇率卻因此提升；故當鍛燒溫度為 700 °C 時，可獲得最佳的選擇率。

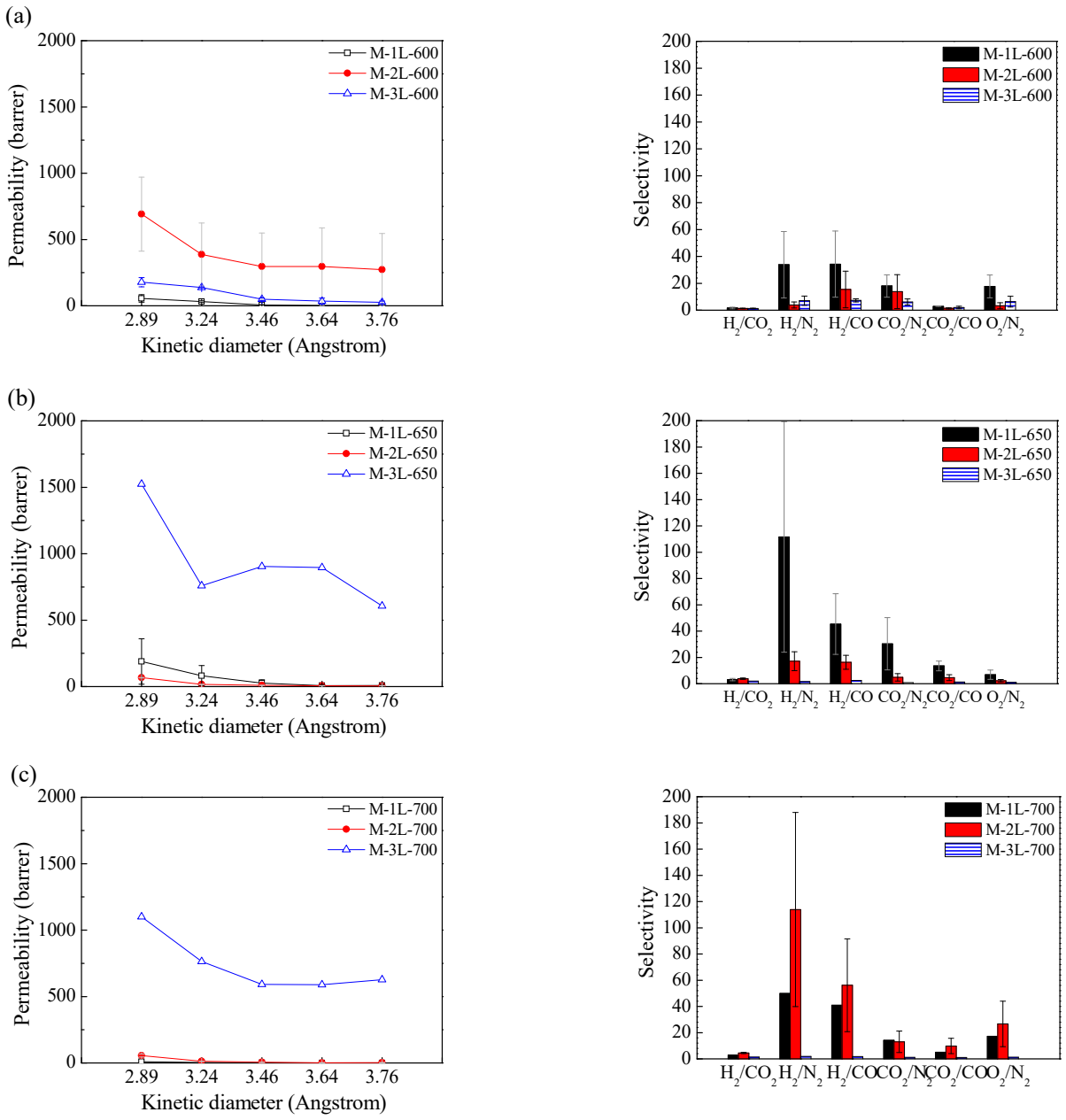

圖 5-5 在不同碳化溫度下(a) 600 °C、(b) 650 °C 及(c) 700 °C 於不同塗佈層數所製得之碳分子篩選薄膜其氣體滲透分選效能(1)氣體滲透率及(2)選擇率。

物質表面之接觸角大小代表液體對其濕潤情形，亦可作為評估此表面親疏水性之依據。為了鑑定疏水材塗佈於碳分子篩選薄膜對疏水性之改質成效，分別針對改質前後之碳膜進行接觸角量測。接觸角量測採動態分析，以每秒一筆，共量測 5 秒之記錄數據方式觀察膜面受液滴浸潤之狀態。量測結果記錄於表 5-2 中(量測結果為 5 秒平均值)。

由接觸角量測結果中發現，經過疏水材塗佈進行膜表面改質後之薄膜的疏水性有顯著提升，且經過 5~6 小時之水氣轉移反應後，薄膜仍能保有相當高之疏水性能。

表 5-2　碳分子篩選薄膜改質前後及反應後之接觸角

Membrane code	Non-modified membrane	Modified membrane	Modified membrane after reaction
Contact angle (°)			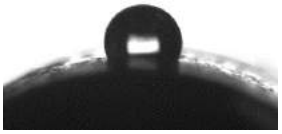
	83.89±2.54 °	106.43±0.76°	104.56±0.69°

5.2.3. 觸媒之基本特性

圖 5-6 為鍛燒前(a)及鍛燒後(b)之 Cu/Zn/SBA-16 觸媒經由 X 光繞射分析儀所繞射之圖譜。與標準圖譜對照後，其晶相轉換結果顯示，未經鍛燒之 Cu/ZnO/SBA16 觸媒主要由綠碳銅鋅礦(Aurichalite，$(Cu_{1-x}Zn_x)_5(OH)_6(CO_3)_2$，ICDD17-0743)，其主要特徵峰為 13.7° (2 0 0)；孔雀石(Malachite，$Cu_2CO_3(OH)_2$；ICDD 41-1390) 以及部分黑銅礦（Tenorite，CuO；ICDD 48-1548）、紅鋅礦（Zincite，ZnO；ICDD 36-1451）等晶相所組成[81,85-86]；而經鍛燒後的觸媒晶相則轉為以 CuO 和 ZnO 為主之組成，主要的特徵峰分別為 CuO 35.6°(111)及 ZnO 31.8°(110)[87]。

Nakamura 等人[88]曾利用 Zn 沉積於 Cu 之單一晶體進行 CO_2 合成甲醇。學者提出當 Zn 沉積於 Cu(111)之上會促進反應的進行，然而，當 Zn 沉積於 Cu(110)和 Cu(100)則會延遲反應進行。當製備出的 Cu/ZnO 觸媒其 Cu(111)特徵峰和 Cu(200)之特徵峰的強度比(intensity ratio)會伴隨前驅物之綠碳銅鋅礦的含量越高而越高之趨勢，代表銅微晶之形態會受到前趨物的改變而有所不同。觸媒前驅物中含有綠碳銅鋅礦組成之觸媒，其衍生出的觸媒選擇性與活性較佳，此結果可歸因於特定表面上的 Cu 位點如 Cu(111)表面若以 ZnO 進行改質可提高 Cu 的分散性[81]。

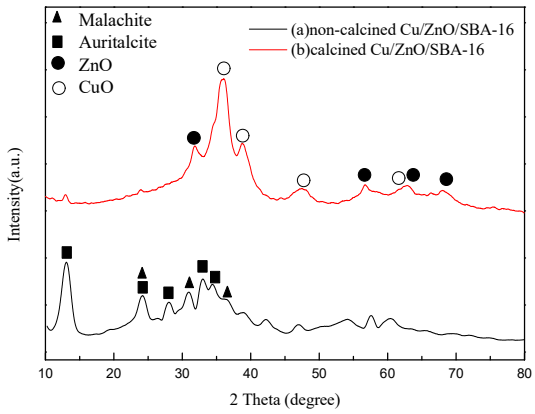

圖 5-6 Cu/Zn/SBA-16 觸媒鍛燒前(a)及鍛燒後(b)之 XRD 圖

圖 5-7 為(a)及 Cu/Zn/SBA-16(b)觸媒於不同倍率下所拍攝的 SEM 圖。利用 FE-SEM 圖可觀察觸媒之表面微結構－由圖(a1)、(a2)可觀察到以水熱合成法合成之 SBA-16 擔體具有球狀外觀型態及其表面微觀樣貌；然而，在以共沉澱法披覆活性相 Cu、Zn 之後，觸媒表面呈現貌似絨毛的形態，由此可推斷活性相沉積於 SBA-16 之外表面上，如圖 5-7 (b1)所示。再將放大倍率增加至 100k 如圖 5-7 (b2)後觀察絨毛結構的微觀形貌，發現實際上是由許多顆粒堆疊而成的板狀結構[89]。

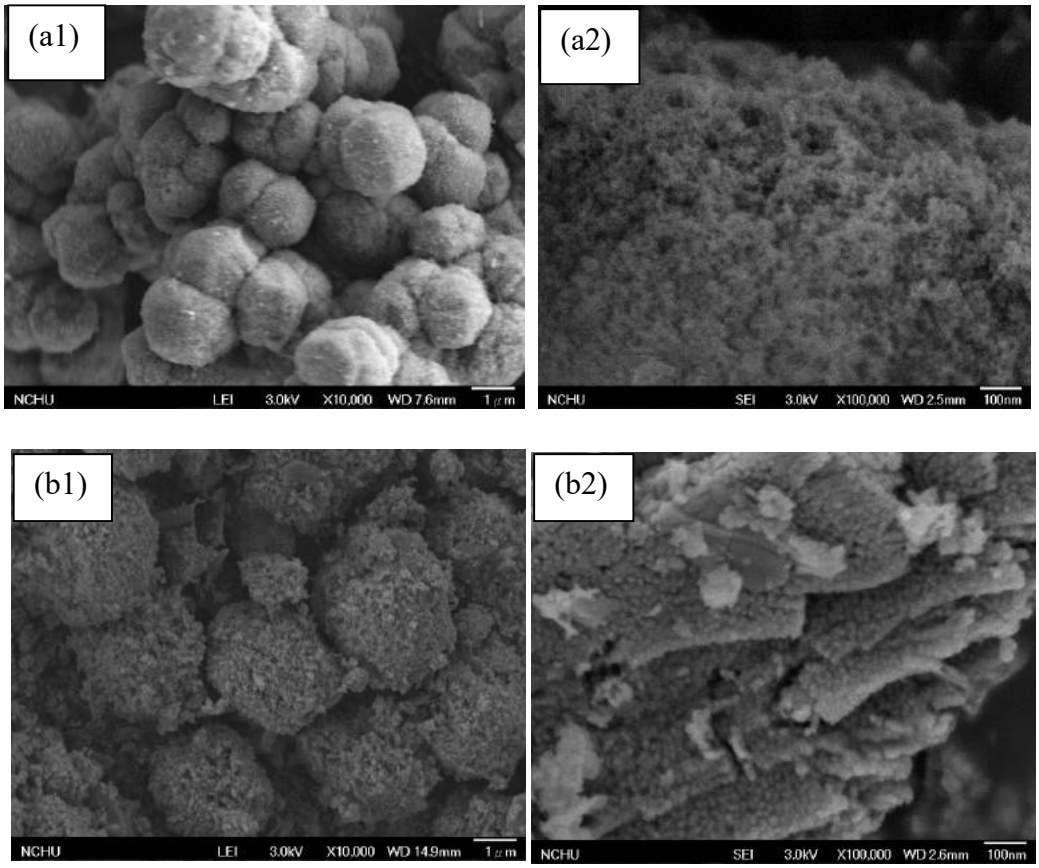

圖 5-7 SBA-16 擔體(a1)SBA-16-10k、(a2)SBA-16-100k 與 Cu/Zn/SBA-16 觸媒 (b1)Cu/Zn/SBA-16-10k、(b2)Cu/Zn/SBA-16-100k 之 FESEM 圖

表 5-3 為 SBA-16 擔體及 Cu/Zn/SBA-16 觸媒經 BET 分析後，並以 BJH 方程式所計算得之比表面積、平均孔徑及孔洞體積。經由分析數據結果顯示，SBA-16 擔體具有高比表面積，且其孔洞型態的分布以中孔和微孔為主，其平均孔徑為 50.18 Å，屬於中孔洞的材料。

經活性相 Cu 和 Zn 的披覆之後，製備而得之 Cu/Zn/SBA-16 觸媒之比表面積相較於 SBA-16 擔體大幅下降，由 611.34 m^2/g 減少至 81.18 m^2/g；而總孔體積亦有減少之趨勢，由 0.7669 cm^3/g 減少至 0.3329 cm^3/g；反之，平均孔徑有所提升，由 50.18 Å 增加至 164.01 Å，且孔洞型態的分布也從以微孔、中孔為主的結構轉變成以中孔、巨孔為主的結構。

由此現象推測可能是因為當活性相金屬負載於擔體時有部分進入其微孔道之中，造成微孔洞比例減少；另外亦有部分沉積於擔體表面，如 SEM 圖 5-7 所示，觸媒表面型貌呈現板狀堆疊，因此造成此結果。

表 5-3 擔體與觸媒之孔洞結構及特性

樣品	S_{BET} (m^2/g)	D_{pore} (Å)	V_{total} (cm^3/g)	V_{micro}	V_{meso} (cm^3/g)	V_{macro}
SBA-16	611.34	50.18	0.7669	0.2579 *(33.63%)*	0.4889 *(63.75%)*	0.0201 *(2.62%)*
Cu/Zn/SBA-16	81.18	164.01	0.3329	0.0313 *(9.4%)*	0.2444 *(73.42%)*	0.0572 *(17.18%)*

5.2.4. 薄膜反應器催化試驗

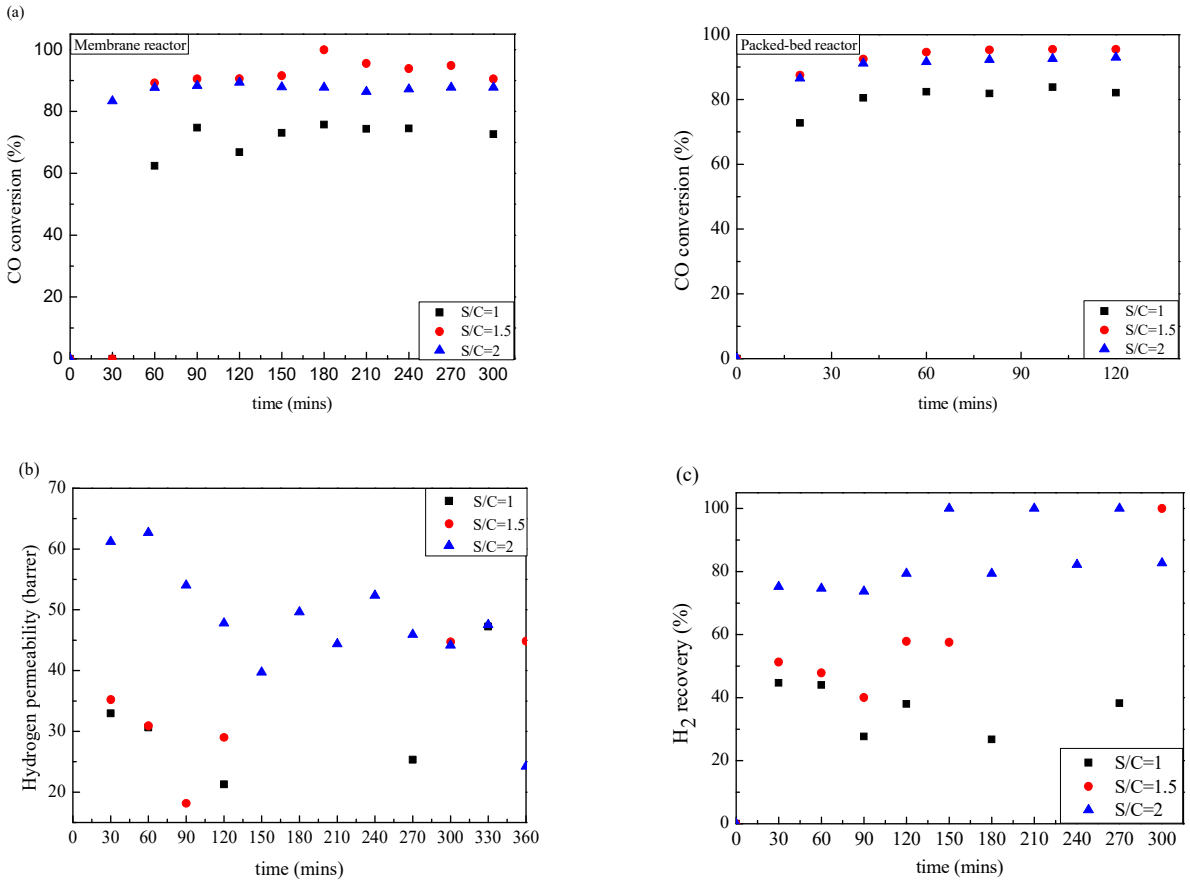

圖 5-8 不同水汽比條件下之(a1) 薄膜反應器與 (a2) 固定床反應器的 (a) CO 轉化率; (b) H_2 通量 (barrer); 及 (c) 氫氣回收率

在本研究的水汽比測試中，固定反應溫度為 300 ºC，分別進行了 S/C=1、S/C=1.5 及 S/C=2 的催化活性試驗。由圖 5-8 (a1)中可觀察到自水汽比 S/C=1 時 X_{CO} 可達 75.75%，當水汽比提升至 S/C=1.5 時可提升 X_{CO} 達 90%以上最高至 100%，然而，當 S/C=2 時，X_{CO} 卻降至 89%；將此結果與(a2)固定床之催化試驗相比較，當 S/C=1 時 X_{CO} 可達 81.36%，當水汽比提升至 S/C=1.5 時可提升 X_{CO} 至 95.43%，當 S/C=2 時，X_{CO}=92.95%，顯示固定床之最佳轉化率未及膜反應器的效能，然其在於 CO 轉化率上卻有較穩定成長的表現。另外，由圖 5-8 (c)可提供催化型膜反應器進行催化測試時其氫氣回收率隨時間的變化趨勢。由圖中顯示出在 S/C=1 和 S/C=1.5 時，氫氣回收率僅有 50~75%，然當水汽比提升至 S/C=2 時，氫氣回收率即可控制於 80%以上甚至達 100%。

為了有效提升膜反應器之 CO 轉化率，遂進行碳膜的改質，在其表面塗佈疏水層並同樣於 S/C=2 下進行水氣反應，結果如圖 5-9 所示。經過測試後發現經過改質的碳膜其 CO 轉化率可在反應半小時後即達平衡狀態並可促使 CO 轉化率達 100%。與未改質之碳膜比較兩者在高水汽量下的 CO 轉化率表現，發現經改質後的碳膜在轉化率方面確實有優化的現象。一般而言，不同觸媒之催化整體趨勢為反應器出口端之 CO 濃度的會與水汽比呈反比；當水汽比越高，意味著能提供更多的反應物，由於觸媒催化活性提升促使 CO 轉化率亦提高，因而降低出口端之 CO 濃度[90]。然而，經由測試結果發現本研究所使用的膜反應器其轉化效果會伴隨水汽比提高而降低，雖與預期結果不符合，但過去有學者[87,90]曾提出當催化反應於不同條件之水汽比下進行，當水汽含量較高，可能會吸附於觸媒表面活性位點並與 CO 發生競爭性吸附的現象，因而導致 CO 轉化率的下降。

而改質後之碳膜雖能提供較佳之 CO 轉化效果，然而，氫氣滲透率卻因為疏水材塗佈造成部分膜孔的阻塞，導致氫氣滲透率大幅下降(圖 5-9(b))。

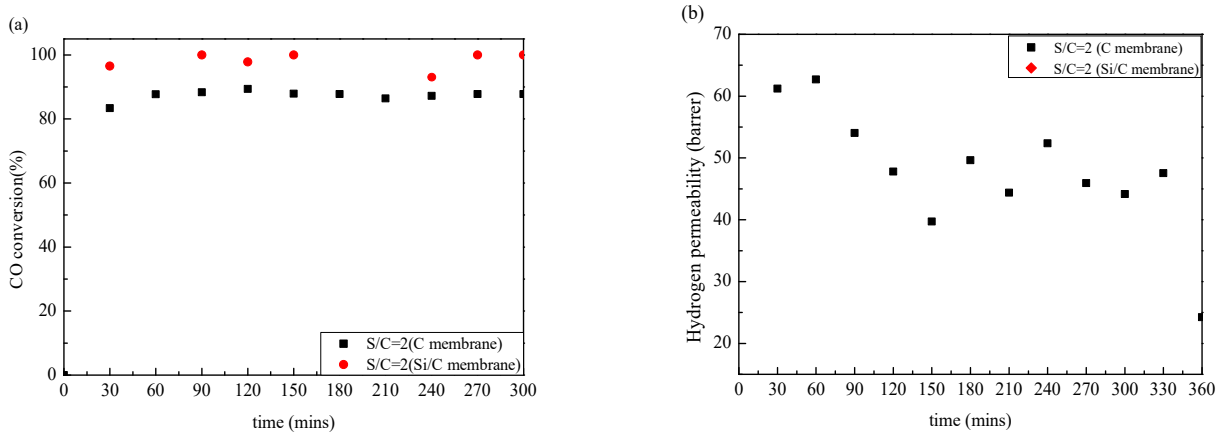

圖 5-9 當 S/C 為 2 時，改質前後之膜反應器的(a) CO 轉化率及(b)氫氣通量

5.3 小結

研究第三年以具有良好熱穩定性、環境耐受度佳及對 H_2/CO_2 具理想滲透分選效果之管柱型碳分子篩選薄膜作為膜材料，探討其作為膜反應器可能衍生之老化現象及疏水性改質之成效。為了優化碳分子篩選薄膜對於氣體之滲透分選效果，探討碳膜之製備條件包含：基材前處理、薄膜浸鍍條件、碳化溫度等。其中，基材前處理經由塗佈 TiO_2 修飾層，再經鍛燒、研磨、拋光處理後，可將基材粗糙度由 642.8 ± 88.52 減少至 109.5 ± 7.5 nm，尤以研磨、拋光處理的效果最佳。而製備所得之薄膜則以 M-2L-700 具有最佳的滲透-選擇率，H_2 滲透率為 55.90±11.37 barrer，O_2 滲透率為 5.4±1.75 barrer，H_2/CO_2 及 O_2/N_2 的選擇率則分別為 5.05 及 15.14。

水氣轉移觸媒 Cu/Zn/SBA-16 係以共沉澱法製備。當膜反應器之操作條件為反應溫度 300 ºC，空間速度 2,500 h^{-1}，水汽比為 1.5 時，膜反應器的 CO 轉化率可達到 99%以上，H_2 的回收率可達 76%，而 H_2 回收率則是隨著水汽比越高而有提升之趨勢，在 S/C=2 時，膜反應器之氫氣回收率亦可達 100%，然其 CO 轉化率卻降至 89%。由於水汽含量高時容易吸附於碳膜活性位基，導致碳膜老化。因此，在研究中利用疏水材進行碳膜改質，並發現其在 S/C=2 時仍可得到高 CO 轉化率；相較於固定床，膜反應器在 CO 轉化率及 H_2 回收率都有更佳的表現。

第六章 結果與建議

根據第一年的研究主題係在管柱式碳分子篩選薄膜的開發，評估製備參數如：溶液組成與濃度、真空輔助系統之影響、塗佈層數、基材浸沒與抽出速度。在此階段的實驗一共設計兩種溶劑、三種濃度、有無真空輔助系統、三種塗層、兩種基材移度速度，對碳膜表面結構觀察與進行氣體滲透試驗，來找出最佳的操作條件。由研究結果發現，使用高揮發性的氯仿做為溶劑，能製備出表面無缺陷的碳分子篩選薄膜，且在浸塗過程中使用真空輔助系統，能增加碳層與基材間的滲入行為，此現象有助於基材被有效修飾，因此大幅提升氣體選擇率。由研究結果發現使用真空輔助系統，以氯仿作為溶劑之 10 wt.% PEI，基材浸漬與浸沒與抽出速度為 1 mm/s、塗佈 5 次，具有最佳的氣體滲透與分選能力，PH_2 為 519、PCO_2 = 308.4、PO_2 = 210.1、PN_2 = 149.7、PCH_4 = 172.9 Barrer、H_2/CH_4 為 7.35、H_2/N_2 為 9.25。

本研究第二年研究主題係在碳分子篩型水氣轉移膜反應器的開發與老化機制評估，主要先針對第一年所開發出來之管柱式碳分子篩選薄膜進行改良，進一步探討鑄膜液濃度、基材浸於鑄膜液內抽真空之浸滯時間以及透過 TiO_2 修飾層改質基材等製程參數，對管柱式碳分子篩選薄膜於氣體分選效能之影響；並製備 Cu/ZnO/SBA–16 低溫水氣轉移觸媒，評估其反應最適當之空間速度、反應溫度等；並將上述兩者結合成為碳分子篩型水氣轉移膜反應器，比較與傳統的觸媒固定床反應器在催化反應表現上之差異。由研究結果顯示，使用高濃度的鑄膜液，以特定的抽真空浸滯時間塗覆低層數之高分子層，大幅提升氣體分子間之選擇率。透過 TiO_2 改質基材，使基材內部之巨孔結構得以受到有效之修飾，能夠有效改善鑄膜液滲入的情形增加薄膜之滲透率。水氣轉移催化反應方面，降低空間速度能夠有效的加速反應達平衡，並提高 CO 轉化率與氫氣生成率。使用碳分子篩型水氣轉移膜反應器進行催化反應，能夠致使氫氣的生成率大幅提升。由研究結果顯示，最佳之碳膜其 H_2/CO_2 選擇率為 3.58；H_2 滲透率為 2312 barrer、CO_2 滲透率為 768 barrer；在固定床催化反應方面，最佳之 CO 轉換率為 82.76%，而膜反應器則可以提升至 86.95%。

本研究第三年成功製備出具高 H_2/CO_2 選擇性的管柱式碳分子篩選薄膜，薄膜係透過三個製備程序的探討，包含(1)基材前處理，此階段又可細分為 Ti 前驅物製備程序探討、Ti 前驅物浸塗參數及機械拋光之條件測試、(2)碳膜浸塗條件及(3)碳化裂解條件等測試。隨後再將以共沉澱法合成之 Cu/Zn/SBA-16 觸媒與管柱式碳分子篩選薄膜整合作為催化型薄膜反應器以進行水氣轉移反應，並進行薄膜反應器疏水性改質前後的反應測試及再生評估。水氣轉移反應測試探討不同水汽比對於膜反應器催化效能如 CO 轉化率、H_2 回收率之影響，並同時藉此評估碳膜在水氣環境下的耐受程度。

由研究結果顯示基材前處理經由塗佈 TiO_2 修飾層，再經鍛燒、研磨、拋光處理後，可將基材粗糙度由 642.8 ± 88.52 減少至 109.5 ± 7.5 nm，尤以研磨加拋光處理的效果最佳。在不同製備條件下所製備而得之薄膜則以 M-2L-700 具有最佳的滲透-選擇率，H_2 滲透率為 55.90±11.37 barrer，O_2 滲透率為 5.4±1.75 barrer，H_2/CO_2 及 O_2/N_2 的選擇率則分別為 5.05 及 15.14。隨後整合水氣轉移觸媒 Cu/Zn/SBA-16 及碳膜構成膜反應器。當操作條件為反應溫度 300 ºC，空間速度 2,500 h^{-1}，水汽比為 1.5 時，膜反應器的 CO 轉化率可達到 99%以上，而 H_2 回收率則是隨著水汽比越高而有提升之趨勢；在 S/C=2 時，膜反應器之氫氣回收率亦可達 100%，然其 CO 轉化率卻降至 89%。由於水汽含量高時容易吸附於碳膜活性位基，導致碳膜老化。因此後續利用疏水材進行碳膜改質，發現膜反應器成功在 S/C=2 時回復到高 CO 轉化效果(約 100%)。

經由本計畫三年度的執行已成功製備出具有良好性能之管柱式碳膜反應器，且經由疏水保護層的塗覆可突破膜反應器之使用限制並維持其高 CO 轉化率的優異性能。未來建議可將膜反應器應用至更複雜的環境氣氛中，如常見的空氣污染氣體－H_2S、SO_2；將水汽比提高或延長反應時間，使之能更接近實廠的應用條件；另外，本研究中選用之疏水材雖能耐高溫，然其在常溫下會自行水解縮合成結晶顆粒，容易在塗佈於膜表層時造成膜孔阻塞，未來可再進一步的探討浸塗條件、溶液稀釋或採用碳氣凝膠(Graphene Aerogel)等方式進行改善。

參考文獻

[1] www.iea.org.

[2] 宋鴻，整體煤氣化聯合迴圈(IGCC)現狀及發展趨勢，第一情報---能源與環境，2009。

[3] Scholes, C.A., Smith, K.H., Kentish, S.E., Stevens G.W., 2010. CO_2 capture from pre-combustion processes-strategies for membrane gas separation. International Journal of Greenhouse Gas Control 4, 739-755.

[4] Steeneveldt, R., Berger ,B., Torp, T.A., 2006. CO_2 capture and storage. Closing the knowing-doing gap. Chem. Eng. Res. Des. 84(A9), 739–763.

[5] Thambimuthu, K., Soltanieh, M., Abandas, J.C., 2005. IPCC Special Report on Carbon Dioxide Capture and Storage. Series Cambridge University Press, Cambridge.

[6] Bracht, M., Alderliesten, P.T., Kloster, R., Pruschek, R., Haupt, G., Xue, E., Ross, J.R.H., Koukou, M.K., Papayannakos, N., 1997. Water gas shift membrane reactor for CO_2 control in IGCC systems: techno-economic feasibility study. Energy Convers. Mgmt. 38, S159–S164.

[7] Xue, E., O'Keeffe, M., Ross, J.R.H., 1996. Water-gas shift conversion using a feed with a low steam to carbon monoxide ratio and containing sulphur. Catal. Today 30, 107–118.

[8] Giessler, S., Jordan, L., Diniz da Costa, J.C., Lu, G.Q.M., 2003. Performance of hydrophobic and hydrophilic silica membrane reactors for the water gas shift reaction. Sep. Purif. Technol. 32, 255–264.

[9] Bredesen, R., Peters, T.A., 2008. In: Peinemann, K.-V., PereiraNunes, S.(Eds.), Membranes in Energy Systems with CO_2 Capture. Series Wiley-VCH, Weinheim, Germany.

[10] J. Sanchez and T.T. Tsotsis, in: Fundamentals in Inorganic Membrane Science and Technology, eds. A.J. Burggraaf and L. Cot (Elsevier, 1996) ch. 11.

[11] Adhikari, S., Fernando, S., 2006. Hydrogen membrane separation techniques. Ind. Eng. Chem. Res. 45, 875–881.

[12] Paglieri, S.N., Way, J.D., 2002. Innovations in palladium membrane research. Sep. Purif. Methods 31, 1–169.

[13] Scholes, C.A., Kentish, S.E., Stevens, G.W., 2009. Effects of minor components in carbon dioxide capture using polymeric gas separation membranes. Sep. Purif. Rev. 38, 1–44.

[14] Lu, G.Q., Diniz da Costa, J.C., Duke, M., Giessler, S., Socolow, R., Williams, R.H., Kreutz, T.G., 2007. Inorganic membranes for hydrogen production and purification: a critical review and perspective. J. Colloid Interface Sci. 314, 589–603.

[15] Lee, L.-L., Tsai, D.-S., 2001. Synthesis and permeation properties of silicon-carbon based inorganic membrane for gas separation. Ind. Eng. Chem. Res. 40, 612–616.

[16] Tseng, H.H., Kumar, I.A., Weng, T.H., Li, Y.L. SBA-15/CMS composite membrane for H_2 purification and CO_2 capture: Effect of pore size, pore volume, and loading weight on separation performance, Microporous & Mesoporous Materials 180 (2013) 270-279.

[17] Harale, A., Hwang, H.T., Liu, P.K.T., Sahimi, M., Tsotsis, T.T., 2007. Experimental studies of a hybrid adsorbent-membrane reactor (HAMR) system for hydrogen production. Chem. Eng. Sci. 62, 4126–4137.

[18] Sa´, S., Silva, H., Sousa, J.M., Mendes, A., 2009. Hydrogen production by methanol steam reforming in a membrane reactor: Palladium vs carbon molecular sieve membranes. J. Membr. Sci. 339,160–170.

[19] Zhang, X., Hu, H., Zhu, Y., Zhu, S., 2006. Methanol Steam Reforming to Hydrogen in a Carbon Membrane Reactor System. Ind. Eng. Chem. Res. 45, 7997–8001.

[20] Agrell, J., Birgersson, H., Boutonnet, M., Melia´n-Cabrera, I., Navarro, R. M., Fierro, J.L.G., 2003. Production of hydrogen from methanol over Cu/ZnO catalysts promoted by ZrO_2 and Al_2O_3. J. Catalysis 219, 389–403.

[21] A´guila, G., Jime´nez, J., Guerrero, S., Gracia, F., Chornik, B., Quinteros, S., Araya, P., 2009. A novel method for preparing high surface area copper zirconia catalysts: Influence of the preparation variables. Appl. Catal. A: General 360, 98–105.

[22] Jones, C.W., Koros, W.J., 1995. Carbon composite membranes: a solution to adverse humidity effects, Ind. Eng. Chem. Res. 34, 164.
[23] Men´endez, J.A., Philips, B., Xia, J., Radovic, L.R., 1996. On the modification and characterization of chemical surface properties of activated carbon: in the search of carbons with stable basic properties, Langmuir 12, 4404.
[24] D. Grosso, How to exploit the full potential of the dip-coating process to better control film formation, Journal of Materials Chemistry, 21 (2011) 17033-17038.
[25] M. Faustini, B. Louis, P.A. Albouy, M. Kuemmel, D. Grosso, Preparation of Sol−Gel Films by Dip-Coating in Extreme Conditions, The Journal of Physical Chemistry C, 114 (2010) 7637-7645.
[26] C. Strobel, A. Kadow-Romacker, T. Witascheck, G. Schmidmaier, B. Wildemann, Evaluation of process parameter of an automated dip-coating, Materials Letters, 65 (2011) 3621-3624.
[27] F.Y. Ding Xiaobin, Xu Nanping, Modeling and control of cermic membrane thickness during dip coating process, Chemical Industry and Engineering (China), 57 (2006).
[28] H.-H. Tseng, P.-T. Shiu, Y.-S. Lin, Effect of mesoporous silica modification on the structure of hybrid carbon membrane for hydrogen separation, International journal of hydrogen energy, 36 (2011) 15352-15363.
[29] Y. Huang, R. Dittmeyer, Preparation of thin palladium membranes on a porous support with rough surface, Journal of Membrane Science, 302 (2007) 160-170.
[30] P. Kumar, J. Ida, S. Kim, V. Guliants, J. Lin, Ordered mesoporous membranes: Effects of support and surfactant removal conditions on membrane quality, Journal of Membrane Science, 279 (2006) 539-547.
[31] Wang, C., et al., Intermediate gel coating on macroporous Al_2O_3 substrate for fabrication of thin carbon membranes. Ceramics International, 2014. **40**(7, Part B): p. 10367-10373.
[32] Nik, O.G., X.Y. Chen, and S. Kaliaguine, Amine-functionalized zeolite FAU/EMT-polyimide mixed matrix membranes for CO_2/CH_4 separation. Journal of Membrane Science, 2011. 379(1–2): p. 468-478.
[33] Ebadi Amooghin, A., M. Omidkhah, and A. Kargari, The effects of aminosilane grafting on NaY zeolite–Matrimid®5218 mixed matrix membranes for CO_2/CH_4 separation. Journal of Membrane Science, 2015. 490: p. 364-379.
[34] Kumar, P., J. Ida, S. Kim, V.V. Guliants, and J.Y.S. Lin, Ordered mesoporous membranes: Effects of support and surfactant removal conditions on membrane quality. Journal of Membrane Science, 2006. 279(1–2): p. 539-547.
[35] Huang, Y. and R. Dittmeyer, Preparation of thin palladium membranes on a porous support with rough surface. Journal of Membrane Science, 2007. 302(1–2): p. 160-170.
[36] Tseng, H.-H., P.-T. Shiu, and Y.-S. Lin, Effect of mesoporous silica modification on the structure of hybrid carbon membrane for hydrogen separation. International Journal of Hydrogen Energy, 2011. 36(23): p. 15352-15363.
[37] Tseng, H.-H., C.-T. Wang, G.-L. Zhuang, P. Uchytil, J. Reznickova, and K. Setnickova, Enhanced H_2/CH_4 and H_2/CO_2 separation by carbon molecular sieve membrane coated on titania modified alumina support: Effects of TiO_2 intermediate layer preparation variables on interfacial adhesion. Journal of Membrane Science, 2016. 510: p. 391-404.
[38] Qi, H., Y. Fan, W. Xing, and L. Winnubst, Effect of TiO_2 doping on the characteristics of macroporous Al_2O_3/TiO_2 membrane supports. Journal of the European Ceramic Society, 2010. 30(6): p. 1317-1325.
[39] Ouellette, R.J. and J.D. Rawn, Introduction to Organic Reaction Mechanisms, in Organic Chemistry. 2014, Elsevier: Boston. p. 75-110.
[40] Atkins, P.W. and L.L. Jones, Chemical Principle –The Quest for Insight. W. H. Freeman and Company, 2008. 4th ed.
[41] Zhao, S., T. Luo, and R.J. Gorte, Deactivation of the water–gas-shift activity of Pd/ceria by Mo. Journal of Catalysis, 2004. 221(2): p. 413-420.
[42] Babita, K., S. Sridhar, and K.V. Raghavan, Membrane reactors for fuel cell quality hydrogen through WGSR – Review of their status, challenges and opportunities. International Journal of Hydrogen Energy, 2011. 36(11): p. 6671-6688.

[43] Abdollahi, M., J. Yu, P.K.T. Liu, R. Ciora, M. Sahimi, and T.T. Tsotsis, Hydrogen production from coal-derived syngas using a catalytic membrane reactor based process. Journal of Membrane Science, 2010. 363(1–2): p. 160-169.
[44] Ladebeck, J.R. and J.P. Wagner, Handbook of Fuel Cells-Fundamentals, Technology and Applications. Vol. Chichester. 2003: Wiley.
[45] Mendes, D., A. Mendes, L.M. Madeira, A. Iulianelli, J.M. Sousa, and A. Basile, The water-gas shift reaction: from conventional catalytic systems to Pd-based membrane reactors—a review. Asia-Pacific Journal of Chemical Engineering, 2010. 5(1): p. 111-137.
[46] Galuszka, J., T. Giddings, and G. Iaquaniello, Membrane assisted WGSR – Experimental study and reactor modeling. Chemical Engineering Journal, 2012. 213(0): p. 363-370.
[47] Basile, A., A. Criscuoli, F. Santella, and E. Drioli, Membrane reactor for water gas shift reaction. Gas Separation & Purification, 1996. 10(4): p. 243-254.
[48] Utaka, T., T. Okanishi, T. Takeguchi, R. Kikuchi, and K. Eguchi, Water gas shift reaction of reformed fuel over supported Ru catalysts. Applied Catalysis A: General, 2003. 245(2): p. 343-351.
[49] Basile, A., G. Chiappetta, S. Tosti, and V. Violante, Experimental and simulation of both Pd and Pd/Ag for a water gas shift membrane reactor. Separation and Purification Technology, 2001. 25(1–3): p. 549-571.
[50] Androver, M.E., E. Lopez, D.O. Borio, and M.N. Pedernera, Theoretical study of a membrane reactor for the watergas shift reaction under non-isothermal conditions. American Institute of Chemical Engineers Journal, 2009. 55: p. 3206-3213.
[51] Moustafa, T.M. and S.S.E.H. Elnashaie, Simultaneous production of styrene and cyclohexane in an integrated membrane reactor. Journal of Membrane Science, 2000. 178(1–2): p. 171-184.
[52] Ma, D. and C.R.F. Lund, Assessing high-temperature water−gas shift membrane reactors. Industrial & Engineering Chemistry Research, 2003. 42(4): p. 711-717.
[53] Basile, A., E. Drioli, F. Santell, V. Violante, G. Capannelli, and G. Vitulli, A study on catalytic membrane reactors for water gas shift reaction. Gas Separation & Purification, 1996. 10(1): p. 53-61.
[54] Kikuchi, E., S. Uemiya, N. Sato, H. Inoue, H. Ando, and T. Matsuda, Membrane reactor using microporous glass-supported thin film of palladium. Application to the water gas shift reaction. Chemistry Letters, 1989. 18(3): p. 489-492.
[55] Tosti, S., A. Basile, G. Chiappetta, C. Rizzello, and V. Violante, Pd–Ag membrane reactors for water gas shift reaction. Chemical Engineering Journal, 2003. 93(1): p. 23-30.
[56] Chiappetta, G., G. Clarizia, and E. Drioli, International congress on membranes and membrane processesanalysis of safety aspects in a membrane reactor. Desalination, 2006. 193(1): p. 267-279.
[57] H.-H. Tseng, C.-T. Wang, G.-L. Zhuang, P. Uchytil, J. Reznickova, K. Setnickova, Enhanced H_2/CH_4 and H_2/CO_2 separation by carbon molecular sieve membrane coated on titania modified alumina support: Effects of TiO_2 intermediate layer preparation variables on interfacial adhesion, Journal of Membrane Science, 510 (2016) 391-404.
[58] T. Okubo, K. Haruta, K. Kusakabe, S. Morooka, H. Anzai, S. Akiyama, Preparation of a sol-gel derived thin membrane on a porous ceramic hollow fiber by the filtration technique, Journal of Membrane Science, 59 (1991) 73-80.
[59] J. Smid, C.G. Avci, V. Günay, R.A. Terpstra, J.P.G.M. Van Eijk, Preparation and characterization of microporous ceramic hollow fibre membranes, Journal of Membrane Science, 112 (1996) 85-90.
[60] S.T. Oyama, Y. Gu, Hydrogen-Selective Silica-Based Membrane, US Patent 7179325, Assigned to Virginia Tech Intellectual Properties Inc., (2007).
[61] M. Imran, S. Riaz, S. Naseem, Synthesis and Characterization of Titania Nanoparticles by Sol-gel Technique, Materials Today: Proceedings, 2 (2015) 5455-5461.
[62] A.V. Vinogradov, V.V. Vinogradov, Low-temperature sol–gel synthesis of crystalline materials, RSC Advances, 4 (2014) 45903-45919.
[63] M. Mulder, Basic Principles of Membrane Technology, Kluwer Acadenic Publoshers, (1996).
[64] H.J. Lee, E. Magnone, J.H. Park, Preparation, characterization and laboratory-scale application of modified hydrophobic aluminum oxide hollow fiber membrane for CO_2 capture using H_2O as low-cost absorbent, Journal of Membrane Science, 494 (2015) 143-153.
[65] H.J. Lee, J.H. Park, Effect of hydrophobic modification on carbon dioxide absorption using porous

alumina (Al_2O_3) hollow fiber membrane contactor, Journal of Membrane Science, 518 (2016) 79-87.
[66] C.W. Jones, W.J. Koros, Carbon Composite Membranes: A Solution to Adverse Humidity Effects, Industrial & Engineering Chemistry Research, 34 (1995) 164-167.
[67] H.-H. Tseng, G.-L. Zhuang, M.-D. Lin, S.-H. Chang, M.-Y. Wey, The influence of matrix structure and thermal annealing-hydrophobic layer on the performance and durability of carbon molecular sieving membrane during physical aging, Journal of Membrane Science, 495 (2015) 294-304.
[68] N.M. Selivanova, N.V. Sautina, D.V. Vezenov, O.V. Stoyanov, Y.G. Galyametdinov, Evaluation of interactions between liquid crystal films and silane monolayers by atomic force microscopy, Journal of Molecular Liquids, 230 (2017) 574-578.
[69] B. Arkles, Hydrophobicity, hydrophilicity and silane surface modification, Gelest Inc, Morrisville, (2011).
[70] C. Picard, A. Larbot, F. Guida-Pietrasanta, B. Boutevin, A. Ratsimihety, Grafting of ceramic membranes by fluorinated silanes: hydrophobic features, Separation and Purification Technology, 25 (2001) 65-69.
[71] A.M. Kansara, S.G. Chaudhri, P.S. Singh, A facile one-step preparation method of recyclable superhydrophobic polypropylene membrane for oil–water separation, RSC Adv., 6 (2016) 61129-61136.
[72] M.-Y. Wey, H.-H. Tseng, C.-k. Chiang, Improving the mechanical strength and gas separation performance of CMS membranes by simply sintering treatment of α-Al $_2O_3$ support, Journal of Membrane Science, 453 (2014) 603-613.
[73] Lima, F.V., P. Daoutidis, and M. Tsapatsis, Modeling, optimization, and cost analysis of an IGCC plant with a membrane reactor for carbon capture. American Institute of Chemical Engineers Journal, 2016. 62(5): p. 1568-1580.
[74] Koc, R., N.K. Kazantzis, W.J. Nuttall, and Y.H. Ma, Economic assessment of inherently safe membrane reactor technology options integrated into IGCC power plants. Process Safety and Environmental Protection, 2012. 90(5): p. 436-450.
[75] Chiesa, P., T.G. Kreutz, and G.G. Lozza, CO_2 sequestration from IGCC power plants by means of metallic membranes. Journal of Engineering for Gas Turbines and Power, 2005. 129(1): p. 123-134.
[76] K. Briceño, D. Montané, R. Garcia-Valls, A. Iulianelli, A. Basile, Fabrication variables affecting the structure and properties of supported carbon molecular sieve membranes for hydrogen separation, Journal of Membrane Science, 415–416 (2012) 288-297.
[77] 王敬婷，利用二氧化鈦中間層改善碳分子篩選薄膜黏附特性與增加氣體分離性能之研究，中山醫學大學職業安全衛生學系碩士論文，(2014)。
[78] 涂逸寧，催化型碳分子篩選膜反應器應用於 IGCC 發電技術之 H_2 純化與 CO_2 捕獲之研究，國立中興大學環境工程研究所碩士論文，(2016)。
[79] H. Qi, Y. Fan, W. Xing, L. Winnubst, Effect of TiO_2 doping on the characteristics of macroporous Al_2O_3/TiO_2 membrane supports, Journal of the European Ceramic Society, 30 (2010) 1317-1325.
[80] A. Matthews, The crystallization of anatase and rutile from amorphous titanium dioxide under hydrothermal conditions, American Mineralogis, 61 (1976) 419-424.
[81] A. Budiman, M. Ridwan, S.M. Kim, J.-W. Choi, C.W. Yoon, J.-M. Ha, D.J. Suh, Y.-W. Suh, Design and preparation of high-surface-area $Cu/ZnO/Al_2O_3$ catalysts using a modified co-precipitation method for the water-gas shift reaction, Applied Catalysis A: General, 462-463 (2013) 220-226.
[82] D. Grosso, How to exploit the full potential of the dip-coating process to better control film formation, Journal of Materials Chemistry, 21 (2011) 17033-17038.
[83] N. Hameed, J. Sharp, S. Nunna, C. Creighton, K. Magniez, P. Jyotishkumar, N.V. Salim, B. Fox, Structural transformation of polyacrylonitrile fibers during stabilization and low temperature carbonization, Polymer Degradation and Stability, 128 (2016) 39-45.
[84] P.J. Sánchez-Soto, M.A. Avilés, J.C. del Río, J.M. Ginés, J. Pascual, J.L. Pérez-Rodríguez, Thermal study of the effect of several solvents on polymerization of acrylonitrile and their subsequent pyrolysis, Journal of Analytical and Applied Pyrolysis, 58 (2001) 155-172.
[85] 梁紹嵐，三維中孔 SBA-16 擔載 Cu/ZnO 觸媒應用於低溫水氣轉移反應之研究，國立中興大學環境工程研究所學士論文，(2017)。

[86] Y. Jeong, I. Kim, J.Y. Kang, H. Jeong, J.K. Park, J.H. Park, J.C. Jung, Alcohol-assisted low temperature methanol synthesis from syngas over Cu/ZnO catalysts: Effect of pH value in the co-precipitation step, Journal of Molecular Catalysis A: Chemical, 400 (2015) 132-138.
[87] S.-i. Fujita, Y. Kanamori, A.M. Satriyo, N. Takezawa, Methanol synthesis from CO_2 over Cu/ZnO catalysts prepared from various coprecipitated precursors, Catalysis Today, 45 (1998) 241-244.
[88] J. Nakamura, I. Nakamura, T. Uchijima, T. Watanabe, T. Fujitani, Model studies of methanol synthesis on copper catalysts, Studies in Surface Science and Catalysis, 101 (1996) 1389-1399.
[89] Y. Jeong, I. Kim, J.Y. Kang, N. Yan, H. Jeong, J.K. Park, J.H. Park, J.C. Jung, Effect of the aging time of the precipitate on the activity of Cu/ZnO catalysts for alcohol-assisted low temperature methanol synthesis, Journal of Molecular Catalysis A: Chemical, 418 (2016) 168-174.
[90] B. Liu, Q. Zong, X. Du, Z. Zhang, T. Xiao, H. AlMegren, Novel sour water gas shift catalyst (SWGS) for lean steam to gas ratio applications, Fuel Processing Technology, 134 (2015) 65-72.

Journal of Membrane Science 510 (2016) 391–404

Contents lists available at ScienceDirect

Journal of Membrane Science

journal homepage: www.elsevier.com/locate/memsci

Enhanced H_2/CH_4 and H_2/CO_2 separation by carbon molecular sieve membrane coated on titania modified alumina support: Effects of TiO_2 intermediate layer preparation variables on interfacial adhesion

Hui-Hsin Tseng [a,b,*], Ching-Ting Wang [a,b], Guo-Liang Zhuang [c], Petr Uchytil [d], Jirina Reznickova [d], Katka Setnickova [d]

[a] School of Occupational Safety and Health, Chung Shan Medical University, No. 110, Sec. 1, Jianguo N. Rd., Taichung City, Taiwan, ROC
[b] Department of Occupational Medicine, Chung Shan Medical University Hospital, No.110, Sec. 1, Jianguo N. Rd., Taichung City, Taiwan, ROC
[c] Department of Environmental Engineering, National Chung Hsing University, Taichung 402, Taiwan, ROC
[d] Institute of Chemical Process Fundamentals v.v.i., Academy of Sciences of the Czech Republic, Czech Republic

ARTICLE INFO

Article history:
Received 15 October 2015
Received in revised form
16 February 2016
Accepted 18 February 2016
Available online 12 March 2016

Keywords:
Carbon membrane
Intermediate layer
TiO_2
Adhesion
Gas separation

ABSTRACT

A new CMS membrane with smaller gas pair H_2/CO_2 and H_2/CH_4 separation factor of approximately 8.3 and 726, with an H_2 permeability of 600.7 Barrer, was synthesized by coating it on titanium gel-modified alumina supports. After calcination, the titanium gel provided an interconnected nano-network intermediate layer for casting dope to penetrate the support and form an interlocking matrix. By adjusting the hydrolysis-condensation rate using acid catalysts, the intermediate layer structure can be modified, which is beneficial for supporting CMS membrane with high adhesion, but not with an interlocking depth too high to increase mass-transfer resistance. Three adhesion mechanisms are proposed in this study to investigate intrinsic adhesion of the selective layer on the TiO_2/Al_2O_3 composite support. These mechanism are mechanical interlocking, chemical bonding, and adsorption. The relationship between permselectivity and adhesion was also evaluated. An adequate/slight pore penetration with strong mechanical interlocking can enhance adhesion without sacrificing high permeance. The new CMS membrane is a promising candidate for electricity generation/hydrogen production with CO_2-capture and oxygen-fuel applications.

1. Introduction

Inorganic membrane-based separation processes are recognized as compelling technologies for H_2 purification and CO_2 capture from power generation systems, such as processes involving the pre-combustion of coal or biomass, in which high-pressure CO_2 and H_2 generated. A high demand for inorganic membrane technology for the separation of these two components exists because of the high temperature and pressure requirements [1,2].

In general, CMS membranes are fabricated via carbonization of a polymer precursor, such as polyetherimide (PEI), polyimide (PI), or poly(furfuryl alcohol) (PFA), at a high temperature in an inert atmosphere or under vacuum, which have exhibited a permselectivity performance exceeding those of their polymeric precursor membranes [3,4]. Such high performances have been observed in O_2/N_2, CO_2/CH_4, CO_2/N_2, H_2/CO_2, etc. [5–10] and some researches [11–16]. The geometry of CMS membrane can be tailored to accommodate characteristics of the mixture to be processed, such as self-standing flat membranes [17,18], asymmetric hollow fiber [19,20], or supported membranes [21–25]. For realistic large-scale gas separation applications, superior CMS dense films and asymmetric hollow fiber are recognized as a viable configuration, whereas hydrogen selective and permeable process are better dealt with using the supported type; for instance, in catalytic membrane reactors, where highly selective supported membranes in tubular configuration are used to achieve optimal integration of the membrane and catalyst [23]. Recently, Koros's groups have fabricated self-standing CMS hollow fiber membranes [19,20] that demonstrated enough mechanical strength to handle high pressure, with a high packing density and low membrane cost compared with supported CMS membranes; however, the permeance is not as high as predicted by the high permeability because a much thicker effective separation layer formed by substructure collapse occurred [19]; in addition, smaller gas separation data were not reported in the paper; thus, the behavior of this CMS in smaller gas pair separation remains unclear. Nevertheless,

* Corresponding author at: School of Occupational Safety and Health, Chung Shan Medical University, No.110, Sec. 1, Jianguo N. Rd., Taichung City, Taiwan, ROC.
E-mail address: hhtseng@csmu.edu.tw (H.-H. Tseng).

http://dx.doi.org/10.1016/j.memsci.2016.02.036
0376-7388/

to reduce membrane thickness to the micron range ($<10\ \mu m$) while increasing mechanical strength, different studies focused on supported membrane [21–25] in which the influence of supporting material is significant to the carbon membrane properties [23,26–28]. These membranes consist of a thin ($<10\ \mu m$) and dense top layer (i.e., selective layer), and a porous supporting layer. A key step in the preparation of ultra-microporous CMS membranes is support preparation [26] because the properties of selective layers strongly depend on support structure, such as surface roughness, porosity, and pore size distribution [27,28].

Numerous studies have processed α-Al_2O_3 into homogeneous and highly porous supports given its availability and low cost [29–31]. However, the highly porous and rougher structure allows for doping solution during polymer casting by penetrating the support layer more easily, thereby resulting in a discontinuous membrane. Furthermore, the thermal expansion coefficient of α-Al_2O_3 largely differs from that of most polymer materials. When the materials are heated to high temperatures, the thin dense polymer film (precursor) coated on the surface of α-Al_2O_3 supports usually cracks [32]. Thus, considering the porous structure and the difference in thermal expansion behavior between α-Al_2O_3 supports and polymer film, the selective layer must be thick; otherwise, the layer must undergo several coating-pyrolysis cycles to prevent cracks from forming during carbonization. However, a relatively low permeability was usually observed [33,34].

An alternative method might be to add an intermediate layer (gutter layer) to form a composite membrane. Recently, a γ-alumina-modified α-Al_2O_3 supported CMS membrane was fabricated by Ma et al. [27] for smaller gas (He, H_2, CO_2, O_2, N_2, and CH_4) and C_3H_6/C_3H_8 separation. By taking advantage of the γ-alumina support, defect-free and 1.6 μm-thick CMS membrane were successfully prepared through a single coating; at room temperature, their membrane showed an O_2/N_2 ideal selectivity of 5.1, and an O_2 permanence of 9.7×10^{-9} mol m^{-2} s^{-1} Pa^{-1} (28.9 GPU) for O_2/N_2 separation. In our previous paper, we described the fabrication of mordenite framework inverted (MFI) zeolite intermediate layers-modified CMS membrane for smaller gas separation [35]. With the a-oriented crystallites of zeolite layer, the intermediate layer provided an additional gutter for gas diffusion, and improved interfacial adhesion by forming coordinate bonds between Si^{3+}(Si–O) and N (–NH bonds of PEI precursor). The CMS layer thickness (~2.6 μm) was obtained through a one-time coating-pyrolysis procedure, and the M1400-MFI-2 showed an O_2/N_2 ideal selectivity of 9 ± 0.7, and an O_2 permeability of 221 ± 15 Barrer (81.85 GPU) for O_2/N_2 separation. These results demonstrated that perm-selectivity and mechanical strength can be simultaneously improved without sacrificing high permeance if a thin and defect-free CMS membrane could be formed on applicable supporting materials, especially on the porous structured intermediate layer.

As noted above, this work focuses on synthesizing a nanonetworked structure of TiO_2 as an intermediate layer into CMS membranes. The following characteristic changes are expected:

1. A nanonetworked structure of TiO_2 intermediate layer provided an interconnected system for the casting dope to penetrate, and modified the “interlocking pattern” between the CMS layer and the support.
2. Increased interactions with the dope through stronger adsorption and possible surface flow.
3. Increase micro-pore volume within the carbon matrix (chain effect).

A sol–gel method is used to prepare the TiO_2 intermediate layer on the Al_2O_3 support surface. This method is the main one used to produce titania in the laboratory scale, and exhibits a number of advantages over conventional methods such as product homogeneity, and a controllable size, crystal phase, and microstructure [36]. In this process, titania is usually prepared via hydrolysis and condensation reactions of titanium alkoxides. Titanium alkoxide hydrolyzes vigorously in water, and many catalysts (typically simple acids, such as nitric acid, hydrochloric acid, acetic acid, and sulfuric acid) have been applied to lower reaction rates [37–39] and control TiO_2 nanonetwork dimensions.

Thus, in the current work, the effects of TiO_2 nanonetwork physicochemical properties on the CMS layer texture and gas separation performance of the CMS membrane were investigated. Preparation variables of the TiO_2 intermediate layer were investigated, and the interaction mechanism (adhesion) [40] between the Al_2O_3 support and CMS layer was also evaluated. Three techniques (field emission-scanning electron microscopy line scanning, Fourier transform infrared spectroscopy, and contact angle) were used to determine individual contributions of mechanical interlocking, chemical bonding, and the adsorption-to-adhesion mechanism. Our results indicate that the TiO_2 intermediate layer controls the interlocking pattern between the selective layer and porous Al_2O_3 support. The CMS membrane supported on the bare Al_2O_3 substrate has a separation performance of $Q_{H_2}=537.5$ Barrer and $\alpha_{H_2/CH_4}=197.6$. After modifying the CMS membrane supported on a TiO_2/Al_2O_3 substrate with a TiO_2 layer, a superior selectivity of $\alpha_{H_2/CH_4}=725.9\pm15.1$, $\alpha_{H_2/CO_2}=8.26\pm0.27$, and $\alpha_{CO_2/CH_4}=87.9\pm4.6$ was exhibited, with an increased hydrogen permeability of 600.7 Barrer.

2. Experimental

2.1. Materials

The titanium tetraisopropoxide (TTIP) was obtained from Sigma Aldrich Co. (USA) and used as the precursor to synthesize the TiO_2 network intermediate layers. The pure polyethyleneimine (PEI, repeat unit MW=592 g/mol) precursor was purchased from Sigma Aldrich Co. (USA). The N-methyl-2-pyrolidone (NMP) solvent was purchased from Mallinckrodt Chemicals Co., USA and was used without further purification. The alumina disk, with an average pore size of 0.14 μm, a thickness of 1.4 mm, and a diameter of 23 mm, was purchased from Ganya Fine Ceramics Co., Taiwan and used as a bare support material.

2.2. Intermediate layer preparation

Bare Al_2O_3 supports were dried overnight and sintered in air at 800 °C with a 2 °C/min heating rate and a 2 h dwell time. The temperature was increased to 1400 °C for 2 h for calcining. The TiO_2 network intermediate layer was prepared using a one-pot sol–gel method and was then coated on the surface of the Al_2O_3 support by spin coating. An initial solution was prepared by mixing 14.65 ml TTIP and 100 ml water-free ethanol as the solvent under mechanical stirring for 2 h to form a homogeneous solution. Then, an specified amount of nitric acid and 1 ml d.d. water were added drop-wise to adjust the pH value to 3, 4, and 5 while stirring. The molar composition of all Ti precursor solutions is listed in Table 1.

After aging for 2 h at room temperature while stirring, the gel was coated on the surface of the Al_2O_3 support by spin coating at 2400 rpm for 18 s. To evaluate the influence of the thickness of the intermediate layer, the coating was performed two to four times. The coated composite supports were dried overnight at 25 °C and then calcined at 400 °C at a 5 °C/min ramping rate with a 2 h dwell time. The composite supports were labeled TiNX-Y where X was the pH value of the solution, and Y was the number of coats.

Table 1
M composition of all Ti precursor solutions.

Code	Molar composition			pH
	TTIP	HNO_3	Ethanol	
TiN3	1	0.242	34.61	3
TiN4	1	0.145	34.61	4
TiN5	1	0.048	34.61	5

2.3. Preparation of supported CMS membranes

The CMS membranes were prepared following the coating-pyrolysis procedures. PEI was dissolved in NMP to form a 10% (w/w) solution. The casting dope was spread on the surface of the composite support by spinning at 2000 rpm for 26 s. The coated film was dried at room temperature for 24 h to allow the solvent to evaporate. The dried films were then pyrolyzed under vacuum first by a curing step at 240 °C for 6 h with 5 °C/min ramping rate and then a carbonization step at 600 °C for 2 h with a 5 °C/min ramping rate. The resulting supported CMS membranes were slowly cooled to room temperature and held in a desiccator containing silica gel; they were tested for permeability within 24 h to avoid any aging effects.

2.4. Characterization of composite support and CMS membranes

The porous structures were measured using N_2 sorption at −196 °C with a PMI automated Brunauer–Emmett–Teller (BET) sorptometer (201AEL).

The crystalline structure was determined by X-ray diffraction (XRD) using a PW1830 X-ray powder diffractometer (Philips) with a Cu-Kα source ($\lambda = 1.5418$ Å) in a wide Bragg angle range ($20° \le 2\theta \le 70°$) with a 2°/min scanning rate.

The surface roughness was measured by atomic force microscopy in the non-contact mode using a C26 Dualscope/Rasterscope scanner (DME, Denmark). The surface morphology and cross-sectional images were examined by field-emission scanning electron microscopy (FE-SEM; JSM 5600).

The initial contact angle of the bare and composite supports was obtained indirectly from the measurement of a sessile drop using a contact angle instrument (Kruss GH11 Mobiledrop, Germany). The PEI casting dope was used as the probe liquid for all measurements. The software recorded the angles on the left and right image of the liquid drop shapes, and at least four measurements at random locations for each sample were performed and averaged.

The mechanical strength was measured in biaxial pressure mode.

2.5. Gas permeation test

A standard vacuum time-lag system was designed to determine the gas permeability through the composite membranes at room temperature (25 ± 2 °C). The membrane with a 3.14 cm^2 effective area was attached to a permeation cell (25 mm disk filters, Millipore, USA) and was degassed by exposing both sides of the membrane in a vacuum for 4 h. Different gases, including H_2, CO_2, O_2, N_2, and CH_4, at a feed pressure of 2 atm were introduced into the upstream side. The gas permeability was calculated from the slope (dP/dt) of the plot of pressure (P) versus time (t) using the following equation:

$$\text{Permeability, } Q = \left(\frac{dP}{dt}\right) \times \frac{V \cdot T_0}{A \cdot \Delta P} \times \frac{L}{T \cdot P_0}, \quad (1)$$

where dP/dt is the rate of pressure increase in the pseudo steady state, V is the downstream gas permeation volume (cm^3), A is the membrane area (cm^2), ΔP is the differential pressure across the membrane, L is the membrane thickness (cm), P_0 is 76 cm Hg, T_0 is 273 K, and T is the measured temperature (K).

The ideal selectivity coefficient of pure gas A/B ($\alpha_{A/B}$) is defined as the ratio of the permeability of A to that of B:

$$\alpha_{A/B} = \frac{Q_A}{Q_B}. \quad (2)$$

The average values and standard deviations were determined from six samples in two batches.

3. Results and discussion

3.1. Crystal phase and morphology of TiO_2 powder

The crystal phase composition of all the xerogels and calcined TiO_2 intermediate layers was measured by XRD analysis. Due to the detection limit, the titanium gels were coated on glass substrates and not on alumina supports (they were dried and peeled off before or after calcination because the alumina support would interfere with the diffraction pattern of TiO_2). As shown in Fig. 1, all the xerogel precursors were amorphous, while the samples calcined at 400 °C appeared to be crystalline and anatase TiO_2 (compared with Card no. 21-1272 anatase of JCPD (Joint Committee on Powder Diffraction Standard)) were observed. Further comparison of TiN3-, TiN4-, and TiN5-cal revealed that the peak height of anatase did not change with the HNO_3/TTIP ratio. The crystal size calculating by the diffraction patterns and Scherre's formula, also indicated that there was no apparent increase in the crystal size of the titania. Each titania had a crystal size range of 21–24 nm. Therefore, the crystal phase and size did not change significantly under different HNO_3/TTIP conditions. An FE-SEM top-view image of the TiO_2 powder is depicted in Fig. 2 where a porous structure-like nano-network is observed.

3.2. Pore structure and topography of TiO_2/Al_2O_3 composite support

Table 2 shows the physical texture, BET surface area, pore diameter, and total pore volume for each sample. The results indicate that after covering a TiO_2 intermediate layer, the surface area (S_{BET}) of the Al_2O_3 support changed significantly, especially with respect to the amount of nitric acid introduced during the

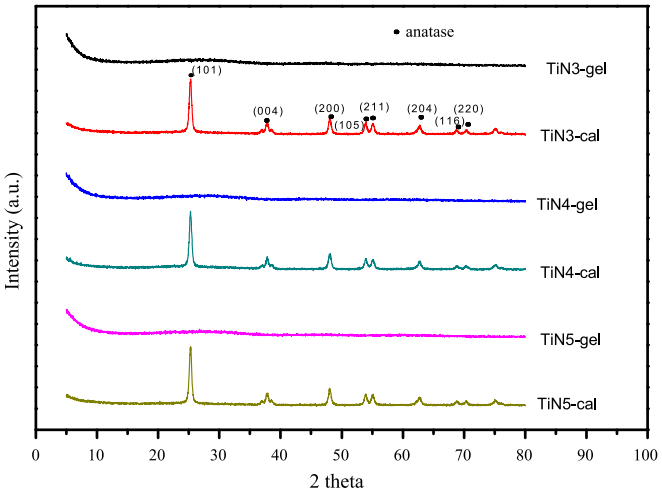

Fig. 1. XRD diffraction patterns of the xerogel and the calcined TiO_2 intermediate layers.

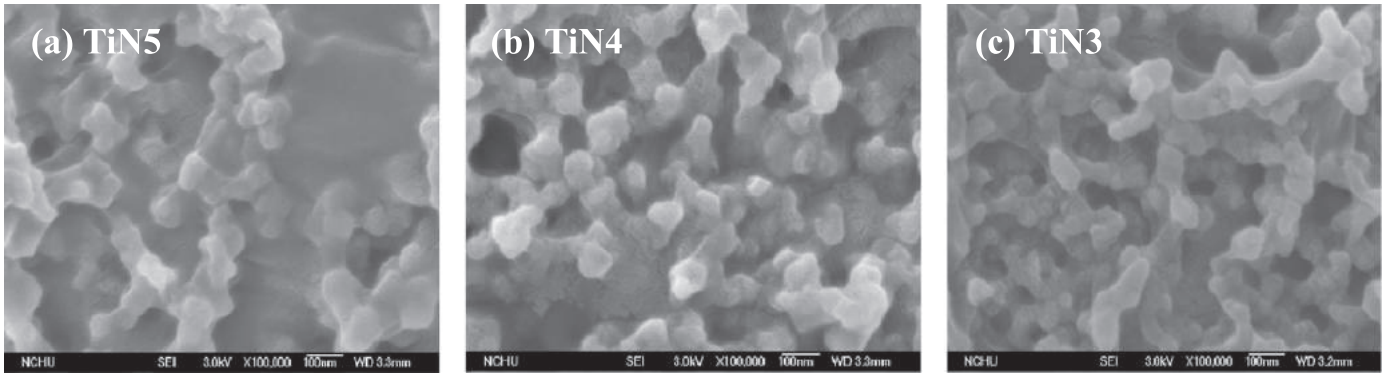

Fig. 2. FE-SEM morphology of the TiO_2 powder prepared with different HNO_3/TTIP molar ratios: (a) TiN5, (b) TiN4, and (c) TiN3.

Table 2
BET surface area, pore volume, and average pore diameter of the TiO_2/Al_2O_3 composite supports.

Code	S_{BET} (m^2/g)	D_{pore} (nm)	BJH adsorption cumulative pore volume of pores between 3.5 Å and 1000 micros radius (cm^3/g)			
			V_{total}	V_{micro}	V_{meso}	V_{macro}
Al2O3	4.3	74.2	0.0080	0.0011 (13.75%)	0.0063 (78.75%)	0.0005 (6.25%)
TiN5-2	9.3	38.5	0.0902	0.0017 (1.88%)	0.0445 (50.44%)	0.0438 (48.55%)
TiN5-3	13.0	27.1	0.0885	0.0024 (2.71%)	0.0487 (55.02%)	0.0372 (42.03%)
TiN5-4	3.8	176.3	0.1686	0.0010 (0.59%)	0.1071 (63.52%)	0.0603 (35.76%)
TiN4-2	10.6	81.1	0.2150	0.0018 (0.83%)	0.1295 (60.23%)	0.0836 (38.88%)
TiN4-3	18.2	62.2	0.2833	0.0032 (1.12%)	0.1998 (70.52%)	0.0801 (28.27%)
TiN4-4	16.4	60.6	0.2489	0.0025 (1.00%)	0.1471 (59.10%)	0.0992 (39.85%)
TiN3-2	13.0	29.6	0.0970	0.0024 (2.47%)	0.0500 (51.54%)	0.0445 (45.87%)
TiN3-3	31.0	9.6	0.0746	0.0046 (6.16%)	0.0420 (56.30%)	0.0278 (37.26%)
TiN3-4	19.2	46.5	0.2238	0.0029 (1.29%)	0.1093 (48.83%)	0.1114 (49.77%)

hydrolysis of the metal-organic precursor and the number of coats. Specifically, the surface area increased from 4.3 m^2/g (Al_2O_3 support) to 13.0 m^2/g (TiN3-2 composite support) when the molar ratio of HNO_3/TTIP increased from 0 to 0.242 (i.e., pH 3) with 2 coats. As the coats increased from 2 to 4, the surface area of the TiN3-2 increased significantly, reaching 31 m^2/g (for 3 coats), but then decreases slightly to 19.2 m^2/g for 4 coats; similar variations were also found for the TiN4 and TiN5 composite supports. This behavior strongly depended on the amount of added nitric acid and the number of coats in the range investigated. However, the change of pore diameter showed an inverse trend compared to the surface area. The pore diameter decreased from 2 to 3 coats then again increased with 4 coats for the TiN5 and TiN3 samples. The mesopores contributed to approximately 78.75% of total pore volume for the Al_2O_3 support, whereas the TiO_2/Al_2O_3 composite support showed macropore contributions ranging from 28.27% to 49.77% of the total pore volume.

Those observations can be explained by structure modifications from coating with a TiO_2 intermediate layer via the sol–gel spin coating method. Previously, the pH value of the precursor solution has been shown to influence the final particle size of the TiO_2 [37] due to its effect on the relative rates of hydrolysis and condensation [38]. In general, sol–gel synthesis can be performed by the hydrolysis and condensation of inorganic salts or alkoxides. The procedures starting from the latter precursors are categorized as conventional sol–gel processes, in which nanoparticles are synthesized during the condensation step, and the particle sizes depend on the reaction rate of condensation. With a low amount of nitric acid catalyst (high pH), a high condensation rate results in rapid solidification; thus, more precursor solution cannot be uniformly introduced onto the surface layer of the support during the spin coating procedure. Therefore, the TiN5 series supports exhibit smaller surface areas and broader pore diameters changes compared to the TiN4 and TiN3 series supports.

Fig. 3 shows the FE-SEM image of the top surface of all of the TiO_2/Al_2O_3 composite supports. Compared to the bare Al_2O_3, the TiN5 supports with a low amount of nitric acid added had a non-uniform surface layer covering a thin TiO_2 discontinuous layer. As the number of coats increased to 3 or 4, the thickness of the TiO_2 layer increased (Fig. 3(d) from the side view of the TiO_2 layer) and possessed many cracks forming an irregular surface. It is clear that an additional TiO_2 layer did not fill the structural pores but covered over the Al_2O_3 layers. This finding agrees with the pore structure results of the TiN5 performed using BET N_2 adsorption, which are presented in Table 2. The average pore diameter of Al_2O_3 was diminished due to the TiO_2 thin film covering. As the number of coats increased to 3, the thickness of the TiO_2 film increased causing the pore diameter and pore volume to decrease. As the coats increased to 4, the thicker TiO_2 layer also influenced the pore structure of the composite support; therefore, the diameter of the pores created in the TiO_2 layer increased, and the micro-cracks in the TiO_2 layer are evidence of the development of a more porous structure.

Fig. 3(e)–(g) shows the top morphology of a TiN4 composite support. As the molar ratio of HNO_3/TTIP increased to 0.145 (pH 4), no significant TiO_2 layer was observed with 2 and 3 coats. This result reveals that the additional titania deposited and filled into the surface layer of the Al_2O_3 support. With the addition of more nitric acid, a lower condensation rate takes place at these molar ratios, resulting in slow gel formation. This phenomenon causes the precursor solution to penetrate the surface layer of the Al_2O_3 support. The TiN_3 composite support showed similar results (Fig. 3 (h)–(j)). Cross-sectional EDS line scanning of TiN3-2, TiN3-3, and TiN4-3 supports confirmed these observations (Fig. 4(a)–(c)), and the ratio of Ti/Al calculated based on the counts were 1.8%, 2.8% and 3.6%, respectively. Those results indicate that intermediate TiO_2 layers entered pores in α-Al_2O_3 supports with more nitric acid. These results suggested that coating an addition layer with

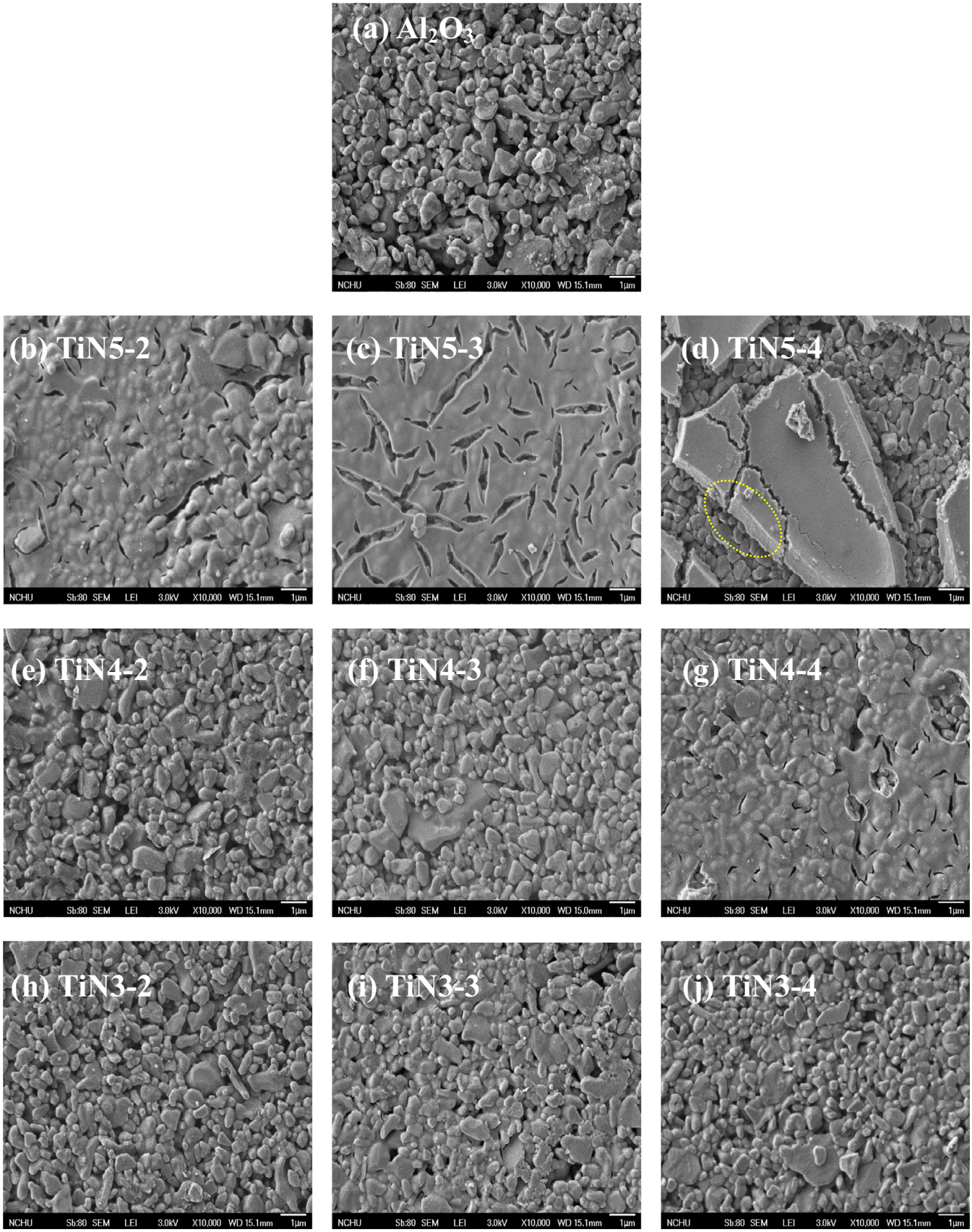

Fig. 3. FE-SEM images of the top surface of the TiO_2/Al_2O_3 composite supports: (a) Al_2O_3, (b) TiN5-2, (c) TiN5-3, (d) TiN5-4, (e) TiN4-2, (f) TiN4-3, (g) TiN4-4, (h) TiN3-2, (i) TiN3-3, and (j) TiN3-4.

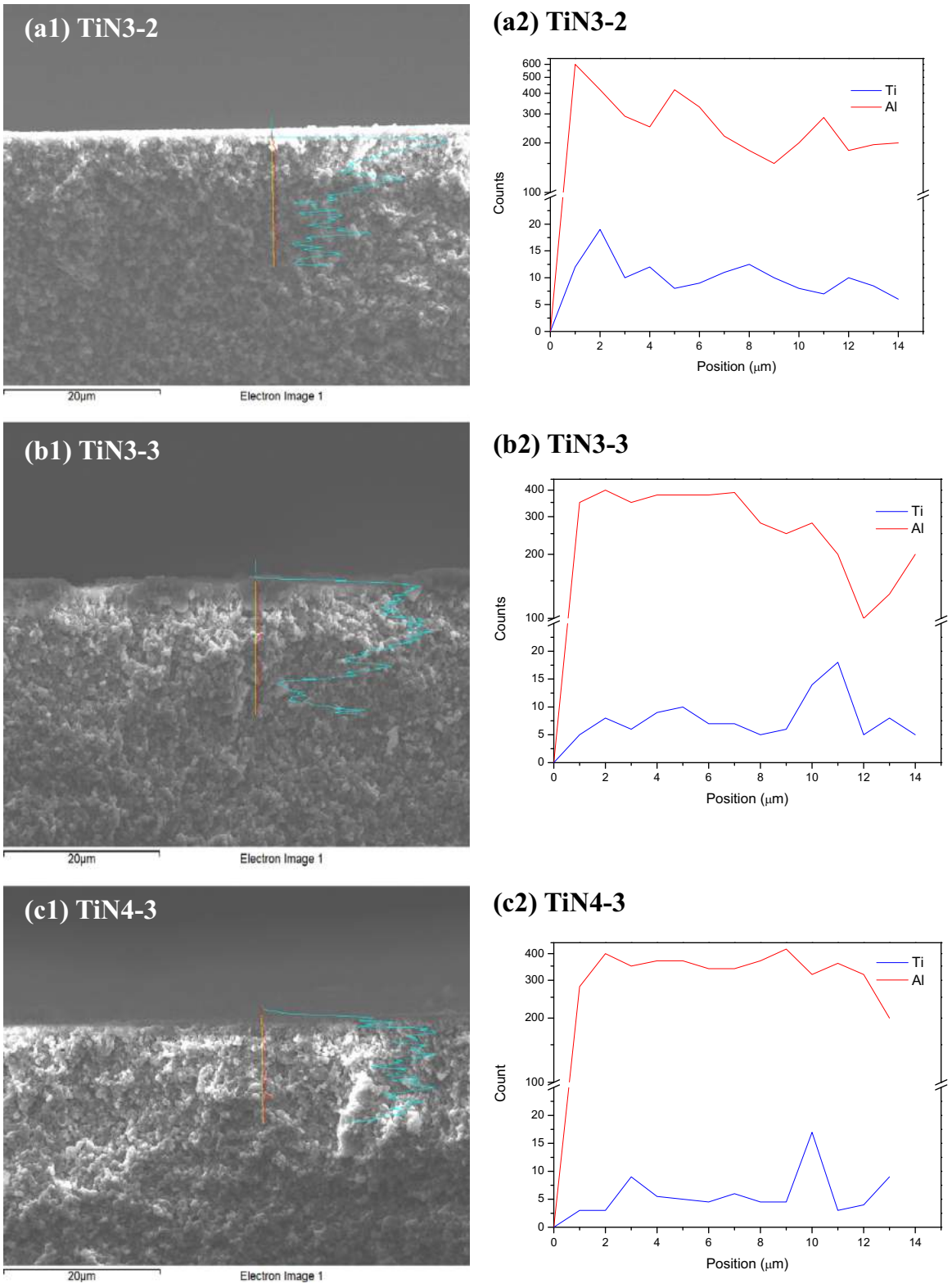

Fig. 4. (1) FE-SEM photographs and (2) EDS line-scanning of the TiO_2/Al_2O_3 composite supports: (a) TiN3-2, (b) TiN3-3, and (c) TiN4-3.

pH 3 and 4 conditions on alumina support may repair some large defects or pinholes existing on the original alumina support, and thus reduce the surface roughness (see Fig. 5). Such improvement in support surface quality is likely to improve the CMS membrane quality as well, especially the selectivity.

Surface topography of the composite supports was further investigated by AFM, and the results are shown in Fig. 5. The results show a surface roughness of 56.8 nm for the bare Al_2O_3 support. When the titania was coated using sol–gel spin coating method, the variation in roughness of all the supports displayed two trends. First, an increase in surface roughness with the number of coats was observed from the series of TiN5 samples. In particular, the topography of the TiN5 samples showed a large difference compared to the original Al_2O_3 support. After covering a titania layer,

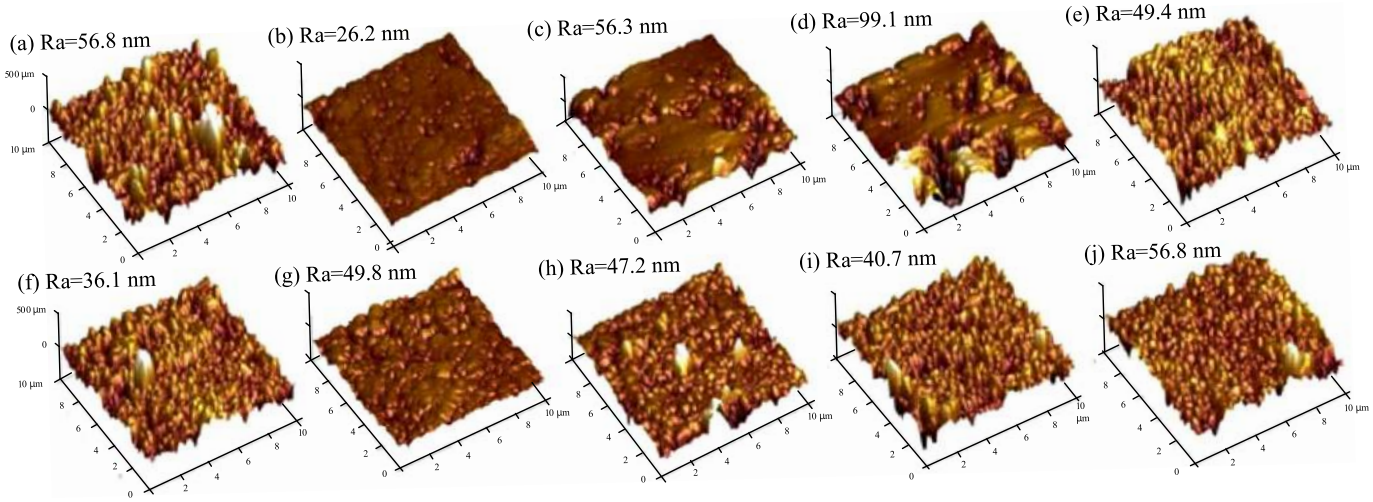

Fig. 5. AFM topography of the TiO_2/Al_2O_3 composite supports: (a) Al_2O_3, (b) TiN5-2, (c) TiN5-3, (d) TiN5-4, (e) TiN4-2, (f) TiN4-3, (g) TiN4-4, (h) TiN3-2, (i) TiN3-3, and (j) TiN3-4.

the depressions of the Al_2O_3 were filled up and resulted in a remarkable decrease in the composite surface roughness from 56.8 nm to 26.2 nm (TiN5-2). However, as the number of coats increased, the surface became rough further due to discontinuous coverage from the TiO_2 layer. Second, a decrease in roughness with an increase in the number of coats was observed from the series of TiN4 and TiN3 samples. The topographies of the TiN3 and TiN4 samples were similar to that of the Al_2O_3, indicating that the

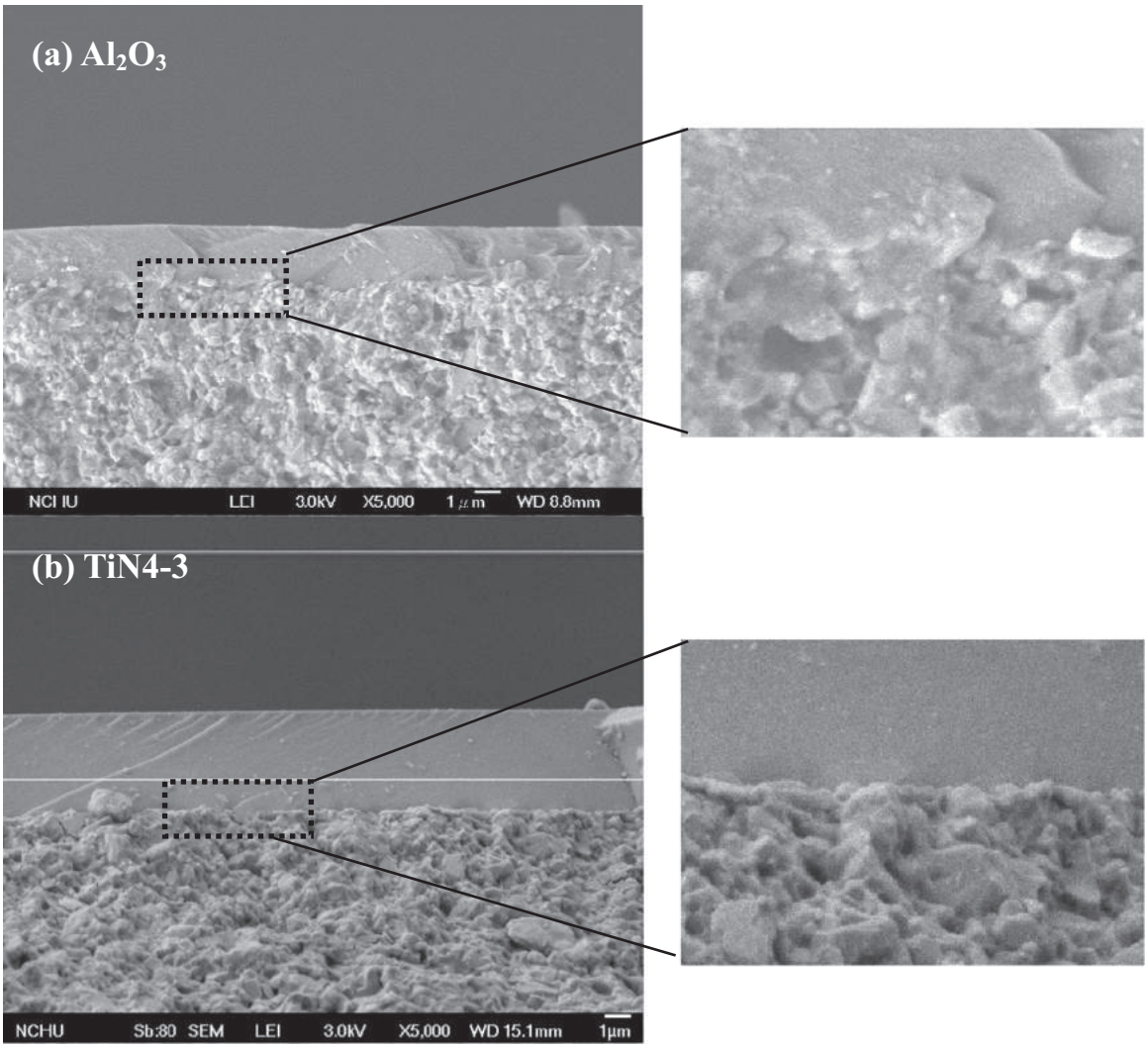

Fig. 6. The FE-SEM images of the CMS layer supported on (a) Al_2O_3 and (b) TiN4-3 support (left), with a more detailed view of the interface (right) at higher magnification.

titania particles were inserted into the surface layer of the Al_2O_3, and the particles size of the TiO_2 was small, as expected. It is obvious that the surface roughness decreased after the sol–gel step even after 4 coats. In conclusion, the introduction of nitric acid in the precursor solution had a noticeable effect on the surface morphology and roughness of the composite support.

3.3. Adhesion mechanism between CMS layer and composite support

The FE-SEM top-view and cross-sectional images of the CMS layer supported on (a) the bare Al_2O_3 and (b) the TiO_2/Al_2O_3 composite support are shown in Fig. 6. The images illustrate that the carbon membrane grown on the top surface of the bare Al_2O_3 support was dense and defect-free with a good adhesion to the support. After the TiO_2 intermediate layer was introduced, the

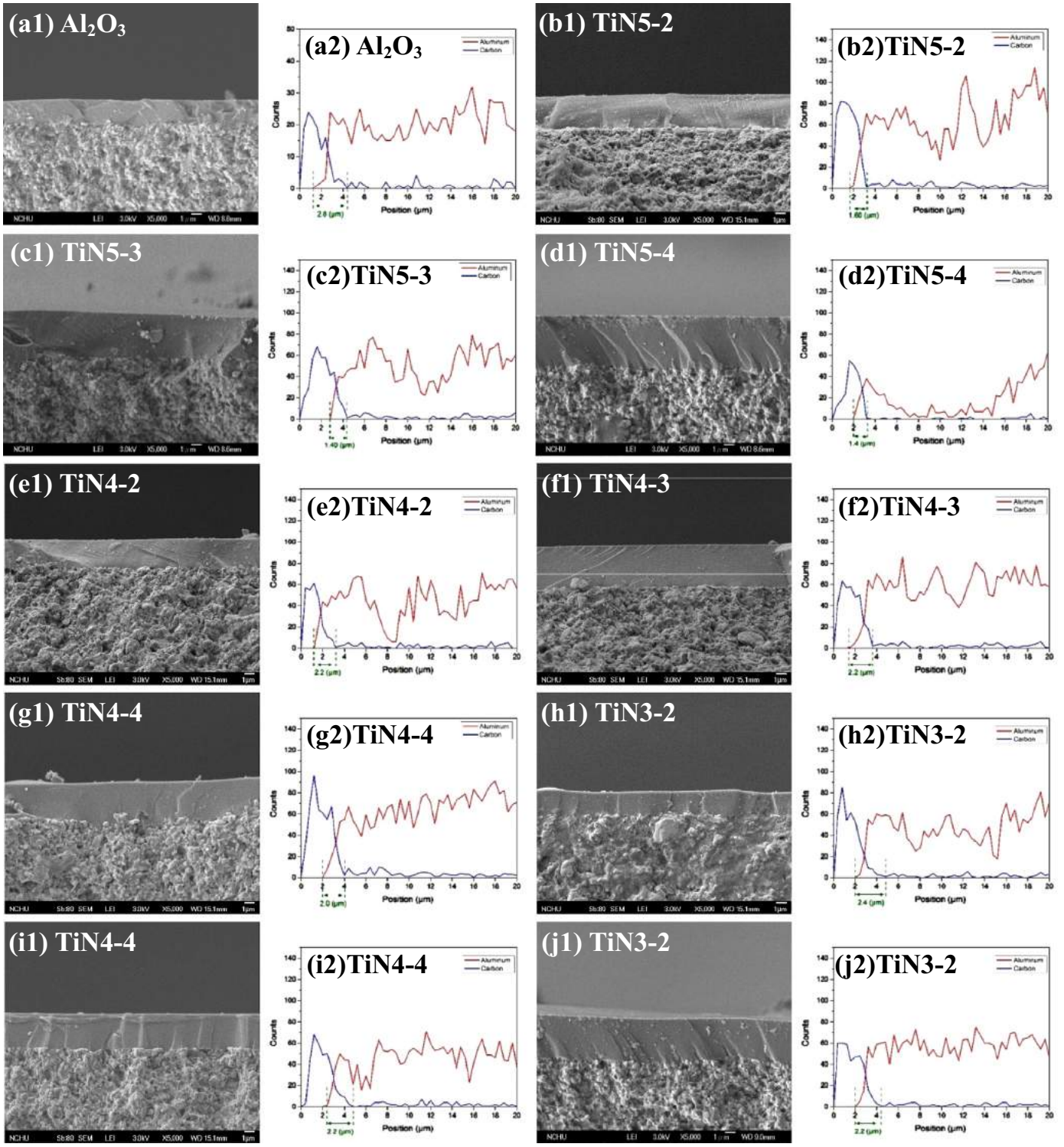

Fig. 7. (1) FE-SEM images and (2) SEM-EDX line scanning spectra of the carbon (blue line) and aluminum (red line) elements of the CMS layer supported on: (a)TiN5-2, (c) TiN5-3, (d) TiN5-4, (e) TiN4-2, (f) TiN4-3, (g) TiN4-4, (h) TiN3-2, (i) TiN3-3, and (j) TiN3-4. (For interpretation of the references to color in this figure legend, the reader is referred to the web version of this article.)

Table 3
Membrane thickness, d-spacing, roughness, interlocking depth, and contact angle of the CMS layer supported on different TiO_2/Al_2O_3 supports.

Code	Al_2O_3	TiN5-2	TiN5-3	TiN5-4	TiN4-2	TiN4-3	TiN4-4	TiN3-2	TiN3-3	TiN3-4
Thickness (μm)	2.13	3.01	4.20	4.50	2.62	3.60	3.64	2.27	3.09	3.60
d-spacing (Å)	4.85	4.71	4.40	4.64	4.70	4.34	4.41	4.56	4.11	3.88
Roughness (nm)	56.8	26.6	56.3	99.1	49.4	45.9	36.1	49.8	47.2	40.7
Interlocking depth (μm)	2.80	1.60	1.40	1.40	2.20	2.20	2.00	2.40	2.20	2.20
Contact angle (deg)	10.5	12.6	20.7	21.0	17.3	16.2	13.4	18.5	16.7	16.2

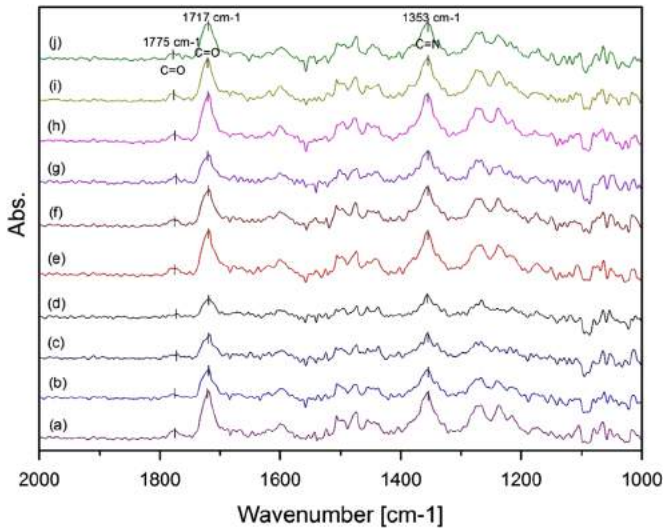

Fig. 8. The FTIR spectra of the PEI polymer film supported on: (a) Al_2O_3, (b) TiN5-2, (c) TiN5-3, (d) TiN5-4, (e) TiN4-2, (f) TiN4-3, (g) TiN4-4, (h) TiN3-2, (i) TiN3-3, and (j) TiN3-4.

morphology of the CMS layers supported on TiO_2/Al_2O_3 composite support (for example TiN4-3) also showed similar results to the layers on the bare Al_2O_3 support. However, upon enlarging the selected zone, the interfaces between the CMS layer and the bare Al_2O_3 and the TiN4-3 were very different. The interface between the Al_2O_3 and the carbon layer were intermingled, but for the TiN4-3 support, a clear interface existed.

To investigate further the effects of the intermediate layer on the interface adhesion of the CMS layer, other TiO_2/Al_2O_3 supports synthesized with different parameters were also selected for deposition of the CMS layer. Based on the observations from the FE-SEM images shown in Fig. 7(a1)–(j1), a thin and defect-free separation layer with uniform morphology was clearly observed on all composite supports. This result reveals that both the bare Al_2O_3 support and the modified composite supports in this study were suitable for the deposition of a thin and defect-free carbon separation layer. However, as shown in Table 3, the membrane thickness of the CMS layer varied with the structure of the composite support, which became thinner as the nitric acid amount increased and the number of coats decreased; the preparation conditions of the CMS layer were the same. Therefore, three adhesion mechanisms are proposed in this study for investigating the intrinsic adhesion of the selective layer on the TiO_2/Al_2O_3 composite support: mechanical interlocking, chemical bonding, and adsorption.

3.3.1. Mechanical interlocking

SEM-EDX line scanning analysis was performed across the CMS membrane to investigate the intrusion (penetration) of the carbon into the TiO_2/Al_2O_3 composite support. The superimposed carbon signal coming from the support layer could indicate the intrusion of carbon in the supports, which can be used as index of the depth of mechanical interlocking. Fig. 7(a2)–(j2) shows the SEM-EDX line scanning spectra of the aluminum and carbon elements obtained along a line drawn in the cross section corresponding to Fig. 7(a1)–(j1). The results reveal that the entire carbon layer penetrated into the composite support, and the deepest interlocking depth was obtained from the bare Al_2O_3 support (Table 3). Meanwhile, for the series of TiN4 and TiN3 supporting membranes with increasing nitric acid in the Ti precursor solution and one coat, the penetration depth of the carbon element in the composite support increased. The rougher surface and more porous structure facilitate the infiltration of the PEI dope solution in the support. However, for the series of TiN5 supporting membranes, we found that the interlocking depth does not correlate well to the roughness or porosity, but to the chemical bonding (see Section 3.3.2.). In general, slight pore penetration can enhance the adhesion between the separation layer and the support layer by mechanical interlocking. However, with an increase in pore penetration, the mass transfer resistance may remarkably increase causing the permeation flux through the composite membrane to decrease (see Section 3.4) [11]. Consequently, modulation of the pore penetration of the interfacial region of the carbon film depended on the variation of the support pore structure and roughness. The strength of mechanical interlocking between the CMS layer and the supports followed the sequence of $Al_2O_3 > TiN3 > TiN4 \gg TiN5$. The supports modified with TiN3 and TiN4 were more conducive to strengthening the mechanical interlocking compared to TiN5-modified one. This result may attributed to the diminish defect or pinholes.

3.3.2. Chemical bonding

In the studied range, the chemical bonding between the series of TiN5 supports and the CMS separation layer was expected to be stronger than others because additional contact area between the TiO_2 intermediate layer and the CMS layer existed due to the higher degree coverage of TiO_2 nano-network.

Fig. 8 shows the typical infrared bands for the PEI polymer film (before carbonization) on bare Al_2O_3 and TiO_2/Al_2O_3 composite supports. The FTIR-ATR spectrum of the PEI (amide group) is characterized by bands at approximately 1775 cm^{-1} (asymmetric stretch of C=O in the amide groups), 1717 cm^{-1} (asymmetric stretch of C=O), and 1353 cm^{-1} (stretch of C–N–C in the amide group) [35]. The intensities of these characteristic peaks were found to gradually decrease when using the TiN5 supports and a qualitative difference in the typical band intensities for the number of coats also can be observed in the three series of TiO_2/Al_2O_3 composite supports. The results indicate that PEI films self-assemble to form H-bonds between the carbonyl and surface hydroxyl groups of the TiO_2. Consequently, when the PEI precursor was coated on the surface of the TiO_2/Al_2O_3 composite supports, the intensity of the PEI bands decreased due to the increase in the amount of PEI bound to TiO_2; this increase is related to the number of hydroxyl groups forming on the surface, i.e., the degree of coverage of TiO_2.

Therefore, good adhesion between the composite support and the CMS layer, which contributes to the interfacial chemical bonds, followed the sequence of $TiN5 > TiN4 > TiN3 > Al_2O_3$, and the influence from the number of coats is as follows: 4 layers > 3 layers > 2 layers.

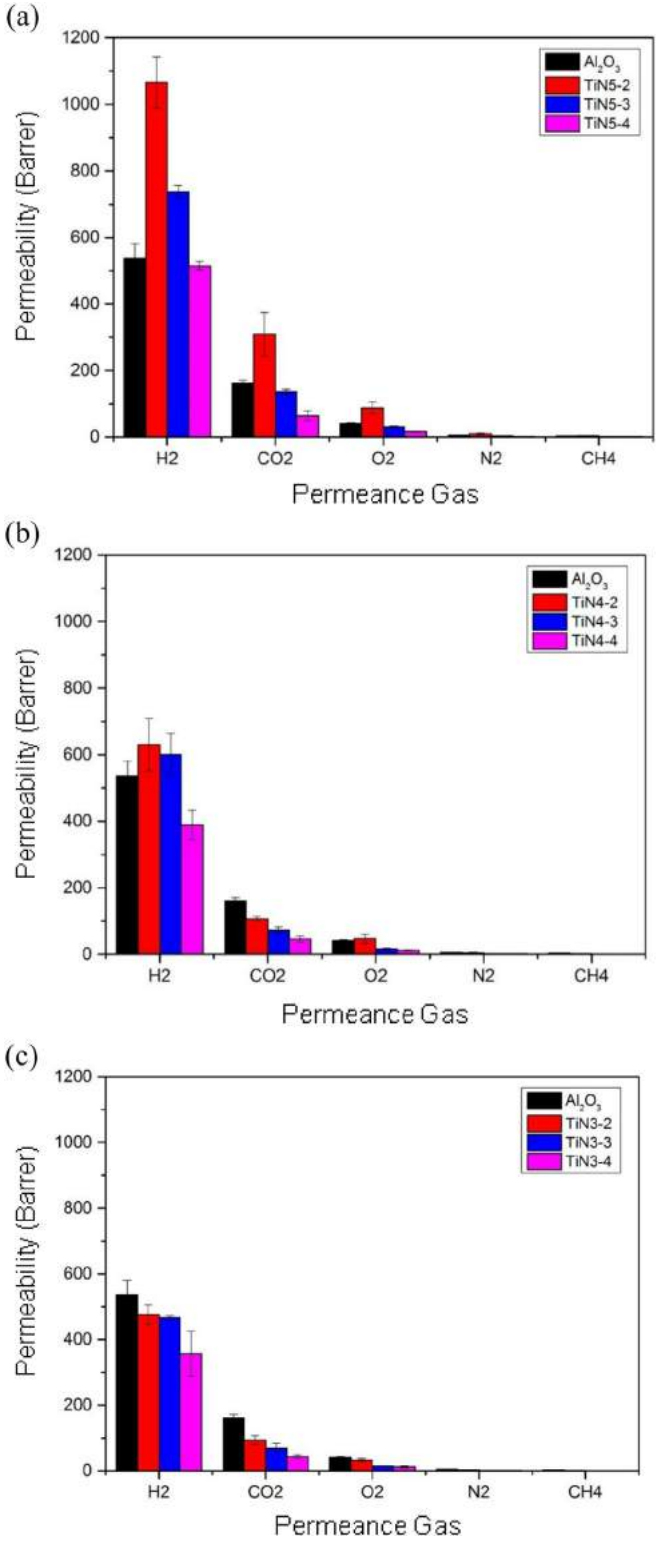

Fig. 9. The gas permeability obtained from the series of (a) TiN5, (b) TiN4, and (c) TiN3 supported CMS membranes.

3.3.3. Adsorption

Table 3 shows the average initial contact angle of the probe fluids (here the PEI dope was used) on the bare Al_2O_3 and TiO_2/Al_2O_3 composite supports. The Al_2O_3 had the smallest contact angle of 10.5°. The TiO_2/Al_2O_3 supports all exhibited similar values and were higher than that of bare Al_2O_3 suggesting that the Al_2O_3 has a low surface energy and the TiO_2/Al_2O_3 supports have high surface energies. The TiN5-3 and TiN5-4 tend to have higher contact angles than the TiN4 and TiN3 series; this result may come from the roughness of the TiN5 support series, in which a rough surface can have a high resistance against dope fluidity and a high contact angle. The contact angles of the TiN4 and TiN3 series composite supports also showed a gradual decrease with a decrease in the composite support surface roughness (the contact angle for TiN4 and TiN3 decreased from 17.3° to 13.4° and from 18.5° to 16.2°, respectively).

Compared to the bare Al_2O_3 support, the larger PEI contact angle for the TiO_2/Al_2O_3 composite support clearly indicated that modification with a TiO_2 intermediate layer did not slightly decrease the adsorption of the composite support; this could result from the hydrophilicity of the polar hydroxyl groups (–OH) found

Table 4
The selectivity of TiO_2/Al_2O_3 supported CMS membranes.

Membrane	Selectivity				
	H_2/CH_4	H_2/CO_2	O_2/N_2	CO_2/CH_4	CO_2/N_2
Al_2O_3	197.6 ± 27.0	3.3 ± 0.1	8.2 ± 0.5	59.7 ± 9.6	32.3 ± 2.1
TiN5-2	240.7 ± 51.9	3.6 ± 0.8	9.0 ± 0.4	68.2 ± 9.6	31.8 ± 2.3
TiN5-3	470.5 ± 4.2	5.4 ± 0.2	9.1 ± 2.5	87.2 ± 3.3	39.4 ± 8.7
TiN5-4	324.0 ± 18.7	8.2 ± 1.8	7.2 ± 1.6	40.6 ± 10.9	27.7 ± 2.5
TiN4-2	365.4 ± 16.7	5.9 ± 0.9	10.3 ± 2.4	63.4 ± 11.7	24.8 ± 8.5
TiN4-3	725.9 ± 15.1	8.3 ± 0.3	8.9 ± 0.5	87.9 ± 4.6	38.2 ± 1.7
TiN4-4	458.6 ± 19.8	8.6 ± 0.8	7.6 ± 0.7	53.8 ± 3.0	29.3 ± 0.8
TiN3-2	316.4 ± 38.5	5.1 ± 0.6	9.2 ± 1.3	61.9 ± 0.6	26.8 ± 4.7
TiN3-3	574.6 ± 121.2	6.8 ± 1.5	8.5 ± 1.4	84.1 ± 0.4	39.4 ± 1.4
TiN3-4	471.5 ± 54.6	8.1 ± 0.5	6.7 ± 1.1	58.5 ± 10.1	24.0 ± 5.0

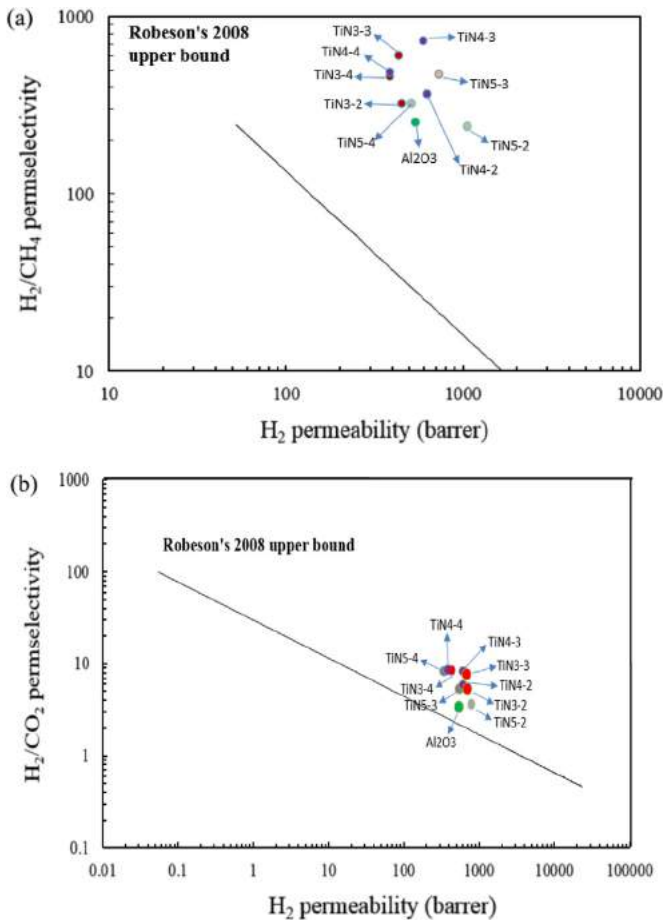

Fig. 10. Performance of the TiO_2/Al_2O_3 supported CMS for the separation of (a) H_2/CH_4 and (b) CO_2/N_2 with respect to the Robeson trade-off line.

Table 5
Gas perm-selectivity of some selected CMS membrane.

Geometry		Thickness (μm)	Permeability (Barrer)[a]			Selectivity					References
			H_2	CO_2	O_2	H_2/CH_4	H_2/CO_2	O_2/N_2	CO_2/CH_4	CO_2/N_2	
Supported type	Precursor										
TiN4-3 (disk)	PEI	3.6	600.7	72.9	17.0	725.9	8.3	8.9	87.9	38.1	This work
Ceramic (disk)		0.15	–	115.8	22.6	–	–	2.8	–	14.3	[43]
γ-alumina/Al_2O_3 (disk)	PI[b]	1.6	–	–	28.9	–	–	5.1	–	–	[23]
AlOOH gel/Al_2O_3 (tube)		3.7	479.1	217.8	104.5	–	2.2	5.3	–	11	[33]
Carbon (disk)	PEI		–	35	19.8	–	–	7.4	25	15	[48]
Self-standing											
Cellophane paper		9	60.3	1.9	0.7	6030	31.2	17.5	193.0	48.3	[42]
6FDA/1,5-ND:ODA(1:1)		–	45.0	45.0	11.0	45.0	1.0	5.5	45.0	22.5	[44]
PIM-6FDA-OH		80–90[c]	2177	556	149	363	3.9	8.9	93.0	32.7	[17]
PBI/Kapton(50/50)			–	119.2	23.2	–	–	12.9	175.2	66.0	[45]
PBI/Matrimid(50/50)			324.0	36.6	11.0	1165.5	8.85	8.7	131.7	29.0	[16]
PIM-6FDA-OH		80–100[c]	–	512	—	–	–	–	88	–	[18]
BTDA-ODA polyimide		30[c]	–	176	61	–	–	15	–	44	[46]
Kapton		42	–	23.0	3.9	–	–	12.4	–	74.1	[47]
PEI/PVP		88–127		56.58		–	–	–	69.0	34.5	[49]

[a] 1 Barrer = 1×10^{-10} cm^3 (STP) cm/(s cm^2 cm Hg).
[b] PI: polyimide (Matrimid).
[c] Thickness of dry polymer membrane.

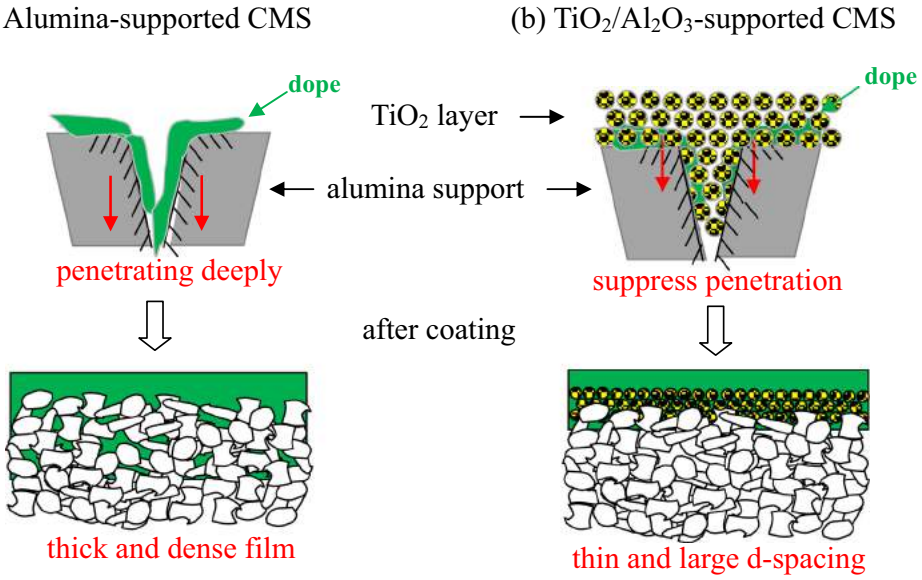

Fig. 11. The proposed interlocking pattern for the CMS membrane supported on (a) alumina and (b) TiO_2/Al_2O_3 supports.

in TiO_2. Thus, an increase in contact angle was observed after adding the TiO_2 intermediate layer. This may result in an increase in the degree of bending of the polymer chain, which enhances the d-spacing values. Based on the above analysis, the adsorption capacity of support is described as $Al_2O_3 > TiO_2/Al_2O_3$ supports.

3.4. Gas separation performance of supported CMS membranes

The bare Al_2O_3 and TiO_2/Al_2O_3 supported CMS membranes were all tested by dynamic state single gas permeation at 298 K to determine their gas permeability and selectivity. As shown in Fig. 9, the gas permeability obtained from all CMS membranes decreased by degrees with the gas kinetic diameter increasing in the following order of PH_2 (2.8 Å) > PCO_2 (3.3 Å) > PO_2 (3.46 Å) > PN_2 (3.64 Å) > PCH_4 (3.8 Å) (the value in the bracket is the dynamic diameter of the gas molecule). This trend is consistent with the molecular sieving mechanism, the dominant mechanism for gas transport through the CMS membrane. After coating with the TiO_2 intermediate layer, the permeabilities of H_2, CO_2, O_2, N_2, and CH_4 through CMS membrane supported on TiN5 series support increased compared to the bare Al_2O_3-supported membrane, but then decreased gradually as the TiN4 and TiN3 supports were used; for example, the H_2 permeability obtained from the bare Al_2O_3-supported CMS was 537.49 Barrer, while the TiN5, TiN4 and TiN3 series values decreased from 1065.92 to 515.08 Barrer to 629.96–388.34 Barrer, and 476.14–357.00 Barrer, respectively. Interestingly, the permeability of H_2 obtained from the TiN5-and TiN4-modified CMS membranes was increased with 2 and 3 coats. This trend could be attributed to the formation of the TiO_2 intermediate layer, which possesses a nano-network structure, and with a dependence on the different adhesion mechanism, the permeability and the selectivity increased simultaneously (shown in Table 4).

The advantage of a TiO_2/Al_2O_3 composite support over the bare

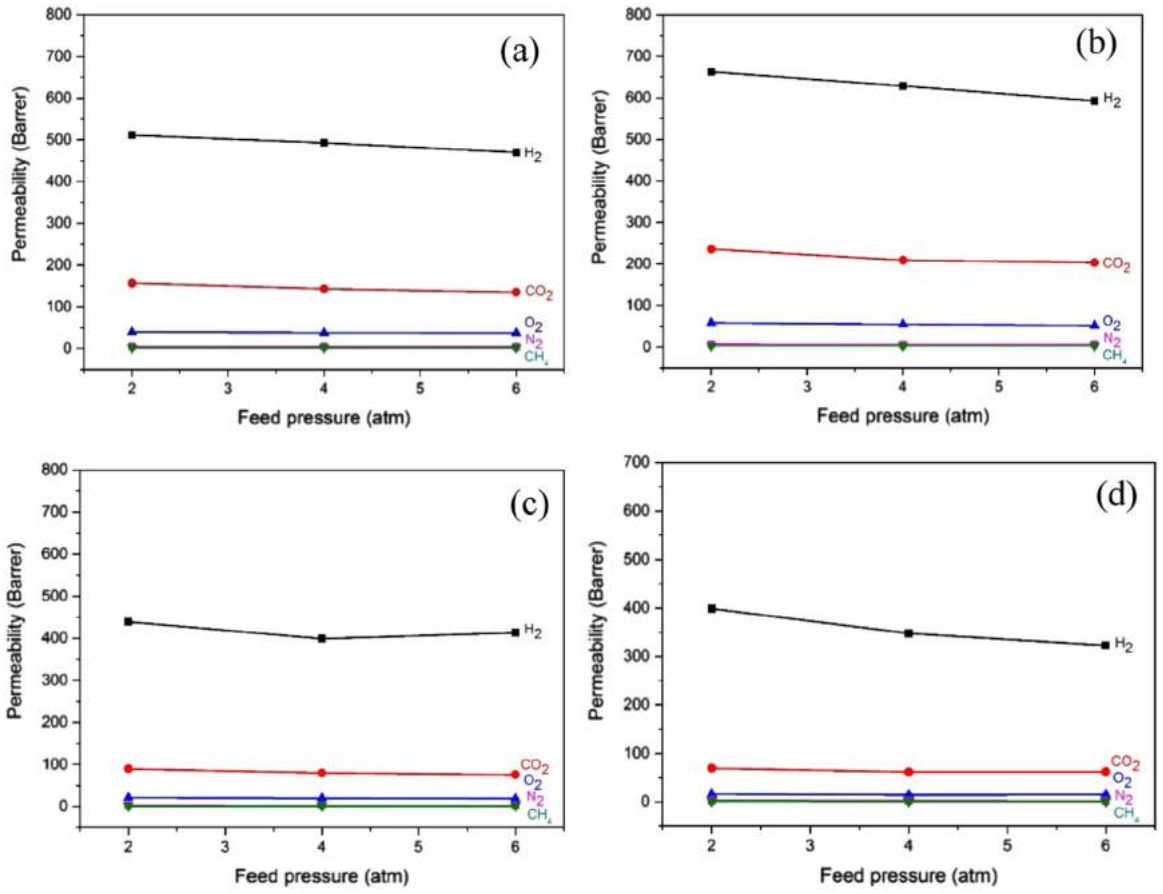

Fig. 12. The effect of feeding pressure on the permeability of the CMS membranes supported by (a) Al_2O_3, (b)TiN4-2, (c)TiN4-3, and (d)TiN4-4 supports.

Al_2O_3 support is the advanced selectivity. As shown in Table 4, the single gas permeability of H_2 obtained from the TiN4-3 supported membrane is 600.74 Barrer, which is slightly higher than that from Al_2O_3 (537.49 Barrer). However, the ideal selectivities for the H_2/CH_4, H_2/CO_2, O_2/N_2, CO_2/CH_4 gas pairs are 725.93 (197.62), 8.26 (3.32), 8.91 (8.18), and 87.94 (59.68) (parentheses indicated the value from the Al_2O_3 supported membrane) showing remarkably enhanced results. It is clear that the TiO_2/Al_2O_3 supported CMS membranes offer higher gas permeabilities and ideal selectivities than the Al_2O_3 supported membrane.

Fig. 10 shows the performances of $C/TiO_2/Al_2O_3$ molecular sieving membranes for the separation of H_2/CH_4 and H_2/CO_2 with respect to the Robeson trade-off line [41]. The results show that the CMS membranes with TiO_2/Al_2O_3 supports not only surpassed the upper-bound line but also show superior permeability and selectivity performance for commercially attractive applications. Further, as shown in Table 5, the results obtained from TiN4-3 supported CMS membranes are also higher than the other reported membranes which are in different structures [16–18,22,33,42–49]. By demonstrating good H_2/CH_4 and H_2/CO_2 separation performance, there is great potential for these materials for use in industrial applications as novel composite CMS membranes.

3.5. The role of adhesion mechanism on the performance of supported CMS membrane

We modified the adhesion between the Al_2O_3 support and the supported carbon membrane by adding a TiO_2 intermediate layer (especially of TiN4 series support). This modification enhanced CMS membrane permeability and increased H_2/CH_4 and H_2/CO_2 perm-selectivities, thereby also enhancing mechanical strength (see Section 3.6). Adhesion mechanisms proposed in this study, such as mechanical interlocking, chemical bonding, and adsorption, might have contributed simultaneously; therefore, discerning the respective contribution of each mechanism is impossible.

However, TiO_2-supported carbon membrane unexpectedly perform better than alumina-supported membrane. As compared to TiN4 series supports, alumina has a higher roughness and interlocking depth, which implies stronger interlocking with the membrane; alumina also has a higher adsorption as suggested by the smaller contact angle. These factors suggest that alumina is a better support than TiO_2. However, this finding contradicts membrane performances found in this work. Table 4 shows that the ideal selectivity of H_2/CH_4 ranges from 240.7 to 725.9, and H_2/CO_2 selectivity ranges from 3.57 to 8.6 (Table 4). These data were obtained from TiO_2/Al_2O_3-supported CMS membrane, which were higher than those of the alumina-supported membrane. H_2/CH_4 and H_2/CO_2 selectivity interestingly have a much greater variation than other gas pairs, whereas the selectivity of O_2/N_2, CO_2/CH_4, and CO_2/N_2 are consistent. This trend may be caused by the high permeation rate of H_2, and exquisite structural changes may cause big variations for H_2 permeation rates. On the other hand, slow gases O_2, N_2, and CH_4, are less sensitive.

In fact, considering the adhesion properties as discussed earlier, the adhesion property, including interlocking mechanism, chemical bonding, and adsorption may not be an appropriate predictor of CMS membrane performance because deep interlocking and strong adsorption may result in a dense matrix, and thus increase mass-transfer resistance. Fig. 11 illustrates the proposed interlocking pattern for the CMS membrane supported on alumina and TiO_2/Al_2O_3 supports. A dense matrix can be formed on the alumina

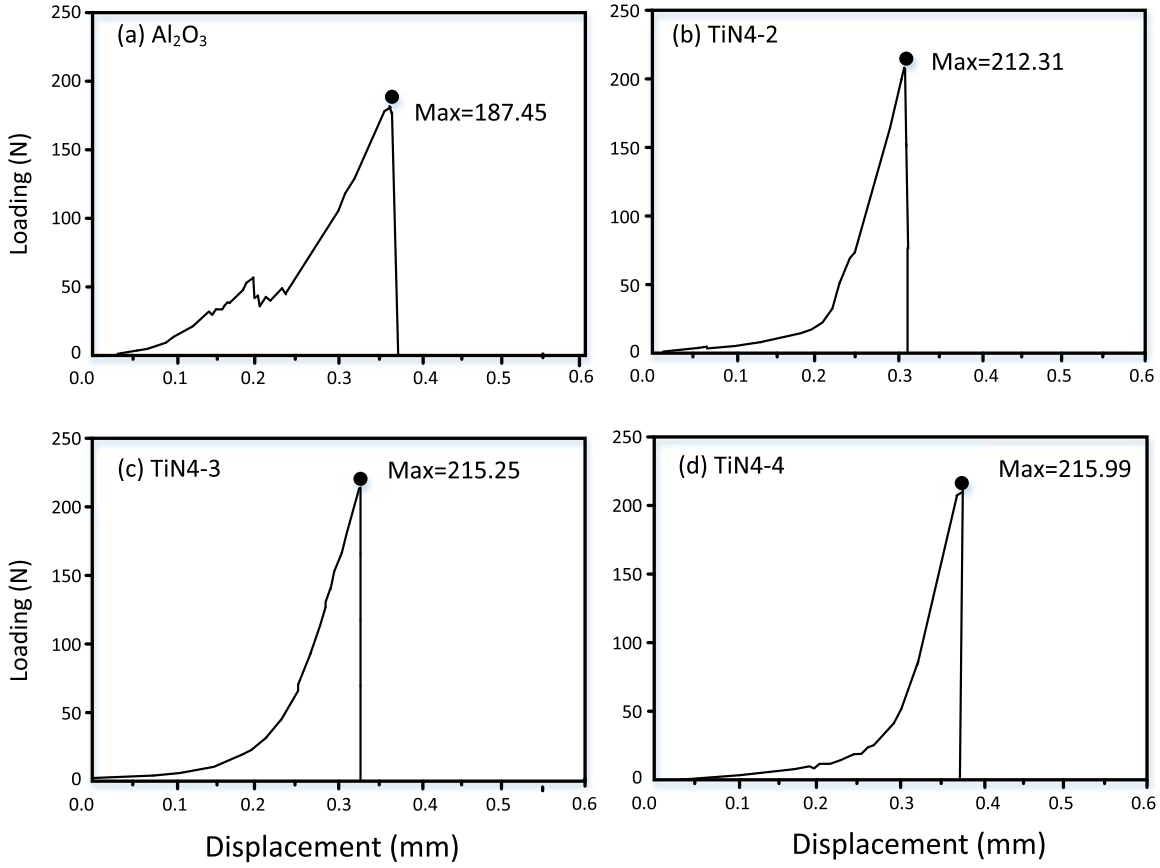

Fig. 13. The mechanical strength of the CMS membranes supported by (a) Al_2O_3, (b)TiN4-2, (c)TiN4-3, and (d)TiN4-4 supports.

support due to deep interlocking and strong adsorption. In this case, the polymer chain penetrated far down the alumina support, and a hard phase formed on the alumina surface (here denoted as vertical interlocking pattern) with good adsorption. When carbonization takes place, the phase becomes more dense with a lower sub-micropore volume. However, alumina modified with TiO_2 intermediate layer provides an interconnected channel for casting dope entering the support. The interconnected open pore structure is capable of producing a large pore volume (Table 2) to interlock with the polymer chain, and narrowing down the connected depth within 2.0–2.2 μm ($<$2.8 μm of alumina support, as shown in Table 3 and Fig. 6). Such interconnected pore structure provides a "networking interlocking pattern" that prevents the formed dense matrix from deep penetration. Thus, we conclude that with a certain interlocking pattern, rather than interlocking depth, the intermediate layer improves CMS membrane performance based on the above results.

3.6. *Mechanical strength TiO_2/Al_2O_3 supported CMS membrane*

In this section, the membrane supported on the TiN4 series supports exhibiting high perm-selectivity performance was chosen to investigate mechanical strength by changing gas feed pressure and using the biaxial method. Fig. 12 shows that H_2, CO_2, O_2, N_2, and CH_4 permeability did not change with increased feed pressure. The feed pressure had no effect on gas permeance, indicating that the membrane can operated up to at least 6 atm. Fig. 13 shows the mechanical strength measured using the biaxial method. The conventional bare Al_2O_3 support has an average strength of 187.45 N. Moreover, for a given axial loading up to 50 N, a discrete point was observed because of crack formation inside the membrane. Axial loading was then continuously increased to 187.45 N, at which the membrane fractured. However, when the Al_2O_3 support was modified with a TiO_2 intermediate layer, the strength increased to 215 N, and no discrete point was observed inside the membrane. The CMS membrane supported on TiO_2-modified support did not have a crack formation stage when the strength was continuously increased to 215 N. Thus, improving the "interlocking pattern" and surface chemical bonding between the support and selective layers instead of the interlocking depth can increase the mechanical strength of the entire membrane.

4. Conclusions

In this study, a Carbon/TiO_2/Al_2O_3 molecular sieving membrane synthesized via a sol–gel spin coating method followed by a carbonization process was proposed for the first time. Significantly influence on the adhesion mechanisms is observed from the TiO_2 intermediate layer coverage on an Al_2O_3 support and the microstructure and surface roughness of the TiO_2/Al_2O_3 composite support, whose fractions strongly depended on the sol–gel conditions, i.e., the molar ratio of HNO_3/TTIP and the number of coatings.

Furthermore, to the best of our knowledge, the adhesion mechanisms of the CMS layer on the TiO_2/Al_2O_3 composite support were evaluated for the first time using EDX-line scanning, FTIR, and contact angle to determine the contribution from mechanical interlocking, chemical bonding, and adsorption, respectively. The results show that the three adhesion mechanisms might simultaneously contribute to the intrinsic adhesion depending on the preparation variables of the TiO_2 nano-network. Therefore, it is difficult to discern the respective contribution of each mechanism; however, based on the gas separation performance, mechanical

interlocking and chemical bonding were the dominant mechanisms affecting the gas perm-selectivity.

Acknowledgment

The authors would like to gratefully acknowledge the financial support provided by the NSC Taiwan program (NSC 100-2221-E-040-004-MY3), and the Taiwanese-Czech Joint Research Project MOST/14/02.

References

[1] A.A. Olajire, CO_2 capture and separation technologies for end-of-pipe applications-a review, Energy 35 (2010) 2610–2628.
[2] G. Lu, J. Diniz da Costa, M. Duke, S. Giessler, R. Socolow, R. Williams, T. Kreutz, Inorganic membranes for hydrogen production and purification: a critical review and perspective, J. Colloid Interface Sci. 314 (2007) 589–603.
[3] A.B. Fuertes, T.A. Centeno, Preparation of supported asymmetric carbon molecular sieve membranes, J. Membr. Sci. 144 (1998) 105–111.
[4] S.M. Saufi, A.F. Ismail, Fabrication of carbon membranes for gas separation-a review, Carbon 42 (2004) 241–259.
[5] H.H. Tseng, G.L. Zhuang, M.D. Lin, S.H. Chang, M.Y. Wey, The influence of matrix structure and thermal annealing-hydrophobic layer on the performance and durability of CMS membrane during physical aging, J. Membr. Sci. 495 (2015) 294–304.
[6] H.H. Tseng, I.A. Kumar, Modification of carbon molecular sieve membrane structure by self-assisted deposition carbon segment for gas separation, J. Membr. Sci. 389 (2012) 223–233.
[7] H.H. Tseng, P.T. Shiu, Y.S. Lin, Effect of mesoporous silica modification on the structure of hybrid carbon membrane for hydrogen separation, Int. J Hydrog. Energy 36 (2011) 15352–15363.
[8] I.A. Kumar, H.H. Tseng, M.Y. Wey, Fabrication and characterization of PPO/PVP blend carbon molecular sieve membranes for H_2/N_2 and H_2/CH_4 separation, J. Membr. Sci. 372 (2011) 387–395.
[9] A.K. Itta, H.H. Tseng, Hydrogen separation performance of CMS membranes derived from the imide-functional group of two similar types of precursor, Int. J Hydrog. Energy 36 (2011) 8645–8657.
[10] H.H. Tseng, I.A. Kumar, T.H. Weng, C.Y. Lu, M.Y. Wey, Preparation and characterization of carbon molecular sieve membranes for gas separation application: the effect of incorporated multi-walled carbon nanotube, Desalination 240 (2009) 40–45.
[11] C.W. Jones, W.J. Koros, Carbon molecular sieve separation membranes-I. Preparation and characterization based on polyimide precursors, Carbon 32 (1994) 1419–1425.
[12] S.G. Anshu, W.J. Koros, Air separation properties of flat sheet homogeneous pyrolytic carbon membranes, J. Membr. Sci. 174 (2000) 177–188.
[13] M. Kiyono, P.J. Williams, W.J. Koros, Effect of pyrolysis atmosphere on separation performance of carbon molecular sieve membranes, J. Membr. Sci. 359 (2010) 2–10.
[14] Y. Xiao, Y. Dai, T.S. Chung, M.D. Guiver, Effects of brominating matrimid polyimide on the physical and gas transport properties of derived carbon membranes, Macromolecules 38 (2005) 10042–10049.
[15] P.S. Tin, T.S. Chung, Y. Liu, R. Wang, Separation of CO_2/CH_4 through carbon molecular sieve membranes derived from P84 polyimide, Carbon 42 (2004) 3123–3131.
[16] S.S. Hosseini, T.S. Chung, Carbon membranes from blends of PBI and polyimides for N_2/CH_4 and CO_2/CH_4 separation and hydrogen purification, J. Membr. Sci. 328 (2009) 174–185.
[17] X. Ma, R. Swaidan, B. Teng, H. Tan, O. Salinas, E. Litwiller, Y. Han, I. Pinnau, Carbon molecular sieve gas separation membranes based on an intrinsically microporous polyimide precursor, Carbon 62 (2013) 88–96.
[18] R. Swaidan, X. Ma, E. Litwiller, I. Pinnau, High pressure pure- and mixed-gas separation of CO_2/CH_4 by thermally-rearranged and carbon molecular sieve membranes derived from a polyimide of intrinsic microporosity, J. Membr. Sci. 447 (2013) 387–394.
[19] L. Xu, M. Rungta, W.J. Koros, Matrimide derived carbon molecular sieve hollow fiber membranes for ethylene/ethane separation, J. Membr. Sci. 380 (2011) 138–147.
[20] L. Xu, M. Rungta, M.K. Brayden, M.V. Martinez, B.A. Stears, G.A. Barbay, W. J. Koros, Olefins-selective asymmetric carbon molecular sieve hollow fiber membranes for hybrid membrane-distillation processes for olefin/paraffin separations, J. Membr. Sci. 423–424 (2012) 314–323.
[21] C. Song, T. Wang, X. Wang, J. Qiu, Y. Cao, Preparation and gas separation properties of poly(furfuryl alcohol)-based C/CMS composite membranes, Sep. Purif. Technol. 58 (2008) 412–418.
[22] H.C. Lee, M. Monji, D. Parsley, M. Sahimi, P. Liu, F. Egolfopoulos, T. Tsotsis, Use of steam activation as a post-treatment technique in the preparation of carbon molecular sieve membranes, Ind. Eng. Chem. Res. 52 (2013) 1122–1132.
[23] K. Briceño, D. Montané, R. Garcia-valls, A. Iulianelli, A. Basile, Fabrication variables affecting the structure and properties of supported carbon molecular sieve membranes for hydrogen separation, J. Membr. Sci. 415–416 (2012) 288–297.
[24] S.C. Rodrigues, R. Whitley, A. Mendes, Preparation and characterization of carbon molecular sieve membranes based on resorcinol-formaldehyde resin, J. Membr. Sci. 459 (2014) 207–216.
[25] M. Teixeira, M.C. Campo, D.A. Pacheco Tanaka, M.A. Llosa Tanco, C. Magen, A. Mendes, Composite phenolic resin-based carbon molecular sieve membranes for gas separation, Carbon 49 (2011) 4348–4358.
[26] W. Deng, X. Yu, M. Sahimi, T.T. Tsotsis, Highly permeable porous silicon carbide support tubes for the preparation of nanoporous inorganic membranes, J. Membr. Sci. 451 (2014) 192–204.
[27] X. Ma, B.K. Lin, X. Wei, J. Kniep, Y.S. Lin, Gamma-alumina supported carbon molecular sieve membrane for proplyene/propane separation, Ind. Eng. Chem. Res. 52 (2013) 4297–4305.
[28] M.Y. Wey, H.H. Tseng, C.K. Chiang, Improving the mechanical strength and gas separation performance of CMS membranes by simply sintering treatment of α-Al_2O_3 support, J. Membr. Sci. 453 (2014) 603–613.
[29] Y. Huang, R. Dittmeyer, Preparation of thin palladium membranes on a porous support with rough surface, J. Membr. Sci. 302 (2007) 160–170.
[30] P. Kumar, J. Ida, S. Kim, V. Guliants, J. Lin, Ordered mesoporous membranes: effects of support and surfactant removal conditions on membrane quality, J. Membr. Sci. 279 (2006) 539–547.
[31] G. Li, H. Qi, Y. Fan, N. Xu, Toughening macroporous alumina membrane supports with YSZ powders, Ceram. Int. 35 (2009) 1641–1646.
[32] H.H. Tseng, K. Shih, P.T. Shiu, M.Y. Wey, Influence of support structure on the permeation behavior of polyetherimide-derived carbon molecular sieve composite membrane, J. Membr. Sci. 405–406 (2012) 250–260.
[33] C. Wang, X. Hu, J. Yu, L. Wei, Y. Huang, Intermediate gel coating on macroporous Al_2O_3 substrate for fabrication of thin carbon membranes, Ceram. Int. 40 (2014) 10367–10373.
[34] W. Zhou, M. Yoshino, H. Kita, K. Okamoto, Carbon molecular sieve membranes derived from phenolic resin with a pendant sulfonic acid group, Ind. Eng. Chem. Res. 40 (22) (2001) 4801–4807.
[35] M.Y. Wey, H.H. Tseng, C.K. Chiang, Effect of MFI zeolite intermediate layers on gas separation performance of carbon molecular sieve (CMS) membranes, J. Membr. Sci. 446 (2013) 220–229.
[36] M.R. Bayati, H.R. Zargar, A. Talimian, A. Ziaee, R. Molaei, Characterization of Al_2O_3-TiO_2 nano porous solar absorbers derived via MAO/sol–gel hybrid process, Surf. Coat. Technol. 205 (2010) 2483–2489.
[37] W. Zhang, S. Chen, S. Yu, Y. Yin, Experimental and theoretical investigation of the pH effect on the titania phase transformation during the sol–gel process, J Cryst. Growth 308 (2007) 122–129.
[38] S. Melada, S.A. Ardizzone, C.L. Bianchi, Sulphated zirconia by sol–gel route. The effects of the preparative variables, Microporous Mesoporous Mater. 73 (2004) 203–209.
[39] C.Y. Wu, Y.L. Lee, Y.S. Lo, C.J. Lin, C.H. Wu, Thickness-dependent photocatalytic performance of nanocrystalline TiO_2 thin films prepared by sol–gel spin coating, Appl. Surf. Sci. 280 (2013) 737–744.
[40] W. Wei, S. Xia, G. Liu, X. Gu, W. Jin, N. Xu, Interfacial adhesion between polymer separation layer and ceramic support for composite membrane, AIChE J. 56 (2010) 1584–1592.
[41] L.M. Robeson, The upper bound revisited, J. Membr. Sci. 320 (2008) 390–400.
[42] M.C. Campo, F.D. Magalhães, A. Mendes, Carbon molecular sieve membranes from cellophane paper, J. Membr. Sci. 350 (2010) 180–188.
[43] L.H. Cheng, Y.J. Fu, K.S. Liao, J.T. Chen, C.C. Hu, W.S. Hung, K.R. Lee, J.Y. Lai, A high-permeance supported carbon molecular sieve membrane fabricated by plasma-enhanced chemical vapor deposition followed by carbonization for CO_2 capture, J. Membr. Sci. 460 (2014) 1–8.
[44] S. Fu, E.S. Sanders, S.S. Kulkarni, W.J. Koros, Carbon molecular sieve membrane structure–property relationships for four novel 6FDA based polyimide precursors, J. Membr. Sci. 487 (2015) 60–73.
[45] S.S. Hosseini, M.R. Omidkhah, A. Zarringhalam Moghaddam, V. Pirouzfar, W. B. Krantz, N.R. Tan, Enhancing the properties and gas separation performance of PBI–polyimides blend carbon molecular sieve membranes via optimization of the pyrolysis process, Sep. Purif. Technol. 122 (2014) 278–289.
[46] Y.K. Kim, H.B. Park, Y.M. Lee, Preparation and characterization of carbon molecular sieve membranes derived from BTDA–ODA polyimide and their gas separation properties, J. Membr. Sci. 255 (2005) 265–273.
[47] K.S. Liao, Y.J. Fu, C.C. Hu, J.T. Chen, Y.H. Huang, M.D. Guzman, S.H. Huang, K. R. Lee, Y.C. Jean, J.Y. Lai, Development of the asymmetric microstructure of carbon molecular sieve membranes as probed by positron annihilation spectroscopy, J. Phys. Chem. C 117 (2013) 3556–3562.
[48] A.B. Fuertes, T.A. Centeno, Carbon molecular sieve membranes from polyetherimide, Microporous Mesoporous Mater. 26 (1998) 23–26.
[49] W.N.W. Salleh, A.F. Ismail, Carbon hollow fiber membranes derived from PEI/PVP for gas separation, Sep. Purif. Technol. 80 (2011) 541–548.

Journal of Membrane Science 495 (2015) 294–304

Contents lists available at ScienceDirect

Journal of Membrane Science

journal homepage: www.elsevier.com/locate/memsci

The influence of matrix structure and thermal annealing-hydrophobic layer on the performance and durability of carbon molecular sieving membrane during physical aging

Hui-Hsin Tseng [a,b], Guo-Liang Zhuang [c], Min-Der Lin [c], Ssu-Hsun Chang [c], Ming-Yen Wey [c,*]

[a] School of Occupational Safety and Health, Chung Shan Medical University, Taichung 402, Taiwan, ROC
[b] Department of Occupational Medicine, Chung Shan Medical University Hospital, Taichung 402, Taiwan, ROC
[c] Department of Environmental Engineering, National Chung Hsing University, Taichung 402, Taiwan, ROC

ARTICLE INFO

Article history:
Received 16 January 2015
Received in revised form
2 July 2015
Accepted 2 August 2015
Available online 13 August 2015

Keywords:
Hydrophobic layer
Thermal annealing
CMS membrane
Gas separation
Aging

ABSTRACT

Although carbon surfaces are generally hydrophobic, the surface oxygen-containing groups act as water molecule sorption sites, reducing the performance of carbon molecular sieving (CMS) membranes over time. In this study, a hydrophobic poly(2,6-dimethyl-1,4-phenylene oxide) (PPO) layer was coated on the surface of PPO- or polyetherimide (PEI)-derived CMS membranes to protect against aging. The permeation properties and anti-aging characteristics of the modified CMS membranes were explored using a single gas permeability test. Furthermore, thermal annealing below the PPO's glass transition temperature was applied to the hydrophobic layer to evaluate its anti-aging effect. The results indicate that the aging of CMS membranes was also determined by the carbon matrix structure and that a smaller pore size could prevent water adsorption and O_2 chemisorption. After the hydrophobic layer was post-treated with thermal annealing, the gas diffusion resistance was diminished, and the initial permeance was retained to approximately 60%, showing slight loss within the testing period.

1. Introduction

After Koresh and Soffer [1] proposed a simple thermal treatment method for producing carbon membranes, carbon molecular sieve (CMS) membranes have become promising candidates for gas separation, particularly CO_2 capture from combustion processes [2]. CMS membranes possess random porous networks typically obtained by pyrolyzing polymer films under vacuum or an inert atmosphere at high temperatures (ca. 450–800 °C). The pyrolysis process vaporizes the labile side groups of the polymer precursor, leaving space between the inter-chains in the carbon matrix; the formed carbon materials contain narrow micropore and ultra-micropore sizes similar to the molecular dynamic diameter of gas molecules (<0.6 nm) [3–5]. This technique generates a highly porous membrane, facilitating gas separation via molecular sieving and surface diffusion mechanisms. Given their high porosity, the CMS membranes exhibit superior perm-selectivity compared to other materials [6–10].

However, CMS membranes experience negative effects in humid environments or air because of oxygen chemisorption, reducing their performance over time [11–14]. Although carbon surfaces are generally hydrophobic, the surface oxygen-containing groups also act as water molecule sorption sites. The additional water molecules are absorbed in sequence, filling the porosity of the carbon matrix through hydrogen bonding and reducing the diffusion pathways available to other permeating species [11]. Saufi and Ismail [15] noted that the separation performance of CMS membranes decreased by as much as 80% over 14 months. This aging phenomenon is caused by the chemisorption and physisorption processes that occur when the material has been exposed to air for a long time. Menendez and Fuertes [13] studied the effect of the storage atmosphere (air, nitrogen, and propylene) on the aging of membranes over time. The storage atmosphere containing oxygen exhibited serious problems; the permeability of N_2, O_2, and CO_2 decreased by nearly 50% after one day of storage and could only partially be regenerated via heat treatment.

Therefore, the regeneration of CMS membranes through physical and chemical treatments to extend their lifespan was evaluated by various techniques. Previous studies have suggested three main strategies to revive CMS membranes: (1) cleaning with an organic agent to remove chemisorbed organic materials by dissolution. Jones et al. [11] demonstrated the regeneration of CMS membranes using propylene. The propylene removed the

* Corresponding author. Fax: +886 4 22862587.
E-mail address: mywey@dragon.nchu.edu.tw (M.-Y. Wey).

http://dx.doi.org/10.1016/j.memsci.2015.08.009
0376-7388/

absorbed compounds from the carbon surface, thereby restoring the gas permeance. However, the use of cleaning agents can be costly. (2) Heating treatment to remove both physisorbed water and chemisorbed organic material. Lagorsse et al. [16] analyzed the impact of removing surface oxygen on the adsorption equilibrium, kinetic transport, and pore structure. The differences compared to the untreated specimens were negligible because of irreversible chemisorption. (3) Using electrochemical treatments to remove organic compounds from the surface of carbon materials [17,18]. This method is advantageous because of its low operating temperature, lack of required agents, and high regeneration efficiency. However, the regeneration process remains costly and difficult even without any apparent carbon loss [19].

In addition to a capacity for regeneration, the carbon membrane should have long-term stable permeance without significant aging to achieve a suitable membrane lifetime. Using coating techniques to form a hydrophobic layer is another favored pretreated method used to extend the lifespan of virgin carbon membranes, allowing the membranes to endure storage in an air or organic gas environment better than CMS membranes. However, to the best of our knowledge, coating of hydrophobic layers on the surface of CMS membranes has rarely been studied. Jones and Koros [11] studied the water-vapor resistance of carbon composite membranes. The highly hydrophobic polymer used as the precursor for the coating layer included poly(4-methyl-1-pentene), in addition to DuPont Teflon AF1600 and AF2400 amorphous fluoropolymer copolymers. The results indicated that coating the CMS membrane with a protective layer can restore the O_2 flux loss from 58% to 11% in the long term. The polymer barrier has a dense structure. Therefore, the permeability exhibited no apparent loss, but the selectivity was reduced.

The main objective of this study was to assess the effect of carbon membrane structure on long-term uses of CMS membranes in applications such as O_2-containing gas separation and to explore the preparation conditions of the hydrophobic layer to prevent or delay aging. Thus, semi-crystal poly(p-phenylene oxide) (PPO) was used as the precursor to the hydrophobic layer of CMS membrane because it shows higher permselectivity nature than other conventional polymers. To maintain the separation performance, the structure of the hydrophobic layer was altered with cast doping of PPO of different viscosities and thermal annealing post-treatment. In addition, two different structures of CMS membranes derived from PPO and polyetherimide (PEI) precursors were fabricated to determine the possible viscosity influence and thermal annealing mechanism and the anti-aging effect. This study aimed to produce a CMS membrane with a longer lifespan for storage under atmospheric conditions. The aging properties of hydrophobic-coated CMS membranes were investigated through long-term operation with H_2, CO_2, O_2, N_2, and CH_4 gas molecules for 30 days.

2. Experimental

2.1. Materials

The PPO and PEI polymer precursors were purchased from Sigma-Aldrich Chemical (USA). N-Methyl-2-pyrrolidone (NMP) and chloroform were supplied by Mallinckrodt Chemical (USA) and used as received. A support substrate (α-Al_2O_3 disk-typed green) with a diameter of 23 mm and thickness of 1.4 mm was purchased from Ganya Fine Ceramics (Taiwan) and used after sintering in our laboratory.

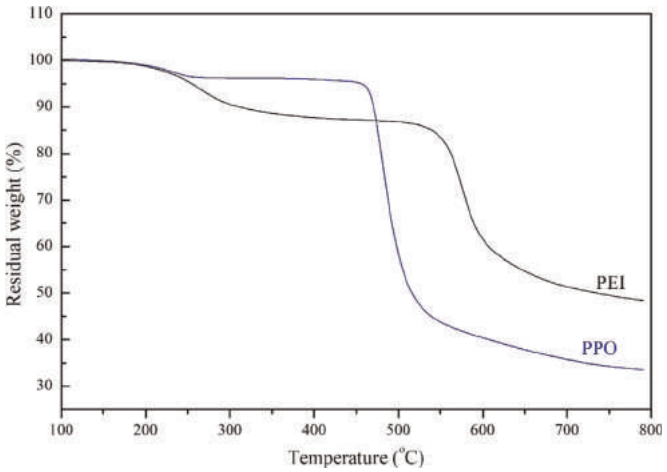

Fig. 1. Thermogravimetric analysis curves obtained from PPO and PEI polymer precursor.

2.2. Preparation

The CMS membranes were prepared using a single coating-pyrolysis cycle procedure. The casting dope was prepared by magnetically stirring PPO and PEI in chloroform and NMP, respectively, at room temperature, forming a homogeneous 10 wt% solution. The dope was spread on the surface of the support substrate by spin coating at 2000 rpm for 18 s. After coating, the polymer film was dried at ambient temperature for 24 h, followed by curing at 240 °C with a 5 °C/min heating rate for 6 h and carbonization at 600 °C with a 5 °C/min heating rate for 2 h under vacuum. The resultant CMS membrane was slowly cooled to room temperature and stored in a desiccator before use. The PPO- and PEI-derived CMS membranes are represented by PO and EI, respectively.

The hydrophobic layer was also coated by spin coating. The desired amount of PPO was dissolved in chloroform using magnetic stirring for 24 h at room temperature to form homogeneous 1.5, 3.0, 5.0, and 7.0 wt% solutions. The viscosity of the various dopes was measured at room temperature using a Brookfield cone-and-plate viscometer (Model HB DV-III) equipped with a CP 52 spindle. The dope was then spread on the surface of the CMS membrane by spin coating and then dried at ambient temperature for 24 h.

Thermal annealing of the hydrophobic layer was conducted with a vacuum furnace equipped with a temperature controller. The coated samples were placed in the furnace and heated to the required temperature of 230 °C under vacuum for 2 h with heating rate of 5 °C/min. After the desired time was reached, the annealed samples were slowly cooled to room temperature and removed from the furnace. Then, all of the samples were kept in plastic bag containing silica gel and started for permeation tests within 24 h. The CMS membrane with different dope concentrations for the hydrophobic layer and thermal annealing are represented by PO-(or EI)-X-Y, in which X represents the dope concentration of the hydrophobic solution and Y represents the presence (HT) or absence (RT) of heat treatment. For example, the PPO-derived CMS membrane with a coated 1.5 wt% hydrophobic layer and thermal annealing is expressed as PO-1.5-HT.

2.3. Characterization

Several analysis techniques were used to characterize the modified CMS membranes. A scanning electron microscope (SEM, JEOL JSM-6700F) was used to observe the outer surface and cross-sectional morphologies of the CMS membranes.

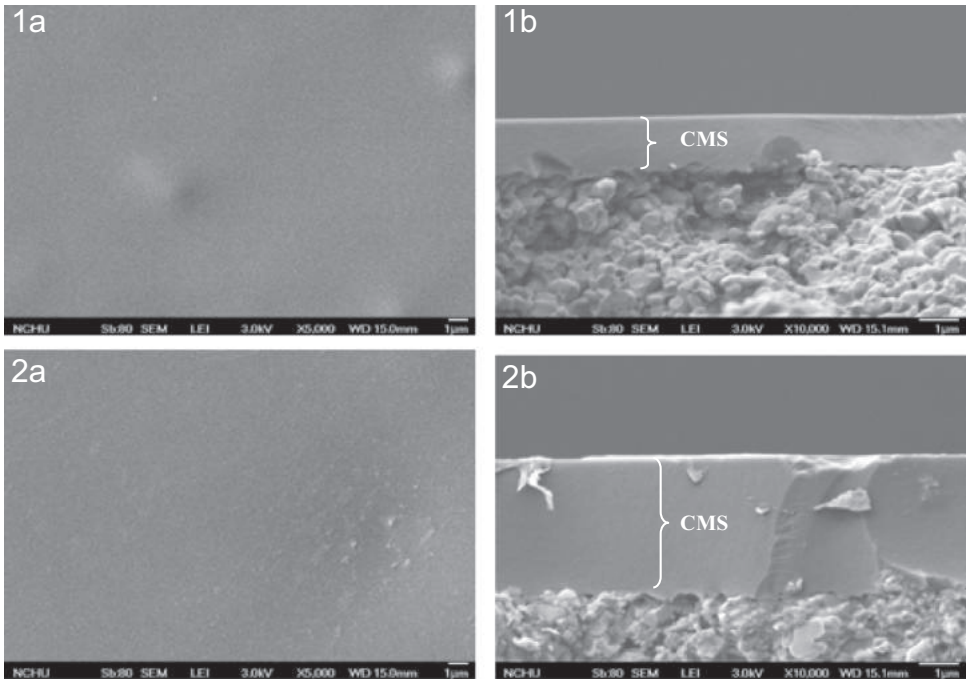

Fig. 2. FE-SEM images of CMS membranes derived from (1) PPO and (2) PEI precursors; (a) top view and (b) cross-sectional view.

Table 1
Permeability of five gases and d-spacing of pristine PO, EI, and EI-500 CMS membranes.

Sample code	d-Spacing (Å)	Thickness (μm)	Permeability (Barrer)					Selectivity		
			H_2	CO_2	O_2	N_2	CH_4	H_2/CO_2	CO_2/N_2	CO_2/CH_4
PO	4.76	1.45–1.75	925.7 ± 124.4	246.3 ± 36.9	85.1 ± 6.6	13.3 ± 4.8	7.1 ± 1.8	3.76	18.5	36.7
EI	4.32	3.66	848.8 ± 132.9	190.4 ± 33.1	64.8 ± 25.3	8.3 ± 4.9	7.4 ± 4.1	4.46	22.9	25.7
EI-500	4.08	4.26	452.3 ± 86.2	92.4 ± 26.5	28.5 ± 5.4	4.6 ± 2.1	3.2 ± 1.2	4.89	20.09	28.9

The d-spacing value of carbon matrix was recorded by X-ray diffraction (XRD) using a PW1830 X-ray powder diffractometer (Philips) with a Cu-Kα source ($\lambda = 1.5418$ Å) and a wide Bragg angle range ($20° \le 2\theta \le 70°$) with a 2°/min scanning rate.

Atomic force microscopy (AFM) was used to examine the surface properties of the CMS membrane. The membrane surfaces were compared in terms of the mean roughness (Ra) of the surface captured using the AFM; the roughness was calculated using the AFM software according to the following equation:

$$R_a = \frac{1}{L_x L_y} \int_0^{L_x} \int_0^{L_y} |f(x, y)| dx\, dy, \tag{1}$$

where $f(x, y)$ is the surface relative to the center plane, whereas L_x and L_y are the dimensions of the surface. The center plane is the plane at which the volumes above and below are equal. The roughness parameters of the membrane surfaces were acquired using AFM in tapping mode with an NS3a D3100 scanner from Digital Instruments.

2.4. Permeation test

The gas permeance through a multilayered composite CMS membrane was measured using a standard vacuum time-lag system. The composite membrane with a 3.14 cm^2 effective area was attached to a permeation cell (25 mm disk fillers, Millipore, USA) and degassed by exposing both sides of the membrane to vacuum overnight. The gases tested in this work included H_2, CO_2, O_2, N_2, and CH_4. The permeance of the pure gases was estimated downstream using a pressure transducer and digital equipment connected to a computer. After the permeation tests started, the membranes were removed from cell after each data point was taken and stored in ambient air.

The gas permeance (cm^3(STP)/cm^2 s cmHg), P/L, was given as follows:

$$\frac{P}{L} = \frac{Q}{A\Delta p} \tag{2}$$

where P is the permeability of the separation layer (cm^3(STP)/cm^2 s cmHg), L is the effective thickness of the separating layer (cm), Δp is the transmembrane pressure difference (cmHg), A is the membrane surface area (cm^2), and Q is the gas flux (cm^3(STP)/s). A gas permeation unit (1×10^{-6} cm^3 (STP)/cm^2 s cmHg) was used in this study. The ideal separation factor for gas A over gas B was given as follows;

$$\alpha_{A/B} = \frac{(P/L)_A}{(P/L)_B} \tag{3}$$

3. Results and discussion

3.1. Characterization and aging of pristine CMS membranes

The thermal properties of the pure PPO and PEI polymers were examined by thermogravimetric analysis (TGA). As shown in Fig. 1, the differential TGA scan curves illustrates that the initial

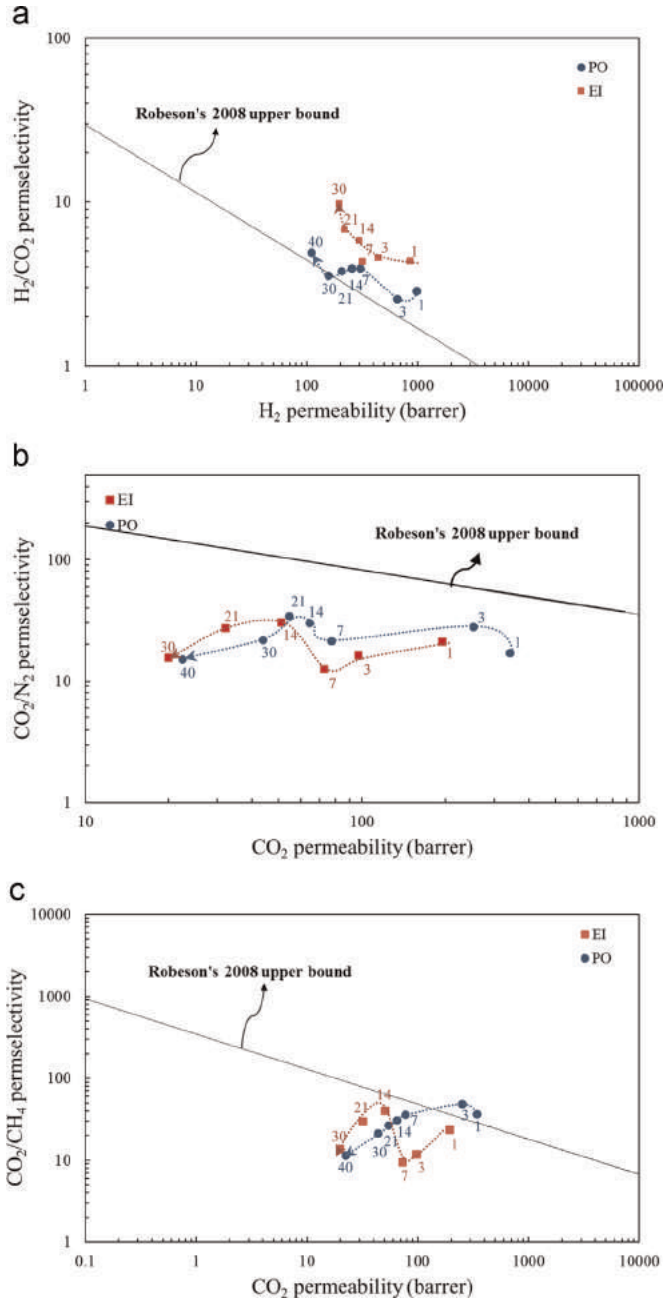

Fig. 3. The variation with time of the perm-selectivity of pristine PO and EI CMS membranes (the number labeled is aging time).

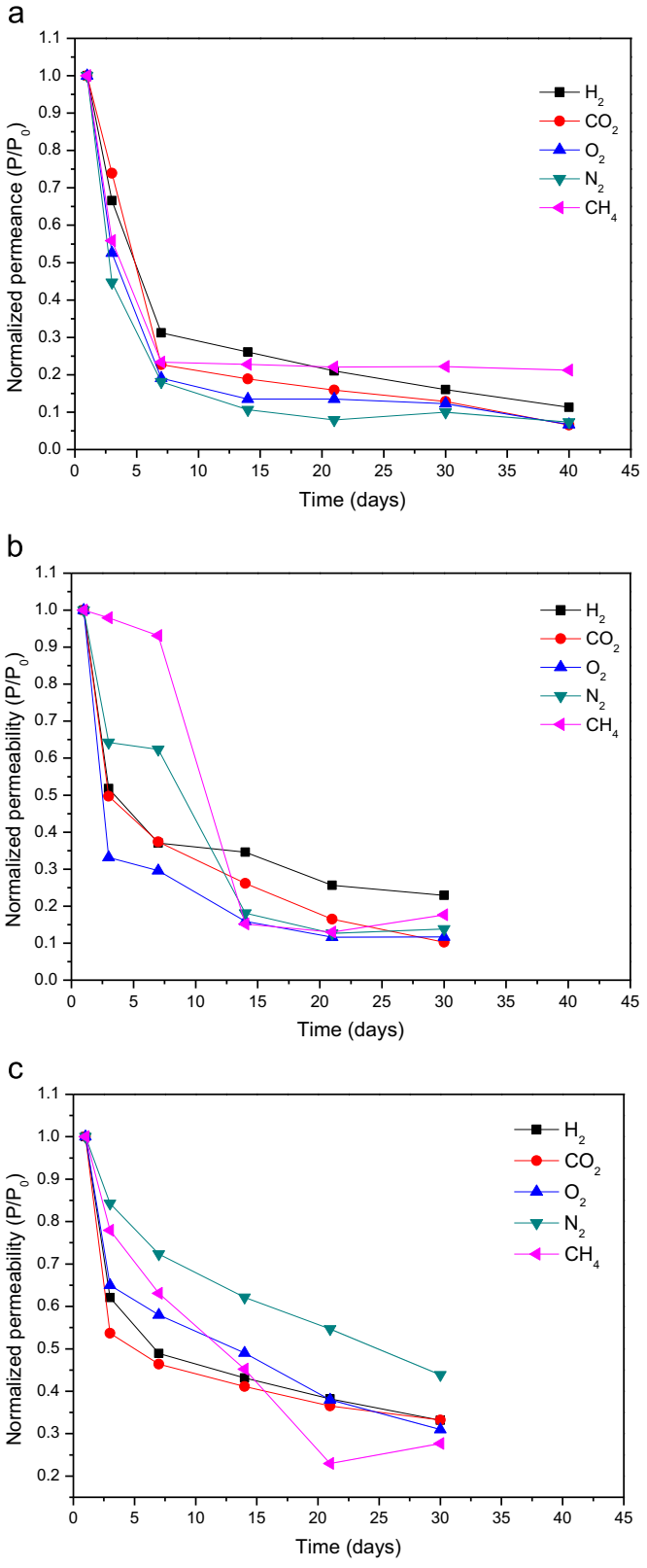

Fig. 4. The normalized permeability (P/P_0) towards H_2, CO_2, O_2, N_2, and CH_4 of (a) PO, (b) EI and (c) EI-500 CMS membranes after exposure to a laboratory air environment at 28 °C.

decomposition temperatures of the PPO and PEI precursors were at 460 °C and 550 °C, respectively, and at the final temperature of 800 °C, the remaining weight percentage of PPO was 36%, which was much lower than that of PEI (50%). In general, the process of dense carbon membrane formation from a thermosetting polymer precursor includes a depolymerization step followed by ring-open polymerization and graphitization [20,21]. The final pore size distribution of the carbon membrane depended on the re-arrangement of the carbon matrix during the pyrolysis procedure. To obtain a critical size ranging from 3 to 7 Å [16], the pyrolysis protocol of carbonization was initiated from 30 °C to 600 °C with a 5 °C/min heating rate and maintained for 2 h for the fabrication of the CMS membranes.

As shown in Fig. 2, the top view (Fig. 2(a)) and cross-sectional view (Fig. 2(b)) of the pristine PO and EI CMS membranes show a smooth surface within a dense structure. These structures are typical of CMS membranes derived from PPO and PEI precursor via the decompose stage followed by carbonization [22]. The thickness of the pristine EI CMS layers differed from that of the PO CMS layers, as the values were approximately 3.66 and 1.45 μm,

Table 2
Surface roughness and thickness of PPO polymer protective layer.

Sample code	Roughness (nm)	Thickness (μm)	Sample code	Roughness (nm)	Thickness (μm)
PO-RT	12.9	1.45[a]	EI-RT	5.2	3.66[a]
PO-1.5-RT	13.0	0.05	EI-1.5-RT	4.4	0.1–0.2
PO-3.0-RT	9.2	< 0.15	EI-3.0-RT	2.2	1.3–1.4
PO-5.0-RT	6.8	0.2 ~ 0.3	EI-5.0-RT	1.5	1.0–1.1
PO-7.0-RT	8.9	1.0 ~ 1.1			

N.D.: Not detected.

[a] Thickness of PPO- or PEI-derived carbon molecular sieve layer.

respectively. This difference may have resulted from different thermal stability of the polymer chain and variation in the matrix structure after carbonization. The PPO is liable to undergo thermal decomposition where the layer would become thinner than the EI layers.

The permeance and aging of pristine CMS membranes was tested using several gases, and the CMS membranes were stored in ambient conditions (laboratory environment) before evaluation at 40 days. As shown in Table 1, the single gas permeabilities of H_2, CO_2, O_2, N_2, and CH_4 determined for the PO and EI CMS membranes followed the order of $H_2 > CO_2 > O_2 > N_2 > CH_4$, which was in accordance with the kinetic diameters of the gas molecules. This is a typical permeation characteristic of CMS membranes, which indicates that the permeation mechanism was dominated by the molecular sieving mechanism. The absolute permeability of PO is approximately 15–20% higher than that of EI based on gradual pore opening, and this variation in permeability could also influence the selectivity.

The variation of permeability and selectivity of PO and EI on virgin CMS membranes over time is illustrated in Fig. 3. Fig. 3 (a) shows the variation over time of H_2 permeability vs. H_2/CO_2 selectivity compared with Robeson's line, Fig. 3(b) and 3(c) shows the perm-selectivity towards CO_2/N_2 and CO_2/CH_4, respectively. The pristine EI CMS membrane exhibited high permeability and permselectivity for separation of gas pairs such as CO_2/CH_4 (α=25.7, P_{CO_2}=190.4 Barrer) and H_2/CO_2 (α=4.46, P_{H_2}=848.8 Barrer). This combination of selectivity and permeability exceeded Robeson's 2008 upper bond limit found for polymeric membranes [23]. Furthermore, the PO membrane showed higher selectivity for CO_2/CH_4 than the EI membrane; however, the H_2/CO_2 selectivity obtained from PO was lower than that of EI. Using the same carbonization protocol to fabricate a CMS membrane from two different polymer precursors (PEI and PPO) probably causes a change in the carbon matrix, where the average pore width is shifted towards the sieving diameter of CO_2 (3.3 Å). This pore narrowing excludes carbon dioxide to a larger extent when PEI is used as the precursor material. Therefore, the pristine carbon membranes prepared in this study are attractive materials for H_2/CO_2 and CO_2/CH_4 separation.

However, a rapid loss of permeability was observed. Immediately after air exposure in the laboratory environment, a decrease in gas permeability was noticed. Fig. 4 presents the permeability of the five gases as a function of aging time for the pristine PO and EI CMS membrane, normalized by the permeability value at an aging time of one day as shown in Table 1. Fig. 4 shows that the permeability rapidly decreased with the aging time during the first few days. For the PO CMS membrane (Fig. 4(a)), the permeability of H_2 and CO_2 decreased by nearly 33% and 26%, respectively, after one day of storage, whereas the permeability of O_2, N_2, and CH_4 decreased by nearly 45–55%. For longer durations (30 days) of storage in the air of the laboratory environment, the permeability was approximately 80–90% decreased for all gases. As expected, the H_2/CO_2 permselectivity (Fig. 3) vs. permeability showed an increase at longer storage times, i.e., 2.2 times higher than that of the fresh sample after 30 days. In contrast, the permselectivities of the other gas pairs (CO_2/N_2 and CO_2/CH_4) did not show an increase; rather, they decreased with aging time.

The storage of EI CMS membranes under the same conditions resulted in a moderate decline in gas permeability. Comparing Fig. 4(a) and 4(b), some appreciable differences existed between PO and EI CMS membranes. For the smaller gases, H_2, CO_2, and O_2, the permeability decreased quickly but remained higher than 10% to 20%, whereas for the larger gases CH_4 and N_2, the permeability decreased slowly by 7% and 38% after seven days, respectively. The EI membrane exhibited a less rapid relative decline in permeability compared with that of PO membrane, which suggests that the matrix structure of the CMS membrane plays a relevant role in the loss of permeability. To evaluate more accurately the effect of the matrix structure of the CMS membrane, the evolution of the permeation properties of a carbon membrane fabricated with a PEI precursor but pyrolyzed at 500 °C, possessing a smaller pore size and lower pore volume [21], was analyzed. For the EI CMS membrane pyrolyzed at 500 °C, the decline in permeance was less than that of the PO or EI CMS membrane pyrolyzed at 600 °C (as shown in Table 1 and Fig. 4(c)). A small change in the effective micropore size can seriously alter the permselectivity performance and aging phenomenon. The results obtained suggest that CMS membranes possessing a smaller pore size undergo partial passivation of the membrane, delaying the aging process. The above assumptions can be verified by the d-spacing value obtained from the X-ray diffraction, which is widely used for characterization the distance between interplanar carbon layers. As indicated in Table 1, the d-spacing value of pristine CMS membranes were followed the sequence of PO (4.76 Å) > EI (4.32 Å) > EI-500 (4.08 Å). Therefore, a smaller in the pore structure of EI and EI-500 was observed.

This is an unexpected and intriguing result that may be attributed to decreased (a) water adsorption or (b) oxygen chemisorption with the smaller pore size. To clarify the dominant aging mechanism of the CMS membrane, aged CMS membranes were thermally regenerated with the pyrolysis conditions (EI and PO were heated to 600 °C and EI-500 was heated to 500 °C for 2 h with a 5 °C/min ramping rate). After thermal regeneration, the recovery of the gas permeance of H_2 and CO_2 followed the order EI-500 > EI > PO, which suggests that CMS membranes having smaller pore size can be regenerated more easily by thermal treatment, although the recovery rate was still low. A possible explanation for this finding is that the molecular size of water is smaller than that of oxygen; the water, is more easily transported into the inner pore to be adsorbed before oxygen chemisorption. Menendez and Fuertes [13] also found that water adsorption on the carbon membrane micropores partially protects them against oxygen chemisorption.

In addition to the matrix structure, there are other potential reasons why the aging behavior of PO at 35 °C differs so markedly from that of EI. One notable difference between PO and EI is the difference in matrix structure and surface roughness, as PO possesses a higher surface roughness and pore volume than EI (as shown in Table 2). Differences in the thickness-dependence of aging for these membranes could be attributed to differences in matrix structure. Kim et al. observed a weakening of the thickness-dependence of the aging rate of thin 6FDA-based polyimide membranes (based on CO_2 permeability data) as the crosslinking treatment [24]. Murphy et al. also observed a smaller difference between the aging rates of relatively bulk PS and thin (400 nm) PS films as the pore volume was increased [25].

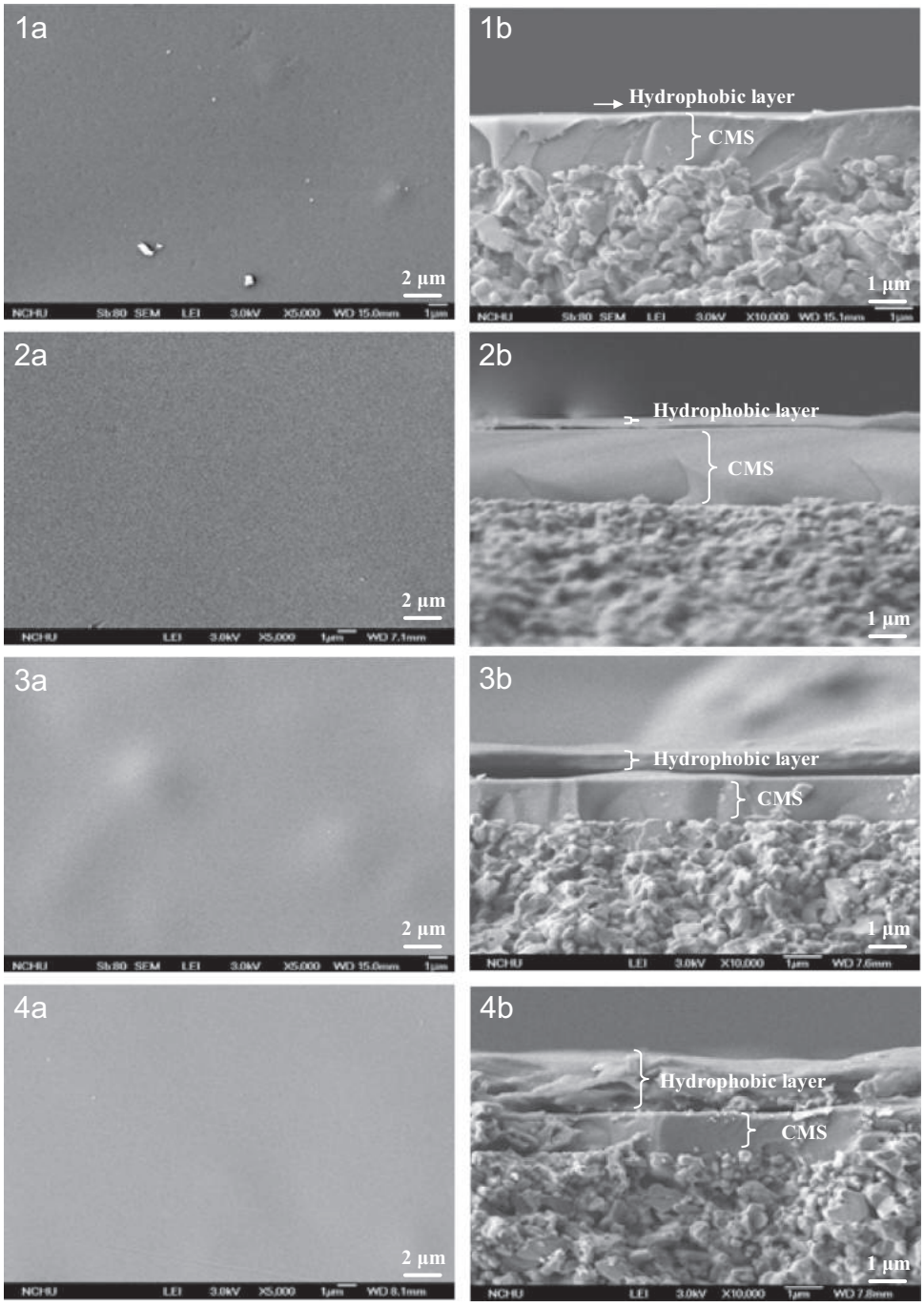

Fig. 5. FE-SEM images of a hydrophobic layer-coated PO CMS membrane: (1) PO-1.5-RT, (2) PO-3.0-RT, (3) PO-5.0-RT, and (4) PO-7.0-RT; (a) top view and (b) cross-sectional view.

Table 3
Viscosity of casting dope with different concentrations.

Sample code	Composition of casting dope (wt%)		Viscosity (Pa s)
	PPO	Chloroform	
1.5% PPO	1.5	98.5	–[a]
3.0% PPO	3.0	97.0	6.9
5.0% PPO	5.0	95.0	10.4
7.0% PPO	7.0	93.0	13.8

[a] Lower detection limit.

3.2. Delaying aging by coating a hydrophobic PPO layer

Different methods were proposed to overcome the decline in permeability of aged CMS membranes over time. First, a hydrophobic PPO film was coated on the surface of the CMS membrane by spin coating to eliminate the H_2O adsorbed into the carbon matrix. In general, fresh PPO polymer membranes have a hydrophobic nature and have good permselectivity toward gas pairs such as CO_2/CH_4. Therefore, the PPO film can be considered to act as a hydrophobic layer to prevent H_2O adsorption and decrease the pore size against O_2 chemisorption. Fig. 5 shows FE-SEM images of

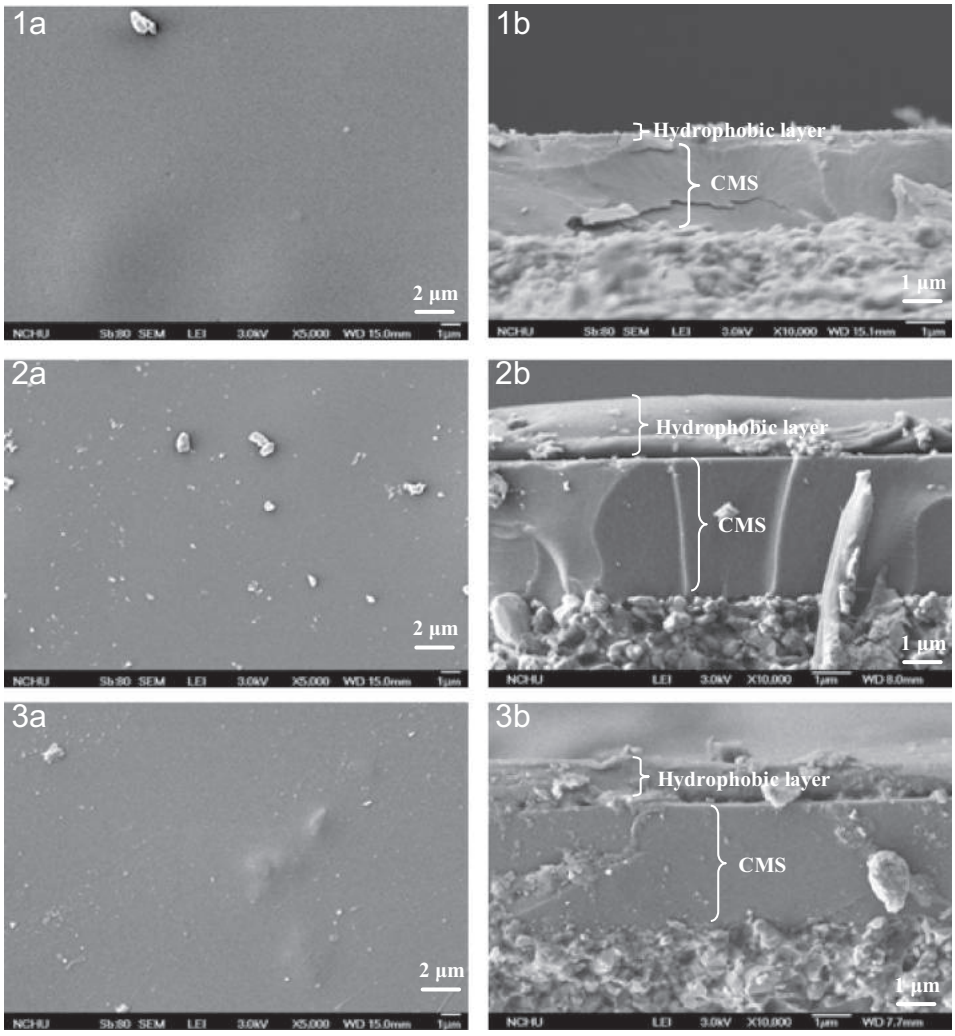

Fig. 6. FE-SEM images of hydrophobic layer-coated EI CMS membrane: (1) EI-1.5-RT, (2) EI-3.0-RT, and (3) EI-5.0-RT; (a) top view and (b) cross-sectional view.

a PPO film-coated PO CMS membrane. The top surface of the modified CMS membranes (Figs. 5(1a)-(4a)) had features similar to those of pristine PO CMS membranes (Fig. 2(1a)). A smooth and dense surface without any defects was formed after dry-phase inversion. A three-layer structure was observed in the cross-section image shown in Figs. 5(1b)-(4b). As shown in Fig. 5(1b), an indistinct PPO film was formed when coating with the 1.5 wt% PPO polymer dope. In general, the low-concentration casting dope could easily spread out or penetrate into the upper level of micropores of CMS layer through the surface pores because of the low viscosity and high fluidity (see Table 3). Thus, the PPO protective layer of the PO-1.5-RT CMS membrane was very thin. Given that the higher polymer concentration increased the viscosity, it also decreased the mobility and extended the phase inversion period during desolvation by solvent evaporation [26]; consequently, the thickness of the PPO hydrophobic layer was proportional to the dope concentration as the dope concentration was increased from 1.5 wt% to 7.0 wt%.

FE-SEM images of PPO film-coated EI CMS membranes are shown in Fig. 6. The hydrophobic layers on the EI CMS membranes were all thicker than those on the PO CMS membranes. The thicker layer on EI may be related to the smooth surface of EI as a consequence of dope accumulation. The surface roughness of the CMS membranes according to AFM analysis is given in Table 2. The roughness of the EI membranes (Ra=5.2 nm) was lower than that of the PO membranes (Ra=12.9 nm); thus, the surface submicroporosity of the EI CMS membrane was lower because its surface was smoother than that of the PO CMS membrane. Therefore, the casting dope may not easily infiltrate into the upper level of micropores through the surface pores of CMS membranes with a smoother surface morphology. Therefore, the hydrophobic layer on the EI CMS membrane was thicker than that on the PO membrane. The surface pore size of the PO and EI CMS membranes was also decreased. As shown in Table 2, the surface roughness of the hydrophobic layer-coated membrane decreased when the viscosity of casting dope was higher.

The change over time of the permeance and selectivity of the modified CMS membrane coated with a hydrophobic layer is illustrated in Figs. 7 and 8 for PO-1.5-RT and EI-1.5-RT, respectively (solid line). Figs. 7(a) and 8(a) show the change over time of the normalized permeance P/P_0 (ratio of the permeance at any time to the permeance of the fresh PO (or EI) membrane), whereas Figs. 7 (b) and 8(b) show the normalized selectivity α/α_0 (ratio of the selectivity at any time to the selectivity of the fresh PO (or EI) membrane). The permeance used here is permeability divided by thickness (P/L) because the values change with the thickness of the coating layer (depending on the % polymer concentration and carbon membrane structure). In Fig. 7(a), the fresh PO-1.5-RT (solid line) exhibits low gas permeance towards all five gases compared to fresh PO, and the permeance remains at only

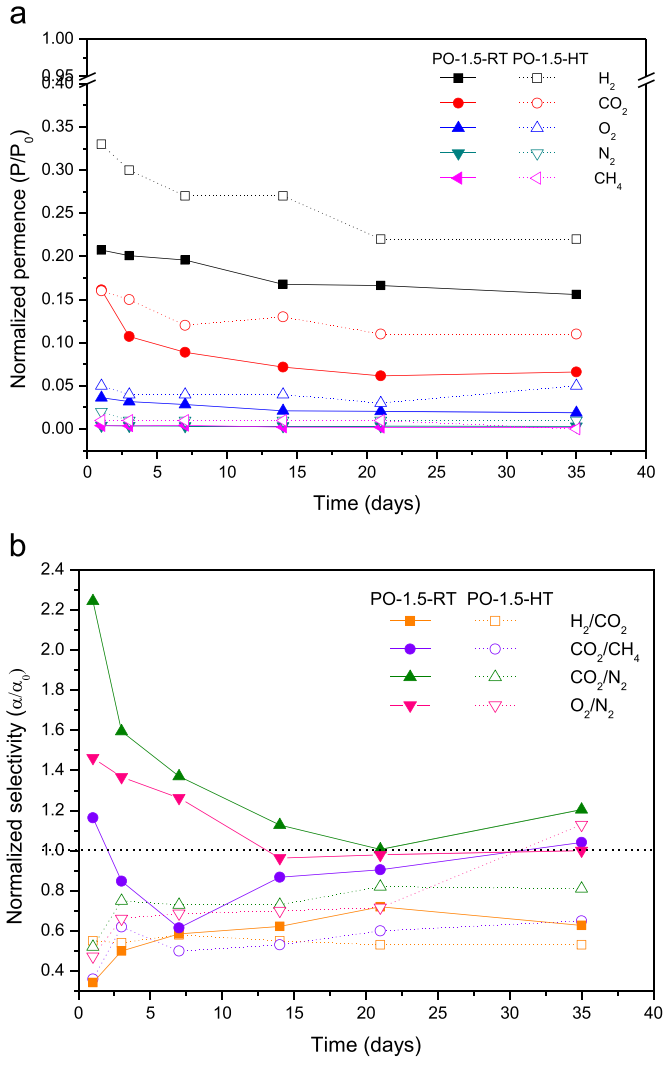

Fig. 7. The (a) normalized permeance (P/P_0) and (b) selectivity (α/α_0) of PO-1.5-RT (solid line) and PO-1.5-HT (dash line) CMS membranes. The permeance of a fresh PO CMS membrane in GPU in the laboratory air environment at 28 °C was: H_2, 578.5; CO_2, 155.94; O_2, 53.19; N_2, 8.31; CH_4, 4.44.

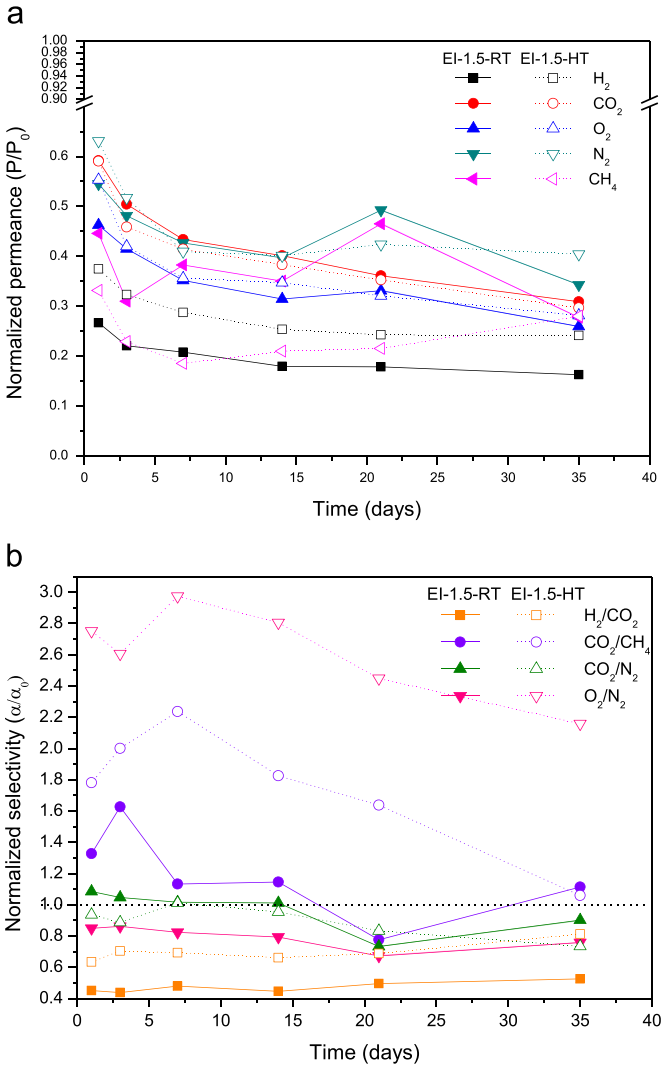

Fig. 8. The (a) normalized permeance (P/P_0) and (b) selectivity (α/α_0) of the EI-1.5-RT (solid line) and EI-1.5-HT (dash line) CMS membranes. Permeance of fresh EI CMS membrane in GPU in the laboratory air environment at 28 °C was H_2, 233.8; CO_2, 52.0; O_2, 17.7; N_2, 2.27; CH_4, 2.01.

approximately 20% for H_2, 16% for CO_2 and negligible for the larger gases O_2, N_2, and CH_4. After 35 days of storage, the permeance losses were small, i.e., within 5%. As expected, coating with a hydrophobic layer clearly reduced membrane aging. Nevertheless, it appears that the hydrophobic layer acts as a gas-resistant layer; as a consequence of the higher resistance to gas diffusion, the permeance of gases decreased dramatically. Furthermore, in this period, the selectivity values also showed an obvious decrease in the fresh PO-1.5-RT membrane. The selectivity of the smaller gas pair α_{H_2/CO_2} in the fresh PO-1.5-RT membrane decreased dramatically, possibly because of the decrease in pore size; thus, both the permeance and small gas pair selectivity were decreased. However, it should be noted out that the selectivity of the small/large gas pairs CO_2/CH_4 and CO_2/N_2 was enhanced. To further evaluate this phenomenon, the permeance of a different modified PO CMS membrane, PO-3.0-RT, was also measured over a period of 35 days, and a remarkable decrease in permeance and selectivity was observed (see Fig. 9). For the modified EI CMS membrane, the change over time of the normalized permeance and the selectivity of EI-1.5-RT are shown in Fig. 8(a) and 8(b) (solid line), respectively. A comparison of Figs. 7(a) and 8(a) reveals that the remaining permeance of EI-1.5-RT was higher than that of PO-1.5-RT, which shows a relatively high normalized permeance of approximately 26% for H_2, 60% for CO_2, and 45–55% for O_2, N_2, and CH_4. In contrast, as observed in Fig. 8(b), the normalized selectivity exhibited a decrease in the first day only for H_2/CO_2 (−55%), whereas a 32% increase for CO_2/CH_4 and an 8% increase for CO_2/N_2 were observed. In this period, the permeance and selectivity values show a stable lifespan. These surprising results indicate that the added extra resistance when coating the hydrophobic layer depended not only on the polymer concentration but also on the carbon matrix structure.

These findings show that coating a hydrophobic layer on the surface of a CMS membrane is beneficial for extending the lifespan of the membrane and preventing the membrane from aging. After coating of a hydrophobic layer, the adsorption capacity of water and the pore size decreased, which may have further reduced the aging caused by oxygen chemisorption.

Although the coating of a hydrophobic layer on the surface of the CMS membrane can extend the long-term stability in the laboratory environmental, a rapid loss of permeability for the fresh-coated membrane was observed on the first day because of the dense structure.

For PO and EI CMS, coating the membranes with PPO hydrophobic layer caused significant decline in the permeance for fresh membranes. This indicates that the transport resistance within the

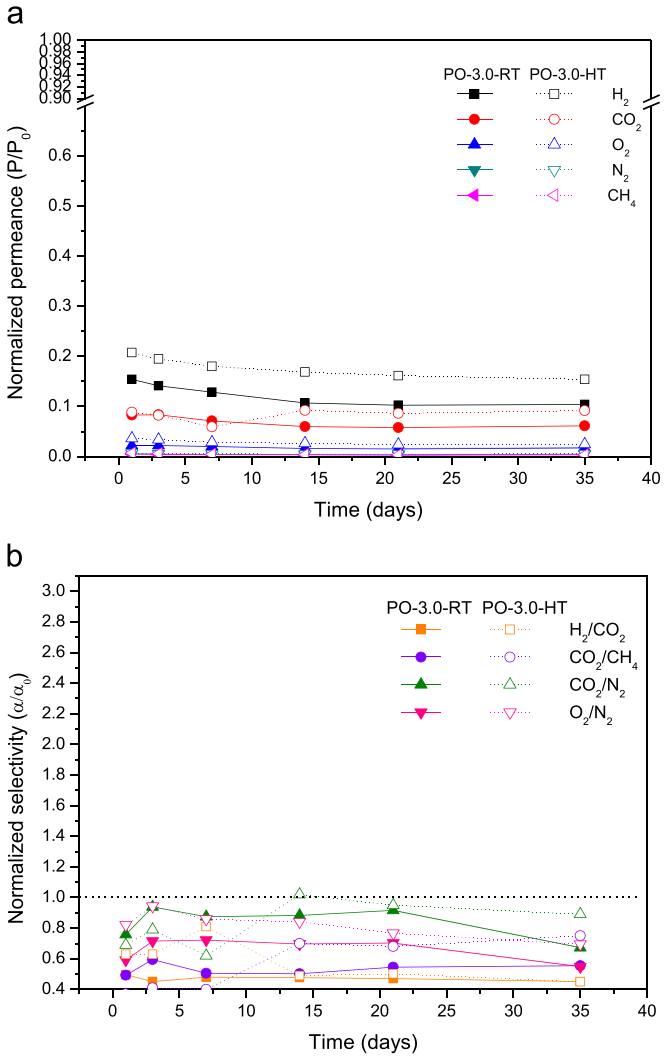

Fig. 9. The (a) normalized permeance (P/P_0) and (b) selectivity (α/α_0) of PO-300-RT (solid line) and PO-3.0-HT (dash line) CMS membranes. The permeance of a fresh PO CMS membrane in GPU in the laboratory air environment at 28 °C was: H_2, 578.5; CO_2, 155.94; O_2, 53.19; N_2, 8.31; CH_4, 4.44.

polymer layer becomes the dominant factor for the entire membrane, any significant permeance/selectivity change within the CMS layer can be hardly seen. Therefore, to really illustrate the effectiveness of coating polymer on preventing the aging of the CMS layer, the permeance of each layer was calculated and presented separately using the resistance-in-series model [20,27].

Based on the hypotheses proposed by Hamad et al. [27] (Fig. 10), the hydrophobic layer that penetrates into the upper level of the PO or EI carbon layer has the same intrinsic permeability as that of the PPO hydrophobic layer (i.e., the L_2 layer). Therefore, the resistance of the upper level of the PO or EI carbon layer is assumed to be combined with the L_2 layer. Then, the overall resistance of the pristine PO and the PO-1.5-RT are defined by the following equations:

Table 4
The overall resistances of pristine and protected CMS membranes.

Sample	Aging time (days)	R_t or $R_{t'}$ (s cmHg cm^{-3})				
		H_2	CO_2	O_2	N_2	CH_4
PO	1	0.055	0.204	0.599	3.832	7.173
PO-1.5-RT	1	0.265	1.266	16.494	982.663	1793.194
	3	0.274	1.905	18.888	1064.552	1992.438
	7	0.281	2.295	21.083	1094.968	1707.804
	14	0.328	2.844	28.243	1127.173	2988.657
	21	0.331	3.321	28.925	1161.329	3586.389
	35	0.353	3.085	31.513	1277.462	3984.877
Sample	Aging time (days)	Permeability of L_2 (Barrer)				
PO-1.5-RT	1	7.5688	1.4995	0.1002	0.0016	0.0009

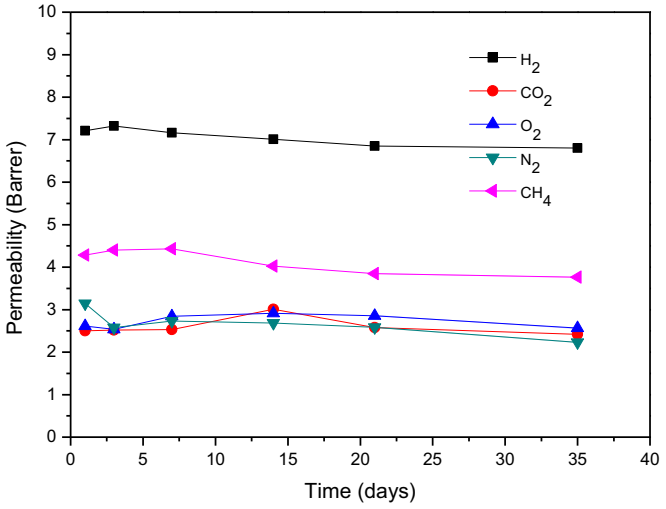

Fig. 11. The aging phenomenon of pure PPO polymer membrane without CMS layer after exposure to a laboratory air environment at 28 °C.

$$R_t = R_1 = \frac{L_t}{P_t A_t} = \frac{L_1}{P_1 A_1} \tag{4}$$

$$R_{t'} = R_2 + R_3 = \frac{L_{t'}}{P_{t'} A_{t'}} = \frac{L_2}{P_2 A_2} + \frac{L_3}{P_3 A_3} \tag{5}$$

where L, P, and A refer to the thickness, permeability and the effective membrane area, respectively; the subscripts 1, 2, and 3 refer to the pristine PO or EI carbon layer, PPO hydrophobic layer, and the lower level of PO or EI carbon layer, respectively; the subscripts t and t' refer to the total resistance of the pristine and protected carbon membrane, respectively. Assuming the permeability of H_2 of PO lower level layer (L_3) is very close to that of pristine PO carbon membrane because of the thickness of L_2 is too thin to be ignored (according to the Fig. 5(1b), the thickness of L_2 is assuming 0.05 μm). By substituting those values into Eqs. (4) and (5), the overall resistance R_t and $R_{t'}$, and the permeability of 1-day L_2 can be calculated. As shown in Table 4, resistance $R_{t'}$ within the

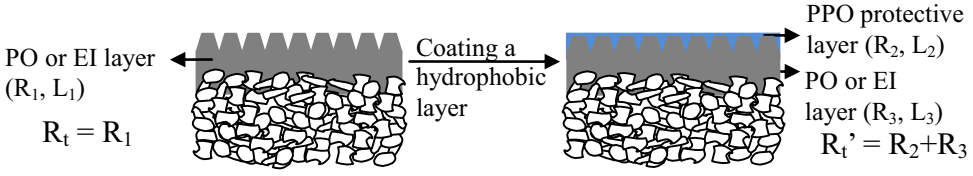

Fig. 10. Schematic representation phases of the PPO protective CMS membranes.

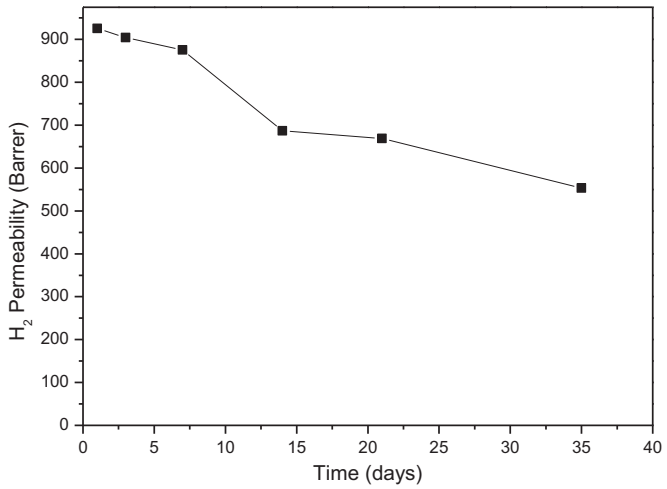

Fig. 12. The separated H_2 permeability of CMS layer calculated based on the resistance-in-series model.

protected membrane is higher than the pristine one, and the permeability of H_2 of 1-day L_2 is only 7.57 Barrer. This indicates that the main disadvantage of coating a hydrophobic polymer is reducing permeance due to the high resistance of polymer film itself.

To really illustrate the effectiveness of coating polymer on preventing the aging of the CMS layer, a pure PPO polymer membrane (without CMS layer) showing the similar H_2 permeability to the protective layer was prepared. The pure PPO membrane was fabricated with the same conditions to that of protective layer but with lower porosity Al_2O_3 support (the supporting material used here is S1500-1-2 that has been investigated in our previously work [28]. The support did not result in any resistance to the gas transport. As shown in Fig. 11, the H_2 permeability almost maintained at 7 Barrer; while CO_2, O_2, N_2, and CH_4 permeability were higher than that of protective layer but also not changed with the aging time significantly. The higher permeability of pure PPO polymer membrane might be resulted from the different support structure [28].

The results indicated that the PPO polymer membrane itself did not show any aging phenomenon for the longer durations (35 days) of storage in the air of the laboratory environment. Therefore, assuming the permeability of H_2 of PO layer is similar to that of pure PPO polymer membrane, and by substituting those values into Eq. (5), the separated H_2 permeability of L_3 changed with time was calculated.

As shown in Fig. 12, based on the calculation according to the resistance-in-series model, the H_2 permeability was slight decreased from 952.6 to 875.7 Barrer during the first 7days, and then decreased to 553.4 Barrer after 35 days. These results demonstrate that the coating polymer layer does effectively slow down the aging behavior of the carbon membrane.

To improve the permeability of the protected CMS membranes, all of them were subjected to a thermal annealing post-treatment to adjust the arraying of the PPO polymer chain.

Thermal annealing is widely used to re-arrange polymer chains to enhance the separation of polymer membranes. In this work, the thermal annealing process took the polymer matrix below its *Tg*, which enabled unpacking of the polymer chains, resulting in a looser matrix. As shown in Figs. 7 and 8, after thermal annealing of the modified CMS membranes, the permeance of most of the gases increased by 10–20% compared to the fresh PO-1.5-RT or EI-1.5-RT membranes. Furthermore, the selectivity towards O_2/N_2 and CO_2/CH_4 was also enhanced significantly. These advantages should facilitate the application of CMS membranes to air or O_2-containing gas separation.

4. Conclusions

CMS membranes are an attractive material for gas separation because of their bimodal pore size distribution and good separation performance combined with permeability and selectivity. However, storage in an air atmosphere causes the CMS membrane to undergo a rapid loss of permeance. In this study, the permeance of CO_2, O_2, and N_2 gases was approximately 80% after 35 days. The selectivity of some gas pairs slightly increased, but this increase could not compensate for the decrease in permeance.

Here, coating of a hydrophobic PPO layer on the surface of a CMS membrane was proposed to extend the lifespan of the membrane. These results show that although the use of CMS membranes for water- or O_2-containing gas separation is serious affected by aging, the lifespan of the membranes can be extending by coating a hydrophobic layer on the surface. The water adsorption capacity can be decreased by the hydrophobic properties of PPO and the pore size can also be decreased to prevent O_2 chemisorption. Although extra resistance will form after coating of a thin film, the gas diffusion resistance can be diminished by altering the polymer concentration and carbon matrix structure. These results suggest that the hydrophobic PPO-modified CMS membrane is more feasible for use after combustion with CO_2/N_2 separation or before natural gas pre-combustion with CO_2/CH_4 separation.

Acknowledgments

The authors would like to thank the Ministry of Science and Technology (MOST), Taiwan, ROC, for financially supporting this research under Contract no. NSC100-2221-E-005-004-MY3.

References

[1] J.E. Koresh, A. Soffer, Study of molecular sieve carbon. Part 1. Pore structure, gradual pore opening, and mechanism of molecular sieving, J. Chem. Soc. Faraday. Trans. 176 (1980) 2457–2471.
[2] C.A. Scholes, K.H. Smith, S.E. Kentish, G.W. Stevens, CO_2 capture from pre-combustion processes—strategies for membrane gas separation, Int. J. Greenh. Gas Control 4 (2010) 739–755.
[3] Z.Y. Yeo, T.L. Chew, P.W. Zhu, A.R. Mohamed, S.P. Chai, Conventional processes and membrane technology for carbon dioxide removal from natural gas: a review, J. Nat. Gas Chem. 21 (2012) 282–298.
[4] D.D. Larikov, S.T.O. Yama, Review of CO_2/CH_4 separation membranes, Membr. Sci. Technol. 14 (2011) 91–115.
[5] J.K. Adewole, A.L. Ahmad, S. Ismail, C.P. Leo, Current challenges in membrane separation of CO_2 from natural gas: a review, Int. J. Greenh. Gas Control 17 (2013) 46–65.
[6] J. Gilron, A. Soffer, Knudsen diffusion in microporous carbon membranes with molecular sieving character, J. Membr. Sci. 209 (2002) 339–352.
[7] H. Yang, Z. Xu, M. Fan, R. Gupta, R.B. Slimane, A.E. Bland, I. Wright, Progress in carbon dioxide separation and capture: a review, J. Environ. Sci. 20 (2008) 14–27.
[8] M. Kiyono, P.J. Williams, W.J. Koros, Effect of pyrolysis atmosphere on separation performance of carbon molecular sieve membranes, J. Membr. Sci. 359 (2010) 2–10.
[9] Y. Zhang, J. Sunarso, S. Liu, R. Wang, Current status and development of membranes for CO_2/CH_4 separation: a review, J. Greenh. Gas Control 12 (2013) 84–107.
[10] A.F. Ismail, K. Li, From Polymeric Precursors to Hollow Fiber Carbon and Ceramic Membranes, in: M. Reyes, M. Miguel (Eds.), Elsevier, 2008, pp. 81–119.
[11] C.W. Jones, W.J. Koros, Carbon composite membranes a solution to adverse humidity, Ind. Eng. Chem. Res. 34 (1995) 164–167.
[12] N. MacDowell, N. Florin, A. Buchard, J. Hallett, A. Galindo, G. Jackson, C. S. Adjiman, C.K. Williams, N. Shah, P. Fennell, An overview of CO_2 capture technologies, Energy Environ. Sci. 3 (2010) 1645–1669.
[13] I. Menendez, A.B. Fuertes, Aging of carbon membranes under different

environments, Carbon 39 (2001) 733–740.
[14] D. Grainger, M.B. Hägg, Evaluation of cellulose-derived carbon molecular sieve membranes for hydrogen separation from light hydrocarbons, J. Membr. Sci. 306 (2007) 307–317.
[15] S.M. Saufi, A.F. Ismail, Fabrication of carbon membrane for gas separation—a review, Carbon 42 (2004) 241–259.
[16] S. Lagorsse, F.D. Magalhães, A. Mendes, Aging study of carbon molecular sieve membranes, J. Membr. Sci. 310 (2008) 494–502.
[17] R.M. Narbaitz, J. Cen, Electrochemical regeneration of granular activated carbon, Water Res. 28 (1994) 1771–1778.
[18] J.A. Lie, M.-B. Hägg, Carbon membranes from cellulose: synthesis, performance and regeneration, J. Membr. Sci. 284 (2006) 79–86.
[19] L. Wang, N. Balasubramanian, Electrochemical regeneration of granular activated carbon saturated with organic compounds, Chem. Eng. J. 155 (2009) 763–768.
[20] H.H. Tseng, A.K. Itta, Modification of carbon molecular sieve membrane structure by self-assisted deposition carbon segment for gas separation, J. Membr. Sci. 389 (2012) 223–233.
[21] A.K. Itta, H.H. Tseng, Hydrogen separation performance of CMS membranes derived from the imide-functional group of two similar types of precursors, Int. J. Hydrog. Energy 36 (2011) 8645–8657.
[22] W.N.W. Salleh, A.F. Ismail, Fabrication and characterization of PEI/PVP-based carbon hollow fiber membranes for CO_2/CH_4 and CO_2/N_2 separation, AIChE J 58 (2012) 3167–3175.
[23] L.M. Robeson, The upper bound revisited, J. Membr. Sci. 320 (2008) 390–400.
[24] J.H. Kim, W.J. Koros, D.R. Paul, Effects of CO_2 exposure and physical aging on the gas permeability of thin 6FDA-based polyimide membranes Part 2. with crosslinking, J. Membr. Sci. 282 (2006) 32–43.
[25] T.M. Murphy, B.D. Freeman, D.R. Paul, Physical aging of polystyrene films tracked by gas permeability, Polymer 54 (2013) 873–880.
[26] J.C. Jansen, M. Macchione, C. Oliviero, R. Mendichi, G.A. Ranieri, E. Drioli, Rheological evaluation of the influence of polymer concentration and molar mass distribution on the formation and performance of asymmetric gas separation membranes prepared by dry phase inversion, Polymer 46 (2005) 11366–11379.
[27] F. Hamad, K.C. Khulbe, T. Matsuura, Comparison of gas separation performance and morphology of homogeneous and composite PPO membranes, J. Membr. Sci. 256 (2005) 29–37.
[28] M.Y. Wey, H.H. Tseng, C.K. Chiang, Improving the mechanical strength and gas separation performance of CMS membranes by simply sintering treatment of α-Al_2O_3 support, J. Membr. Sci. 453 (2014) 603–613.

附件六

科技部補助專題研究計畫出席國際學術會議心得報告

日期：106 年 12 月 13 日

計畫編號	MOST　103－2221－E－040－001－MY3		
計畫名稱	碳分子篩型水氣轉移膜反應器於 IGCC 系統捕獲 CO_2 及提升 H_2 產率之開發與老化再生機制評估		
出國人員姓名	曾惠馨	服務機構及職稱	中山醫學大學/職業安全衛生學系
會議時間	106 年 12 月 8 日至 106 年 12 月 10 日	會議地點	泰國蘇美島
會議名稱	(中文) 2017 第二屆環境工程與永續發展國際研討會 (英文) 2017 2nd International Conference on Environmental Engineering and Sustainable Development(CEESD 2017)		
發表題目	共四篇，請見附件		

一、 參加會議經過

此次參與的研討會為 2017 2nd International Conference on Environmental Engineering and Sustainable Development(CEESD 2017)是由亞太地區的科學與工程之研究院所主辦，而並由香港中小型企業聯合會(HKSME)所協辦，地點位於泰國蘇美島的 Prana Resort 。由於本校亦同時獲教育部教學創新計畫之補助，故此行亦一同帶領本研究室五位四年級大專生同學一同與會，並進行論文的口頭報告共四篇。

CEESD 2017 的研討會議題主要是與環境工程相關之最新研究，會議的議程共為期三天，而其中演講議程共分成 3 個時段，包含有 keynote speech、口頭論文發表及海報論文發表。與會人員以中港台地區的研究學者為主，及少數來自美國及印度的研究單位。藉由面對面學術交流分享，不僅可了解目前相關領域的研究現況，以及為未來合作尋找全球合作夥伴的機會，也增加了學生國際的視野。其中賴炯橦同學更於研討會中獲取**最佳報告獎**的佳績，在參與研討會的過程中學生除了藉由演講者的發表來了解目前對於環境的研究成果，也藉由親自上台口頭報告以及對台下學者的提問所回答來訓練口頭報能力和增加臨場應對的能力，透過此次的學術交流，學生不僅從中獲得了許多相關研究的新知識，也對未來進入研究所有了更具體的學習方向。

二、與會心得

參與本次在泰國舉辦的第二屆環境工程與永續發展研討會，除了有助認識中港台相關領域的研究團隊，建立未來共同合作及跨領域整合的機會與契機，對於本團隊後續研究有相當大的幫助。

<table>
<tr><th colspan="2">活動剪影</th></tr>
<tr><td> 
</td><td> 
</td></tr>
<tr><td>舉辦研討會之會場</td><td>師生合影</td></tr>
<tr><td> 
</td><td> 
</td></tr>
<tr><td>學生於研討會進行口頭發表</td><td>授予獲獎學生最佳報告之榮譽</td></tr>
</table>

三、發表論文全文或摘要

Catalytic behavior of Cu/ZnO catalyst loaded on 3D mesoporous SBA-16 for water–gas shift reaction

Yu-Lun Tu[1], Jing-Yi Li[2], Ming-Yen Wey[3], and Hui-Hsin Tseng[4]*

[1] Bachelor degree student, Chung Shan Medical University, Taiwan, ROC
[2] PhD student, National Chung Hsing University, Taiwan, ROC
[3] Professor, National Chung Hsing University, Taiwan, ROC
[4] Professor, Chung Shan Medical University, Taiwan, ROC

* Presenting author. Tel: +886 911730582, Fax: +886 4 23248194, E-mail: ellie20061205@gmail.com

Abstract

Catalysts for low-temperature WGS (LT-WGS) reaction should be pyrophoric and require long and tedious pretreatment procedures. These catalysts are also susceptible to chemical poisoning and can be easily deactivated thermally. The presence of carbonate species formed on the catalyst surface leads to the deactivation of the LT-WGS catalyst due to the blockage of active sites. The dispersion and crystal size of Cu/Zn/SBA-16 catalysts fabricated through co-precipitation using 3D mesoporous SBA-16 should be evaluated to improve the activity and stability of the LT-WGS catalyst. Cu/ZnO/SBA-16 catalyst was synthesized through co-precipitation for LT-WGS. Cu/ZnO catalysts were fabricated using 3Dmesoporous SBA-16 with different Cu/Zn/Si (1/1/1, 2/2/1, 3/3/1) molar ratios and calcination temperatures (350 °C, 400 °C, and 450 °C). The activities of the catalysts for the WGS reaction were tested in a fixed bed reactor at 3 atm with different steam/CO ratios (S/C=1.0, 1.5, 2.0) and reaction temperatures (200 °C, 250 °C, and 300 °C). Results indicated that different Cu/Zn/Si molar ratios influenced the particle size of active Cu and the dispersion of Cu, leading to varied catalytic activities. Based on the XRD pattern, the precursor of 3/3/1-Cu/ZnO/SBA-16 was identified as aurichalcite. The FE-SEM image revealed the laminated structure of 3/3/1-Cu/ZnO/SBA-16. According to the activity test, the CO conversion rate and H_2 yield of 3/3/1-Cu/ZnO/SBA-16 were found to be 86% and 51%, respectively. (220 words)

Superhydrophobic carbon membrane for separation of water-in-oil emulsions

Ko-Tung-Lai[1], Yi-Fan Chu[1], Hui-Hsin-Tseng[2]*

[1] Student, School of Occupational Safety and Health, Chung Shan Medical University, Taichung 402,Taiwan, ROC

[2] Professor, School of Occupational Safety and Health, Chung Shan Medical University, Taichung 402,Taiwan, ROC

* Presenting author. Tel: +886 9 39643117, Fax: +886 4 23248194, E-mail: lackwhile307@gmail.com

Abstract

With the rapid development of industrial technology, oil field mining and refinement produce large amounts of oily sludge, which causes serious damage to the environment. The high water content in the sludge enhances the difficulty of pollution treatment. In this regard, purification of oil/water systems has been an important research topic. Membrane filtration is a simple system that exhibits high efficiency for oil/water separation. In this study, hydrophobic and oleophilic carbon membranes were prepared through spin coating and pyrolysis and tested for their oil/water separation performance. The pore size and its distribution in the carbon membranes were adjusted by changing (1) the number of coating and (2) the concentration of the polymer solution. Field-emission scanning electron microscopy(FE-SEM) and contact angle analyses were conducted to observe the morphology and hydrophobicity of the carbon membranes, respectively. The results possessing both hydrophobicity and oleophilicity, which is benefit for high flux separation of water-in-oil emulsion and anti-fouling. Furthermore, the membrane performance in terms of permeate flux was affected by spin coating times and the concentration of polymer solution, the water content of the feed liquid and transmembrane pressure. With the increase of coating times and the concentration of polymer solution on the membrane structure, the pore size of surface of carbon membrane becomes denser, and the permeation flux of pure oil or oil-water mixture is decreasing but with the rejection rate increased. The permeation flux was 2551 L/m^2-h, and the penetration water content was only 0.03% at 0.037 bar. In the test results, the contact angles for diesel and water were 0°and 143°, respectively. Therefore, the fabricated carbon membranes possessing hydrophobicity and oleophilicity are suitable for high flux separation of water-in-oil emulsion under low pressure. (281words)

Effect of PEG additive on PVDF membrane morphology and protein separation at different pH values

Yi Chen Lin[1], and Hui Hsin Tseng[2],*

[1] B.S. student, School of Occupational Safety and Health, Chung Shan Medical University. Taichung, Republic of China (ROC)

[2] Professor, School of Occupational Safety and Health, Chung Shan Medical University. Taichung, Republic of China (ROC)

* Presenting author. Tel: +886 975758791, E-mail: a0929556275@gmail.com

Abstract

The effect of different molecular weights and doses of polyethylene glycol (PEG) pore-former on PVDF membrane morphology and hydrophilicity were investigated. We adjusted the pH of the feed protein solution from 3 to 11 to enhance the protein permeate flux and protein rejection for the evaluation of the electric repulsive force. The morphology of PEG/PVDF blend membranes were analyzed by scanning electron microscopy. The pore size distribution and porosity of the membrane were characterized. The contact angle was able to provide membrane hydrophilicity. The performance of the membranes was evaluated with respect to pure water flux, pure water recovery rate, and protein rejection. Field emission-scanning electron microscopy results showed that the membrane surface crystal remarkably decreased, whereas surface pore size obviously increased when the molecular weight of PEG increased from 600 to 6000. The pore size distribution showed that the pore sizes increased. The results indicated that highly molecular PEG had higher water flux, and protein rejection was poor. In solution pH, the most severe fouling was observed at the isoelectric point of bovine serum albumin (pH 4.7), where the electric repulsive force between the foulant and membrane was negligible. When the pH away isoelectric points which had less severe membrane fouling. Overall, optimal balance between protein rejection and pure water flux was observed in solutions containing PEG 600 and dose in 6 wt%, and excellent protein permeate flux was observed in feed solution at pH 11. (237 words)

Esterification/transesterification of waste cooking oil to biodiesel using bifunctional NaOH/SBA-16 catalyst

Fan-Ya Kao [1], Ming-Yen Wey[2], and Hui-Hsin Tseng [3]*

[1] Student, Chung Shan Medical University, Taiwan, ROC
[2] Professor, National Chung Hsing University, Taiwan, ROC
[3] Professor, Chung Shan Medical University, Taiwan, ROC

* Presenting author. Tel: +886 954022326, Fax: +886 4 23248194, E-mail: gracetaka123@gmail.com

Abstract

For biodiesel production, heterogeneous acid–alkali bifunctional catalysts were used for the esterification of free fatty acids (FFAs) and transesterification of triglycerides. Then, palmitic acid and water was added to canola oil such that the resulting mixture had the same properties as waste cooking oil. Bifunctional catalysts were synthesized by using alkali NaOH-impregnated acid SBA-16 as heterogeneous catalyst. The support and catalyst were characterized through X-ray diffraction (XRD), Scanning electron microscope (SEM), Transmission electron microscopy (TEM) and Hammett indicator analyses. SEM results show the sphere-shaped SBA-16 with uniform particle size ranging from 2.5 μm to 2.8 μm and the internal structure of hexagonal parallel channels. The low-angle XRD analysis results indicated that SBA-16 exhibited characteristic peaks at 2θ of 0.84°, 1.17°, and 1.47°. The 3D mesostructure of SBA-16 was expected to increase the mass transfer and improve the yield of the biodiesel. After the impregnation of NaOH, the characteristic peaks at 0.84° remained, indicating that the active phase of NaOH was dispersed well on the surface of the mesoporous SBA-16. In addition, the esterification/transesterification results indicated that NaOH/SBA-16 catalyst enabled the methyl ester yield to reach 95.5% in 8 h of reaction time under the following operation conditions: reaction temperature of 65 °C, methanol-to-oil molar ratio of 6:1, FFA content of 1%, and water content of 0.5. Under the same conditions, compared with canola oil without palmitic acid and water, yield can only reach 66.6% of the yield. The reasons that the addition of palmitic acid and water can increase yield are pH 5–5.4 for SBA-16 and pH 10–15 for NaOH, which can respectively be used for esterification of FFA and transesterification of triglycerides to biodiesel simultaneously. (279 words)

103年度專題研究計畫成果彙整表

計畫主持人：曾惠馨	**計畫編號：**103-2221-E-040-001-MY3
計畫名稱：碳分子篩型水氣轉移膜反應器於IGCC系統捕獲CO2及提升H2產率之開發與老化再生機制評估	

成果項目					量化	單位	質化 （說明：各成果項目請附佐證資料或細項說明，如期刊名稱、年份、卷期、起訖頁數、證號...等）
國內	學術性論文	期刊論文			0	篇	
		研討會論文			1		李靜怡、涂逸寧、曾惠馨、魏銘彥，碳分子篩選膜反應器應用於H2純化與CO2補獲之研究，第28屆環工年會，空氣污染控制技術研討會（台南，嘉南藥理大學）（獲最佳論文獎）
		專書			0	本	
		專書論文			0	章	
		技術報告			0	篇	
		其他			0	篇	
	智慧財產權及成果	專利權	發明專利	申請中	0	件	
				已獲得	0		
			新型/設計專利		0		
		商標權			0		
		營業秘密			0		
		積體電路電路布局權			0		
		著作權			0		
		品種權			0		
		其他			0		
	技術移轉	件數			0	件	
		收入			0	千元	
國外	學術性論文	期刊論文			4	篇	12.Hui-Hsin Tseng*, Ching-Ting Wang, Guo-Liang Zhuang, Petr Uchytil, Jirina Reznickova, Katka Setnickova, Enhanced H2/CH4 and H2/CO2 separation by carbon molecular sieve membrane coated on titania modified alumina support: Effects of TiO2 intermediate layer preparation variables on interfacial adhesion, Journal of Membrane Science, 510 (2016) 391-404. 15.Hui-Hsin Tseng, Guo-Liang Zhuang, Min-Der Lin, Ssu-Hsun Chang, Ming-Yen Wey, The influence

					of matrix structure and thermal annealing-hydrophobic layer on the performance and durability of CMS membrane during physical aging, Journal of Membrane Science 495 (2015) 294-304. 另有兩篇論文審查中
		研討會論文	3		1. Wen-Hsiung. Lai, Guo-Liang Zhuang, Ming-Yen Wey, Hui-Hsin Tseng, Development of Reclaimed Tire Rubber-Derived Carbon Membrane for Hydrogen Separation,14th International Conference on Inorganic Membranes (ICIM), July 10-13,2016, Georgia Tech Global Learning Center, Atlanta USA. (Poster) 2. Po-Yu Cheng, Hui-Hsin Tseng*, Ming-Yen Wey, Preparation and characterization of tubular carbon molecular sieving membrane by vacuum-assisted dip-coating method and their gas separation properties, 12th World Filtration Congress, April 11-15, 2016, Taipei Taiwan. 3. P. Y. Cheng, M. Y. Wey and H. H. Tseng*, Fabrication of Tubular Carbon Molecular Sieve Membranes by Dip-Coating Method for Gas Separation, The 9th Conference of Aseanian Membrane Society (AMS9), 19-21 July 2015, Howard Civil Service International House, Taipei.
		專書	0	本	
		專書論文	0	章	
		技術報告	0	篇	
		其他	0	篇	
	智慧財產權及成果	專利權 發明專利 申請中	0	件	
		專利權 發明專利 已獲得	0		
		專利權 新型/設計專利	0		
		商標權	0		
		營業秘密	0		
		積體電路電路布局權	0		
		著作權	0		
		品種權	0		

		其他	0		
	技術移轉	件數	0	件	
		收入	0	千元	
參與計畫人力	本國籍	大專生	0	人次	
		碩士生	3		鄭博育，以真空輔助浸塗法製備管柱式碳分子篩選薄膜之結構特徵與氣體分選效能之探討，碩士論文，104年7月畢。 涂逸寧，催化型碳分子篩選膜反應器應用於IGCC發電技術之H2純化與CO2補獲之研究，碩士論文，105年7月畢。 李靜怡，疏水型矽/碳分子篩選膜反應器建構與水氣轉移反應之應用，碩士論文，106年7月畢。
		博士生	1		莊國良，利用高分子廢棄物製備氣體分離薄膜之可行性研究，博士論文，106年7月畢
		博士後研究員	0		
		專任助理	0		
	非本國籍	大專生	0		
		碩士生	0		
		博士生	0		
		博士後研究員	0		
		專任助理	0		
其他成果 （無法以量化表達之成果如辦理學術活動、獲得獎項、重要國際合作、研究成果國際影響力及其他協助產業技術發展之具體效益事項等，請以文字敘述填列。）			1. 獲邀演講 Hui-Hsin Tseng, Key factors in optimizing the ultra-microporous structure of carbon molecular sieve membrane for H2 purification and CO2 capture, International Membrane Conference in Taiwan, Taiwan Membrane Society. Hui-Hsin Tseng, Carbon membrane for clean energy, CO2 capture, and water/oil separation, 13th Conference on Environmental Protection and Nanotechnology, May 27, 2016, National Taiwan University, Taipei, Taiwan. 2. 國際合作 與捷克皇家學院進行相關領域之國際合作，除共同發表論文外，亦正進行捷克專利與台灣專利的申請。		

科技部補助專題研究計畫成果自評表

請就研究內容與原計畫相符程度、達成預期目標情況、研究成果之學術或應用價值（簡要敘述成果所代表之意義、價值、影響或進一步發展之可能性）、是否適合在學術期刊發表或申請專利、主要發現（簡要敘述成果是否具有政策應用參考價值及具影響公共利益之重大發現）或其他有關價值等，作一綜合評估。

1. 請就研究內容與原計畫相符程度、達成預期目標情況作一綜合評估
   ■達成目標
   □未達成目標（請說明，以100字為限）
   　□實驗失敗
   　□因故實驗中斷
   　□其他原因
   說明：

2. 研究成果在學術期刊發表或申請專利等情形（請於其他欄註明專利及技轉之證號、合約、申請及洽談等詳細資訊）
   論文：■已發表　□未發表之文稿　□撰寫中　□無
   專利：□已獲得　■申請中　□無
   技轉：□已技轉　□洽談中　■無
   其他：（以200字為限）

3. 請依學術成就、技術創新、社會影響等方面，評估研究成果之學術或應用價值（簡要敘述成果所代表之意義、價值、影響或進一步發展之可能性，以500字為限）
   本研究已成功地開發管柱式碳分子篩膜的製備方法，不僅對小氣體分子，如H2/CO2分子對，具有理想的滲透選擇率，更可進一步整合水氣轉移反應，做為膜反應器材料，提高反應的轉化率及產率。研究結果指出，於管柱式碳分子篩膜中填充自製的Cu-Zn/SBA-16觸媒，在低溫3000 oC時，可對CO+H2O->H2+CO2反應，展現高CO轉化率(99%)及高H2產率(76%)；且經由塗佈疏水層於碳膜表面，可有效地減緩碳膜的老化現象，而更適於長時間的操作。因此，本技術的開發，預期將有助於潔淨燃煤發電技術的提升、氫能產業的應用及二氧化碳分離與純化之應用；此外，三年的研究成果已逐步發表於國際知名期刊，如Journal of Membrane Science等，兼具學術及應用價值。
   其對於產業預期之貢獻如下：
   （1）發電業、工業、運輸業：國內產生二氧化碳的主要排放源為能源使用工業，因此本研究之碳分子篩薄膜，將可應用於上述產業以達二氧化碳之排放減量目的。
   （2）潔淨能源生產工業，氫能工業：可整合產氫製程，提高氫氣純度及產率。

4. 主要發現

本研究具有政策應用參考價值：□否 ■是，建議提供機關經濟部,
（勾選「是」者，請列舉建議可提供施政參考之業務主管機關）

本研究具影響公共利益之重大發現：■否 □是

說明：（以150字為限）

本研究開之技術，可於低溫3000 oC時，可對CO+H2O->H2+CO2反應，展現高CO轉化率(99%)及高H2產率(76%)；且經由塗佈疏水層於碳膜表面，可有效地減緩碳膜的老化現象，而更適於長時間的操作。預期將有助於潔淨燃煤發電技術的提升、氫能產業的應用及二氧化碳分離與純化之應用。